MODELLING DEFORMATION IN A DC SMELTING FURNACE LINING

by

A.H. Kotze

submitted in partial fulfilment of the requirements for the degree

M.Eng Metallurgical Engineering

in the

Faculty of Engineering, Built Environment and Information Technology
Department of Materials Science and Metallurgical Engineering

of the

University of Pretoria

Under Supervision of
Dr J.H. Zietsman
Prof. S. Kok

on

April 20, 2020

DECLARATION ON PLAGIARISM
UNIVERSITY OF PRETORIA
Faculty of Engineering, the Built Environment and Information Technology
Department of Materials Science and Metallurgical Engineering

The University places great emphasis upon integrity and ethical conduct in the preparation of all written work submitted for academic evaluation. While academic staff teach you about systems of referring and how to avoid plagiarism, you too have a responsibility in this regard. If you are at any stage uncertain as to what is required, you should speak to your lecturer before any written work is submitted.

You are guilty of plagiarism if you copy something from a book, article or website without acknowledging the source and pass it off as your own. In effect you are stealing something that belongs to someone else. This is not only the case when you copy work word-by-word (verbatim), but also when you submit someone else's work in a slightly altered form (paraphrase) or use a line of argument without acknowledging it. You are not allowed to use another student's past written work. You are also not allowed to let anybody copy your work with the intention of passing it off as his/her work.

Students who commit plagiarism will lose all credits obtained in the plagiarised work. The matter may also be referred to the Disciplinary Committee (Students) for a ruling. Plagiarism is regarded as a serious contravention of the University's rules and can lead to expulsion from the University.

The declaration which follows must be appended to all written work submitted within the department. No written work will be accepted unless the declaration has been completed and attached.

I (full names) _____

Student number _____

Topic of work _____

Declaration
1. I understand what plagiarism is and am aware of the University's policy in this regard.
2. I declare that this report is my own original work. Where other people's work has been used (from a printed source, internet or any other source), this has been properly acknowledged and referenced in accordance with departmental requirements.
3. I have not used another student's past written work to hand in as my own.
4. I have not allowed, and will not allow, anyone to copy my work with the intention of passing it off as his or her own work.

Signature _____

Dedication

To God, Andrea, Daleen, and Nico

Acknowledgements

During the course of completing this study several people contributed to the work and my personal development.

- The project sponsor and my supervisor Dr Johan Zietsman, thank you for the opportunity to be part of this work.
- Prof Schalk Kok, thank you for your continued guidance and support and especially for always believing in me.
- To Andrea Steyn, without you this would never have been possible, your encouragement and support made all the difference.
- To Willem Roos, thank you for all the talks, late night sessions and support; both in working together and in this study.
- To my colleagues, Admartha Sibanda, Chris van Zyl, and especially Brandon Janse van Vuuren thank you for your support and understanding.
- Finally, I would like to thank my parents and my family for their unwavering support and encouragement.

Contents

List of Figures

List of Tables

Nomenclature

α	Thermal expansion K^{-1}
β	Angle between tangential line on hearth and r-axis
$\Delta\delta_P$	Sum of shell and lining radial displacement (m)
ΔC	Incremental change in circumferential length (m)
ΔR	Incremental change in furnace radius (m)
ϵ	Emissivity
κ	Optical thickness or opacity
μ	Poisson ratio
Ω	Albedo for single scattering
ρ	Density ($kg\,m^{-3}$)
σ	Stress (Pa)
σ_S	Scattering coefficient
σ_{11}	Principal stress 1 (Pa)
σ_{22}	Principal stress 2 (Pa)
σ_{33}	Principal stress 3 (Pa)
τ_{max}	Maximum shear Stress (Pa)
ε	Strain
ε_C	Hoop Strain
C	Compression (Pa)
c_P	Specific heat capacity ($J\,kg^{-1}\,K$)
E	Young's Elasticity (Pa)
E_i	Elasticity modulus at i=L Lining and i=s Shell (m)
h	Heat transfer coefficient ($W\,m^{-2}\,K^{-1}$)
i_0	Zero-order moment of radiation intensity ($W\,sr\,m^{-2}$)

I_1 First Principal Invariant (Pa)

i_b Blackbody radiation intensity ($\mathrm{W\,sr\,m^{-2}}$)

lte Linear thermal expansion ($\%$)

n Strain hardening coefficient

N_C Number of expansion joints in circumferetial direction ()

N_R Number of expansion joints in radial direction ()

P Radial Pressure (Pa)

Q_B Density of blanket ($\mathrm{kg\,m^{-3}}$)

R Radius (m)

$R_{expansion}$ Total expansion allowance (m)

S Coordinate along path of radiation (m)

S_C Circumferential Stress (Pa)

S_c Compression Yield point (Pa)

S''_C Hoop stress (Pa)

S_t Tensile Yield point (Pa)

S_y Yield stress (Pa)

$ST_{\frac{L}{S}}$ Ratio of lining stiffness to shell stiffness

T Temperature (°C)

t Thickness (m)

t Time (s)

T_b Bulk fluid temperature (°C)

t'_l Thickness under compression loading (m)

t_s Shell thickness (m)

u Displacement in the radial direction

w Displacement in the z direction

Subscripts

θ In the tangential direction

l Lining

r In the radial direction

s Shell

z In the axial or z direction

Part I

Introduction

Chapter 1

Background

1.1 Smelting Industry

1.1.1 Impact of Electrical Supply on South African Smelters

The smelting industry is one of the backbones of the South African economy. This builds on the mining sector which is estimated as the fifth largest in the world measured by GDP (Kearney 2012). The total contribution to South Africa's GDP in 2015 by the mining, metals, and minerals industry was between 8 and 22%. Despite this the industry has been facing challenges over the past few years. Some of the most significant challenges are labour unrest and electricity supply, both of which lead to plant closures, temporarily or even permanently. (Zietsman and Kok 2016)

In early 2012 Eskom (South Africa energy supplier) started paying smelters to shut down their furnaces in an attempt to stabilise the power grid. South Africa has been experiencing an energy crises since 2008 which has steadily been growing worse with intermittent bouts of *load shedding* and preferential agreements with smelters to use less electricity. (Naidoo 2012)

The situation has been steadily declining with mass lay-offs as late as January 2019 (Steyn 2019) Eskom from their side has been requesting multiple increases in the electricity price. According to Steyn (2019), any additional increases will result in more smelters having to close their doors. This trend has already started with multiple smelters closing down or companies moving their smelting operations out of South Africa.

Apart from the obvious challenges with the current situation such as profitability, the impact of mass job cuts, and the stability of the entire industry; smelters themselves face significant challenges when they have to switch off furnaces in order to save electricity. These type of operations need to be planned thoroughly and can easily lead to failure of the furnace lining when furnaces are started up again.

Any failure of linings lead to financial losses due to the cost of repairs or total reline as well as the loss in production during these times. The reader is referred to the work by Belt (2011) for an understanding of the financial impact of furnace maintenance.

1.1.2 Ilmenite Smelting in South Africa

Together with Australia, South Africa accounts for more than 50% of the total supply of titanium mineral concentrates and is the second largest producer. Motsie (2008) further explains the challenges faced by this industry referring to a lack of skills and technology. He explains the rising demand for titanium metal applications in the world but highlights that the industry faces tremendous challenges to meet this rise in demands.

Considering the significant role that ilmenite smelting plays in South Africa and in the world, along with the challenges mentioned above, it was decided to consider this process for evaluation.

Two of the major players in the industry are located in the Richards Bay area, Richards Bay Minerals and Tronox's KZN Sands just outside of Empangeni. Tronox owned Namakwa Sands is also a major contributor to South Africa's total ilmenite production. (Motsie 2008)

1.2 Furnace Technology

Richards Bay Minerals make use of four six in line AC electric arc furnaces. These furnaces are rectangular and have six electrodes in-line. A typical six in-line furnace is shown in Figure 1.1.

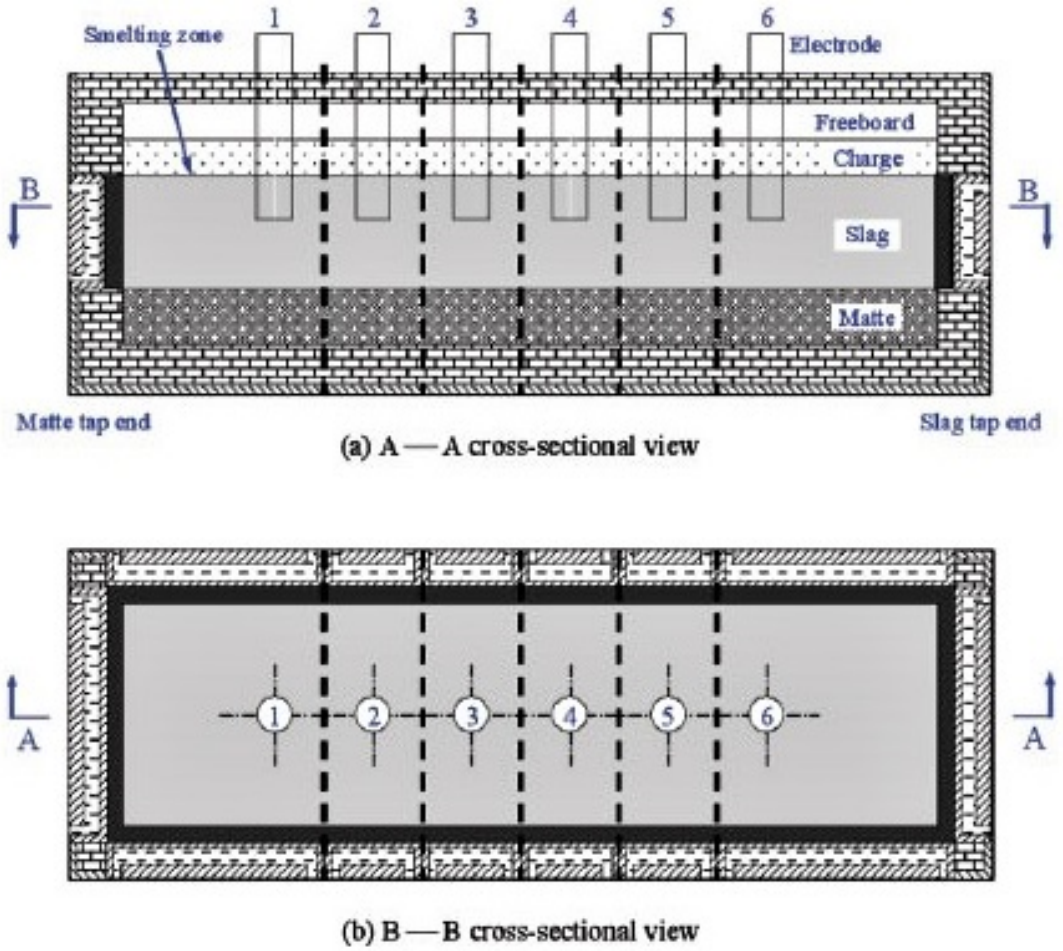

Figure 1.1: Depiction of a rectangular six in-line AC furnace (Pan, Sun, and Jahanshahi 2011)

Both Namakwa and KZN Sands make use of DC furnace technology. This technology was first tested and developed by Mintek in 1992 to 1994 (Gous 2006). Ilmenite along with Anthracite is fed through a hollow central electrode into the furnace. The result of the process is a TiO_2 rich slag and pig iron metal bath forming in the furnace. (Kotze, Bessinger, and Beukes 2006)

DC arc furnaces have also gained increasing popularity in the smelting of other ores such as chromite to produce ferrochrome (Reynolds and Jones 2004). A DC arc furnace refers to a pyrometallurgical vessel that has a conical roof, either a flat or a domed base and is contained by a cylindrical steel shell. The furnace walls and hearth is lined using refractory material to contain the molten materials and, usually, makes use of a central graphite electrode although dual electrode DC furnaces can also be found (Figure 1.2 show the difference between these two configurations) (Jones et al. 2011). Both Namakwa and KZN Sands make use of a traditional DC furnace design. (Kotze, Bessinger, and Beukes 2006)

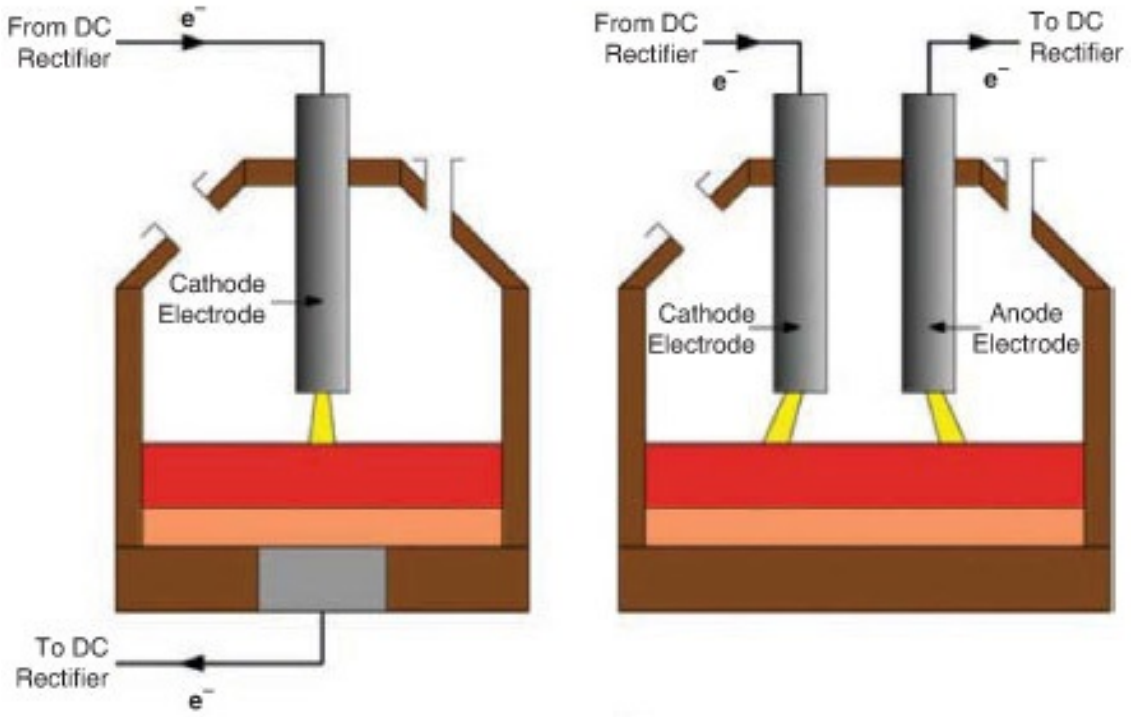

Figure 1.2: Traditional DC on the left vs dual-electrode DC on the right (Reynolds 2012)

The thermal insulation by the refractory lining minimize heat losses and protect the metal structure of the furnace by preventing thermal shocks to, and deformation of, the outer enclosure and steel frame of the furnace. Two types of refractory linings are used; a continues solid which is applied as a composite and a second type which is built from pre-cast bricks. (Boisse et al. 2001)

The high-titania slag is typically operated at a temperature of 1700 °C (Zietsman and Pistorius 2004), the metal bath is usually 150 °C cooler than the slag. This temperature difference causes partial solidification of the slag in direct contact with the metal bath. The temperature is not constant throughout the slag bath, with hot zones formed around the electrode and arc. In addition to these temperature differences, the furnace operates with a freeze lining; solidified slag against the furnace wall. This prevents the titania slag from attacking the MgO refractory lining. (Pistorius 2008)

During transient conditions such as start-ups, shut-downs, maintenance shut-downs and reduced load the refractory lining expand and contract causing stress and strain.

1.2.1 Lining Failure

A case study for the failure of lining can be found in Chirasha and Shoko (2007). Even though the lining failure is recorded for a High Carbon Ferrochrome (HCFeCr) furnace, the lessons from this experience is applicable for any smelting furnace lining. The Zimbabwe Alloys HCFeCr furnace can be seen in Figure 1.3. Some of the major contributors toward the failure of the lining was due to:

1. Bricks were lined directly against the shell.
2. The brick to brick expansion was not adequately allowed for from the base of the furnace to the side walls.

The furnace was commissioned in August 2000, but production started to deteriorate in 2003. From 2003 to 2005 the furnace continued to preform below expectations. After the first 18 months

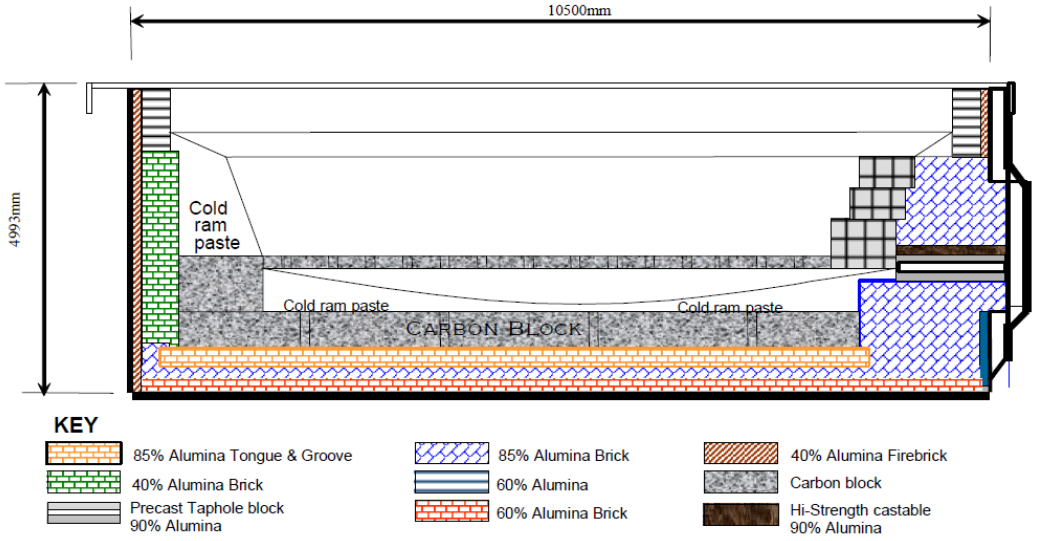

Figure 1.3: Refracotry lining design of Zimbabwe Alloys HCFeCr furnace (Chirasha and Shoko 2007)

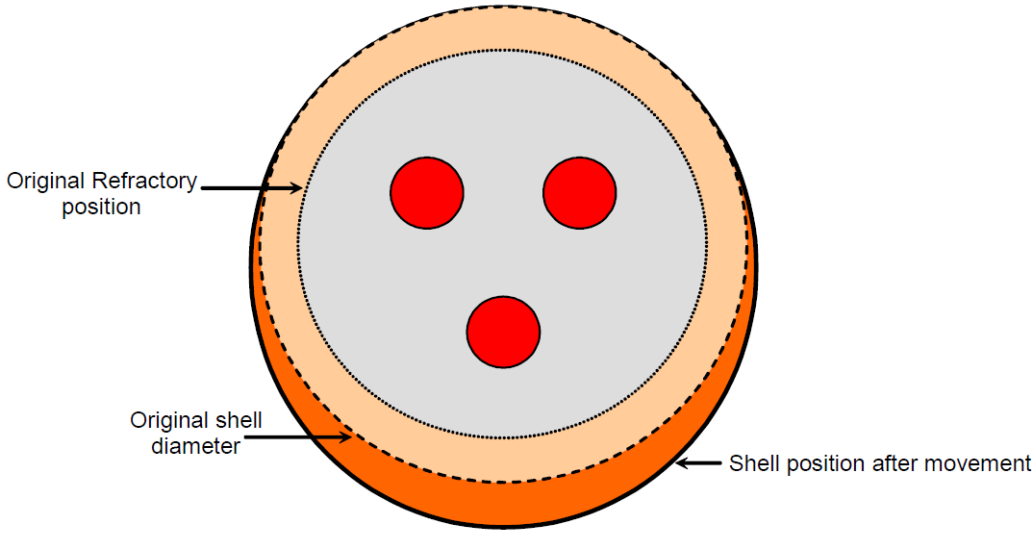

Figure 1.4: Deformation of the Zimbabwe Alloys HCFeCr furnace after 18 months in opperation (Chirasha and Shoko 2007)

of production the furnace started to show significant deformation. The furnace deformation can be seen in Figure 1.4, some of the most significant movements are listed below:

- Taphole lifted 400 mm
- Taphole shifted 200 mm to the right
- Furnace base lifted 300 mm to 400 mm from the horizontal support beams

As a result of this movement the furnace shell cracked vertically from the base on either side of the taphole. After several attempts were made to save the lining an investigation was carried out to find the root cause of the furnace failure. Upon breakout of the furnace it was discovered that the expansion of the bricks and the distortion of the lining in different areas resulted in penetration by the furnace content of the lining. Chirasha and Shoko (2007) describes the following as lessons learnt:

- Any weakness in lining design can lead to loss of production and premature furnace failures.

- The expansion allowance and gaps between bricks and the lining and shell must be calculated correctly and accurately.
- Expansion allowance is relevant to the type of refractory and subsequent refractory material properties.

From this example and several other lining failures in industry it can be deduced that a thorough understanding of lining behaviour has not yet been obtained. In order to prevent these types of failures the effects of all mechanical elements as well as chemical corrosion needs to be understood. This will lead to better furnace design and operation for all furnace types. If furnace operation and design can be better understood mitigating the electricity challenge in South Africa will become less of a problem.

Chapter 2

Research Strategy

2.1 Research Focus

2.1.1 Topic

Modelling Deformation in a DC Smelting Furnace Lining

2.1.2 Question

What are the influences of the stress-strain relationship, expansion allowance, and thermal cycles on the displacement, stresses, and strains of the refractory lining of a DC arc furnace?

2.1.3 Purpose

Due to the increased volatility of the electricity supply in South Africa, combined with demands for higher output from smelters there has been an increase in the challenges faced by the industry. Multi-physics modelling provides a cheaper alternative to trial and error and costly failed campaigns. With the use of multi-physics modelling, investigations of different designs and operational practises can be done t a fraction of the cost. The purpose of this study is to investigate the use of linear stress strain relationships and different Young's Moduli, along with the allowed expansion influence on the mechanical response of the furnace. This is the first step to incorporating all phenomena in a multi-physics model to achieve full scale furnace modelling and simulations.

2.2 Research Objectives

The objectives of this project is to gain a better understanding of:

- the influences of different stress-strain relationships on refractory behaviour for typical operational temperatures.
- the effects allowed expansion has on lining behaviour for typical operational temperatures.
- a theoretical understanding of the effects thermal cycles can have on the lining.

2.3 Research Scope

The scope does not include any chemical corrosion of the lining and will be limited to a DC smelter furnace used for ilmenite smelting. Bath flow and their influences are not included in the scope

of this work. The scope of the theoretical study is limited to an understanding of the mechanical material properties of refractory materials and the influence of allowed expansion. A theoretical study also includes the influence of thermal cycles on the lining and lining failure. The modelling analysis focus only on thermal distribution in the lining and the subsequent displacement, stresses, and strains due to thermal expansion and mechanical loading.

The study is limited to the displacement, stresses, and strains in the sidewalls and the hearth, the mechanical response of the roof is not included.

Part II

Literature Review

Chapter 3

Refractory Lining and Materials

In this chapter the influence of material properties on lining mechanical responses is investigated. The effect of considering different load types when analysing the mechanical response are also explored. The difference between material properties for different types of refractories are considered along with shortcomings in generally available data for refractories. Different modes of lining failure are investigated along with the influence that expansion joints have on this.

3.1 Load Types

In order to analyse the mechanical response of any material, the two types of load that can affect the object needs to be understood. Loading can be either stress induced or strain induced. A stress induced load is due to some or other force acting on an object. This can be a body force such as gravity or a point or distributed load such as the force pushing a block across a surface which in turn opposes the movement with a distributed frictional force (Schacht 1995). A strain induced load results from the deformation of an object. This is typically ascribed to thermal type loadings which causes thermal expansion, as observed in refractory linings (Larosche 2009; Schacht 1995).

There are several factors that influence the type of loading on a refractory lining. According to Schacht (1995) and Yilmaz (2003) the thermal load is the primary loading on a refractory lining. Most linings are constrained by an external steel structure, this results in thermal expansion forces in the lining; strain induced loading. The analysis of a refractory structure consists of two parts; a thermal analysis to give insight into the lining temperature distribution and a mechanical analysis to evaluate the stresses, strains and displacements as a result of the temperature distribution, the constraint on lining expansion as well as any stress induced loads (Schacht 1995).

3.2 Material properties

When choosing the material properties for a lining the following needs to be considered (Schacht 1995; National Productivity Council, India 2006):

- the stiffness of the external steel support structure
- the severity and nature of the transient process temperatures
- the magnitude of the process temperature
- the severity of the process chemistry

The life of a refractory lining is dependent on two summarising factors, the harshness of chemical corrosion of the lining, and the severity of loads and mechanical response. The mechanical response

can again be divided into the thermal loading and the stress and strain induced loading. (Schacht 1995) The chemical influence is outside the scope of this study and will not be considered further.

3.2.1 Thermal Properties

Since the primary purpose of refractory linings is to restrict heat flow, all material properties pertaining to thermal heat conduction are usually readily available from refractory suppliers. The required properties in the case of transient thermal analysis is:

- thermal conductivity
- specific heat
- density

For steady state analysis the specific heat and density is not required. (Papathanasiou, DalCorso, and Piccolroaz 2016).

3.2.2 Mechanical Properties

For a short term (i.e. neglecting the influence of cyclic loading and creep) mechanical analysis under strain loading the most important material properties are:

- elastic modulus
- Poisson's ratio
- coefficient of thermal expansion

It is also important to know the ultimate tensile and compressive strain. For long term analysis the time dependant response of the material, such as creep, will have to be defined. (Schacht 1995; Papathanasiou, DalCorso, and Piccolroaz 2016)

For a stress induced loading analysis, the ultimate tensile and compressive stresses rather than strains would be required in addition to the material properties already listed. In the case of refractories, the properties needed for a complete strain analysis is often hard to come by and, according to Schacht (1995), are often based on inaccurate testing methods. In contrast, several tests has been developed to describe the ultimate tensile and compressive strengths of refractories. This is also the most readily available data for different refractory materials and is often used to select the *strongest* or best refractory. However, most refractory structures are at least partially restrained, very few refractory structures are predominantly exposed to stress induced loads, with stresses due to body loads typically in the range of 0.2 MPa to 1.0 MPa. While the thermal expansion stresses could be in the range of 15 MPa to 40 MPa or in some cases even higher. When doing analysis on most furnaces the only stress induced loading is due to gravity forces and hence the material properties required are the density of the refractory material. The stress induced loading for a furnace is significantly lower than the strain induced loading. (Schacht 1995)

With this in mind in order to analyse refractory linings a complete definition of the stress-strain behaviour of the material has to be known. The stresses induced can only be defined based on the stress-strain relationship since the loading is largely strain-controlled. This means that the stress is resultant of a strain in the lining and the relationship between stress and strain has to be known. The *strongest* refractory should be chosen based on the greatest ultimate crushing strain rather than the greatest ultimate crushing strength. (Schacht 1995)

From a list of recommendations published in Schacht (1995) the following is clear:

- To only have the ultimate crushing strength of a refractory is inadequate to understand if the refractory material will be able to resist the strain-controlled loading.
- To analyse the strain controlled loading condition, the complete stress-strain relationship under crushing of the material needs to be known.
- This stress-strain data will give insight to *if*, *how much*, and *where* expansion allowance will have to be made.
- The data needed for this stress-strain relationship is often unavailable and the testing methods for this data has not been standardised.

Thermal Expansion Behaviour

Thermal expansion of a material is the same for both heating and cooling. Some refractory expansion data do not increase linearly with temperature, in this case the expansion coefficient is temperature dependant, and to define the linear thermal expansion coefficient will require the curve to be broken up into smaller pieces between increments of temperature.

The thermal expansion is applicable between the temperatures T_i and T_R.

$$\alpha_i = \frac{LE_i\%}{100(T_i - T_R)} \tag{3.1}$$

LE_i is the linear expansion expressed as a percentage at T_i. Data for refractory expansion is highly dependent on the chemistry of the specific refractory and could deviate from typical values. In the case of unfired bricks the thermal expansion can vary greatly due to shrinkage, which occurs due to drying and sintering, at high temperatures. (Schacht 1995)

Table 3.1 shows typical coefficients of thermal expansion for different types of refractories.

Table 3.1: Estimated Coefficeint of Thermal Expansion for various types of refractories (Schacht 1995).

Type of Refractory Brick	$\alpha \times 10^{-3}$ mm mm^{-1} °C^{-1}
Fireclay Brick	5.4 - 6.12
60 to 70% Alumina	6.3 - 6.84
80 to 90% Alumina	7.25 - 7.92
99% Alumina	9.0 - 9.36
Zircon	4.5 - 4.86
Chrome	8.82 - 9.18
Magnesite 92%	14.0 - 14.2
Conv. Silica 300 °C	30.6 - 31.3
Conv. Silica 1300 °C	10.1 - 10.6
Super Silica 300 °C	35.0 - 35.5
Super Silica at 1300 °C	10.1 - 10.6
Fired Dolomite	13.3
Resin Bond Dolomite	11.5

Linear VS Non-Linear Material Behaviour

The stress and strain behaviour of a material can either be classified as elastic or inelastic. It is important to understand whether a material is elastic or inelastic as this greatly influences the behaviour under loading and unloading. According to Hibbeler (2011) linear elastic behaviour of a material is when the stress is proportional to the strain. However, this should not be confused as a material can be non-linear elastic, any non-linear behaviour should not be assumed to be non-elastic (Enterfea 2019). Bot linear and non-linear elastic material are defined as elastic due to its ability to return to an unloaded state, or with no permanent deformations, after loading (Enterfea 2019). As can be seen from Figure 3.1, refractories become more non-linear at higher temperatures. (Schacht 1995; Enterfea 2019)

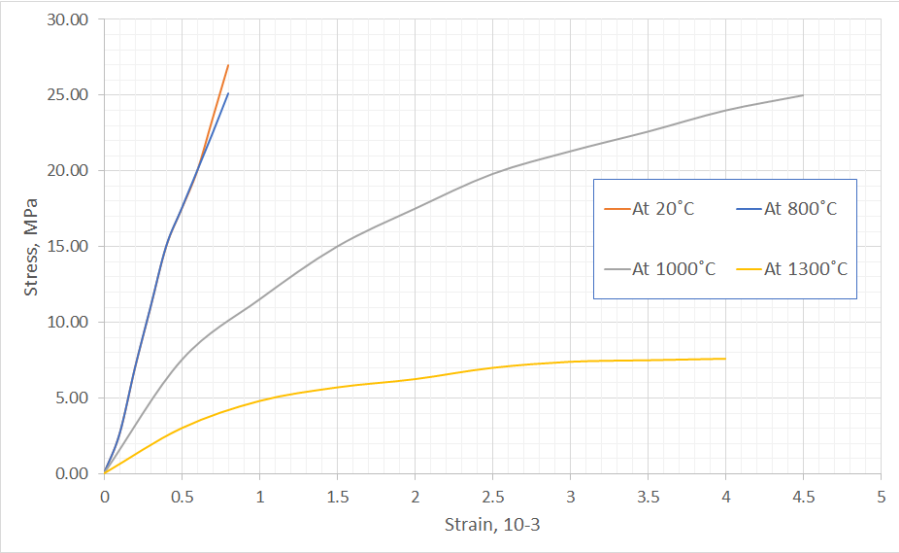

Figure 3.1: Linear behaviour of aluminium based refractory at lower temperatures with increasing non-linearity as temperatures increase. (Schacht 1995)

In addition to a material being elastic or inelastic, it can be classified as either ductile or brittle, depending on the stress-strain characteristics. A ductile material can sustain permanent deformation without losing its ability to resist a load (Schacht 1995). Ductile materials can be classified as having $\varepsilon_f \geq 0.05$ and having a yield strength that is the same for tension and compression and is easily identifiable (Budynas and Nisbett 2011). A brittle material can be described as any material that suddenly loses its ability to carry a load under increasing deformation (Schacht 1995), it does not have an easy identifiable yield strength and has $\varepsilon_f \leq 0.05$. Brittle materials are usually classified by the ultimate tensile and compressive strengths. (Budynas and Nisbett 2011)

A typical ductile material is often described using Equation (3.2).

$$\sigma = K\varepsilon^n \tag{3.2}$$

K is the stress when $\varepsilon = 1$ and n is the strain hardening coefficient. (Schacht 1995) Strain hardening occurs when a material has started to deform plastically and the load is then removed. This results in a greater elastic region and a smaller plastic region. It is important to note that the slope of the elastic deformation remains the same. The phenomena of strain hardening is shown in Figures 3.2a to 3.2b. (Hibbeler 2011)

Stress-Strain Data for Refractories

The cold-crushing strength of a refractory is often supplied as the only mechanical property to consider for strength. However, as shown for superduty fireclay (Figure 3.3), there is a difference

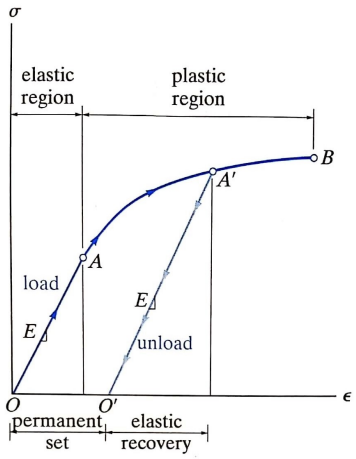

(a) Loading and unloading after plastic deformation of ductile material.

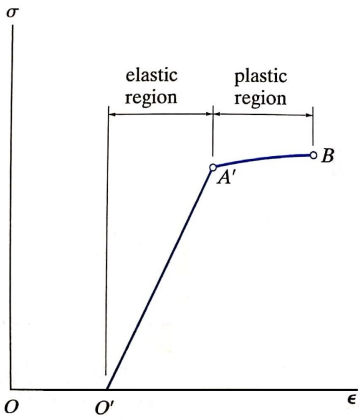

(b) Strain hardening resulting in changed stress-strain response of material.

Figure 3.2: Explanation of strain hardening (Hibbeler 2011).

between the stress-strain data at different temperatures.

Note how the fireclay remains linear up to temperatures exceeding 540 °C, above 980 °C significant non-linear flow is observed. The specified cold crushing strength on the data sheet for the firecaly is 17.2 MPa to 28 MPa. Experiments measured the crushing strength in excess of 50 MPa. This is significantly different from the reported values.

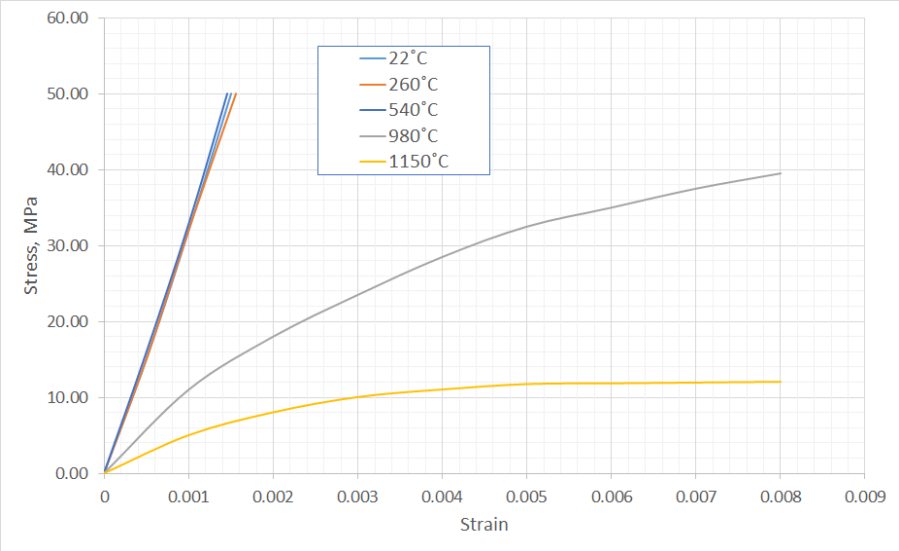

Figure 3.3: Compressive stress-strain data on a superduty fireclay brick for varying temperatures (Schacht 1995).

Figure 3.4 shows the results from further test work conducted by Schacht (1995). A separate test on the same fireclay brick was done until failure for a temperature of 540 °C and 1090 °C. The 540 °C curve shows a slightly lower strength than that of the test data in Figure 3.3. This difference is attributed to differences in the samples used. The stress at a temperature of 1090 °C in Figure 3.4 falls between the results of 980 °C and 1150 °C at a strain of 0.008 as shown in Figure 3.3. Failure only occurs at a strain of 0.04 and a strength of over 60 MPa at 1090 °C, which is significantly higher than the provided cold crushing strength.

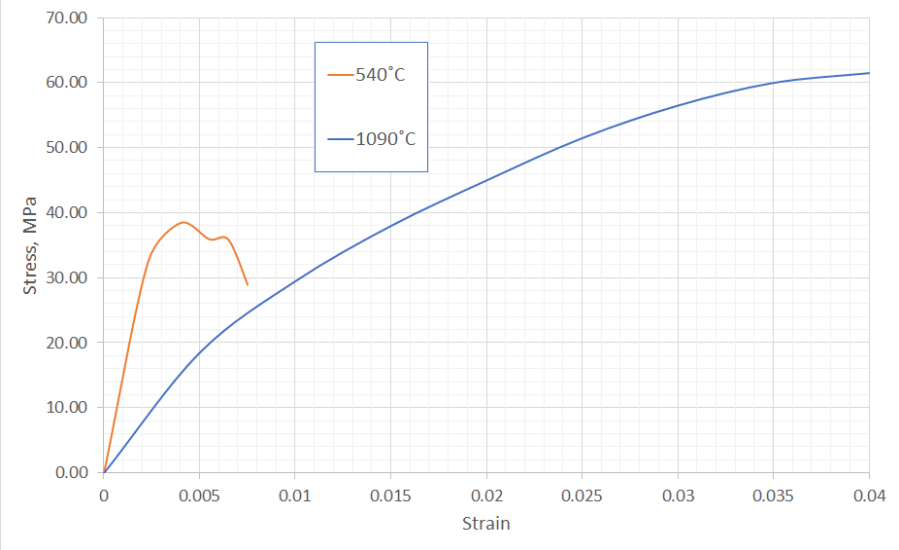

Figure 3.4: Compressive stress-strain data on a superduty fireclay brick until failure (Schacht 1995).

In Figures 3.5a to 3.5d work done by Schacht (1995) shows four basic stress-strain curves for three different 60% MgO dead burned bricks. A stress-strain relationship is also presented for 60% MgO chemically bonded brick. Notice how the MgO bricks tend to keep to a linear relationship at much higher temperatures than the fireclay. The cold crushing strength is not available for bricks 1,2 and 4, however, it is expected to be in the range of 20 MPa to 59 MPa. For brick three the cold crushing strength is listed as 69 MPa. (Schacht 1995)

These examples act as an illustration that the cold crushing strength cannot be used as an

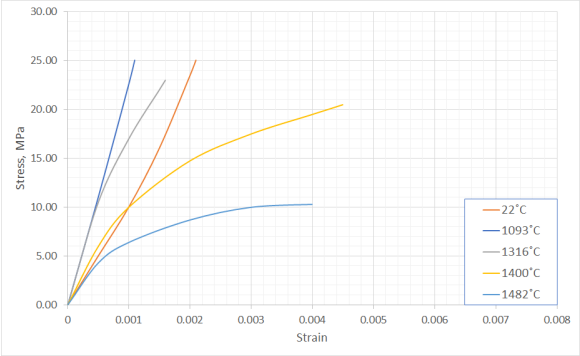

(a) Direct bond brick 1

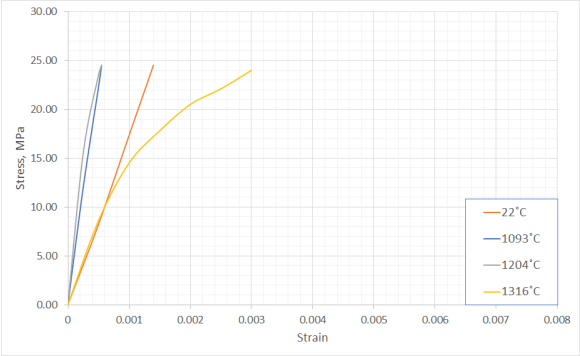

(b) Direct bond brick 2

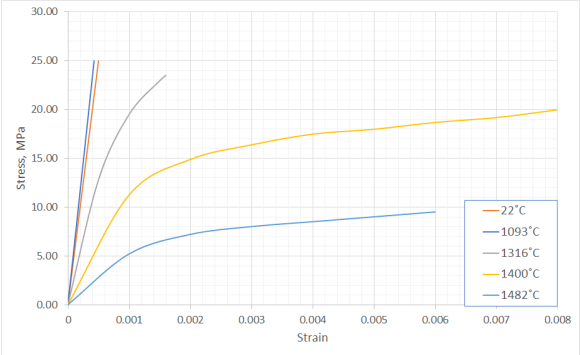

(c) Direct bond brick 3

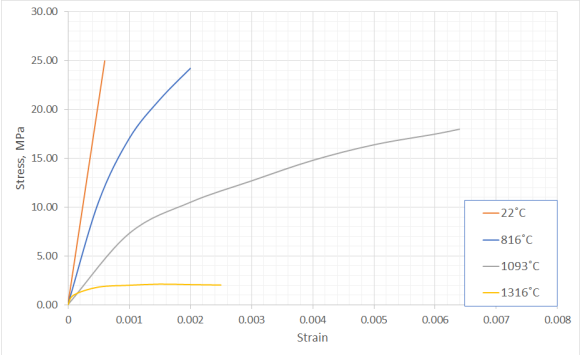

(d) Chemically bond brick

Figure 3.5: Compressive stress-strain data on 60% MgO bricks (Schacht 1995).

indication of the failure. Rather, the full stress-strain data under compressive loading for different temperatures has to be known and quantified. (Schacht 1995)

Creep of Refractories

Creep is the time-dependent permanent deformation of a material under a load. Both the temperature and the stress play a significant role in the rate of creep. In general, creep strength will decrease at higher temperatures. (Hibbeler 2011)

The temperature at which creep needs to be considered is known as the creep threshold temperature and varies for different types of refractories (Schacht 1995). The entire refractory lining is not exposed to the same temperature, but rather a temperature gradient exists through the refractory lining. This is especially prevalent in cylindrical vessels. Of the entire lining only a small part of the hotface is exposed to temperatures at which creep is significant. The resulting total expansion force in this hotface region is quite small compared to the remainder of the lining expansion force. (Schacht 1995) According to Schacht (1995) neglecting to include creep on this small region when evaluating the total thermal expansion would not result in significant error. This is because the region has already had significant deformation due to instantaneous plastic straining, which would be the much larger of forces generated. If the creep response should be included it would result in a lower expansion force generation by the hotface. However, more recent studies stress the relevance of including creep response in refractory linings as well as provide methods to genrate the required data at high temepratures (Ferber, Weresczak, and Hermrick 2006). Ferber, Weresczak, and Hermrick (2006) also stress the importance of considering creep data for furnace optimization but also admit to the lack of high temperature creep data available. As it falls outside of the focus of this study, creep will not be further included.

3.3 Modes of Failure

There is no general accepted theory for failure that can be applied to all materials in all stress states. Several hypotheses have been formulated and tested, over the years these have become general practise, up to the point that they are generally referred to as *failure theories*. (Budynas and Nisbett 2011)

In classical elastic theory, the hydrostatic stress is referred to as the first principal invariant (I_1), described in Equation (3.3). The general rules regarding flow is that the hydrostatic stress state does not cause yielding. (Schacht 1995)

$$I_1 = \sigma_{11} + \sigma_{22} + \sigma_{33} \tag{3.3}$$

σ_{11}, σ_{22}, and σ_{33} is the principle stresses. (Schacht 1995)

3.3.1 Failure Criterion

From Budynas and Nisbett (2011) the general accepted criteria for failure are described in the following sections.

Maximum Shear Stress for Ductile Materials

This criterion predicts that yielding will occur when the maximum shear stress is the same as or exceeds the maximum shear stress in a tension-test of the same material for yielding. This is a very conservative criterion and is based on the 45° slip lines when a specimen is subjected to a tensile test where the shear stress is also a maximum. For a tensile test the normal stress is $\sigma = \frac{P}{A}$ and the maximum shear stress is $\tau = \frac{\sigma}{2}$. Equation (3.4) and Equation (3.5) can be used to determine failure based on the principal stresses ordered such that $\sigma_{11} \geq \sigma_{22} \geq \sigma_{33}$.(Budynas and Nisbett 2011)

For the unique case of plane stress the criterion is presented visually in Figure 3.6.

$$\tau_{max} = \frac{\sigma_{11} - \sigma_{33}}{2} \geq \frac{S_y}{2} \tag{3.4}$$

$$\sigma_{11} - \sigma_{33} \geq S_y \tag{3.5}$$

Distortion Energy for Ductile Materials

According to the distortion energy criterion yielding will occur when the second main invariant (the distortion strain energy per unit volume) reaches or exceeds the distortion strain energy per unit volume for yield in a simple tension or compression test (Equation (3.6)).

$$\sqrt{\frac{(\sigma_{11} - \sigma_{22})^2 + (\sigma_{22} - \sigma_{33})^2 + (\sigma_{33} - \sigma_{11})^2}{6}} \geq S_y \tag{3.6}$$

The actual Von Mises stress (σ') is calculated using the left side of Equation (3.6). Again the case for plane stress is presented in Figure 3.6.

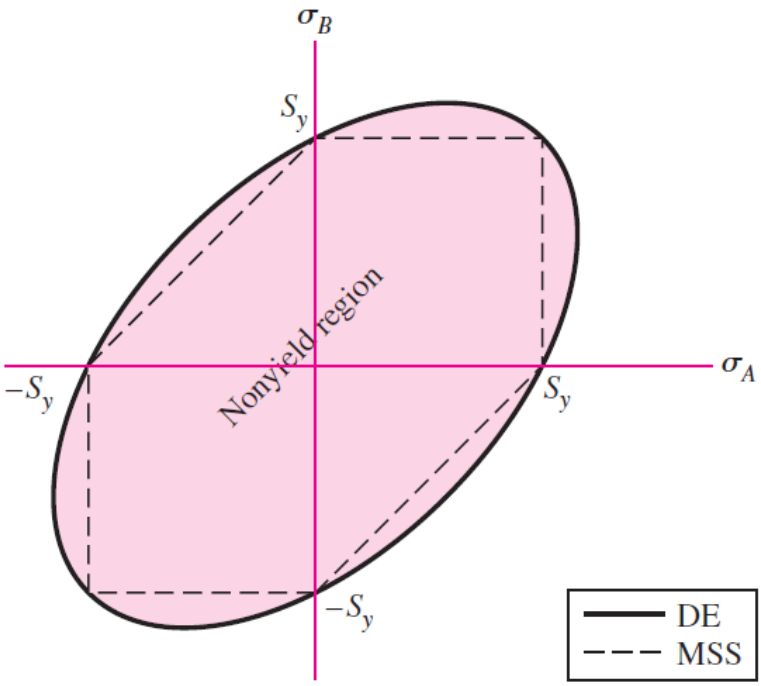

Figure 3.6: Maximum shear stress and distortion energy failure criteria for plane stress (Budynas and Nisbett 2011).

Coulomb-Mohr for Ductile Materials

This criterion can be used for the cases where the compressive strength (S_c) and tensile strength (S_t) are not the same. This criterion is expressed as

$$\frac{\sigma_1}{S_t} - \frac{\sigma_3}{S_c} = 1 \tag{3.7}$$

.

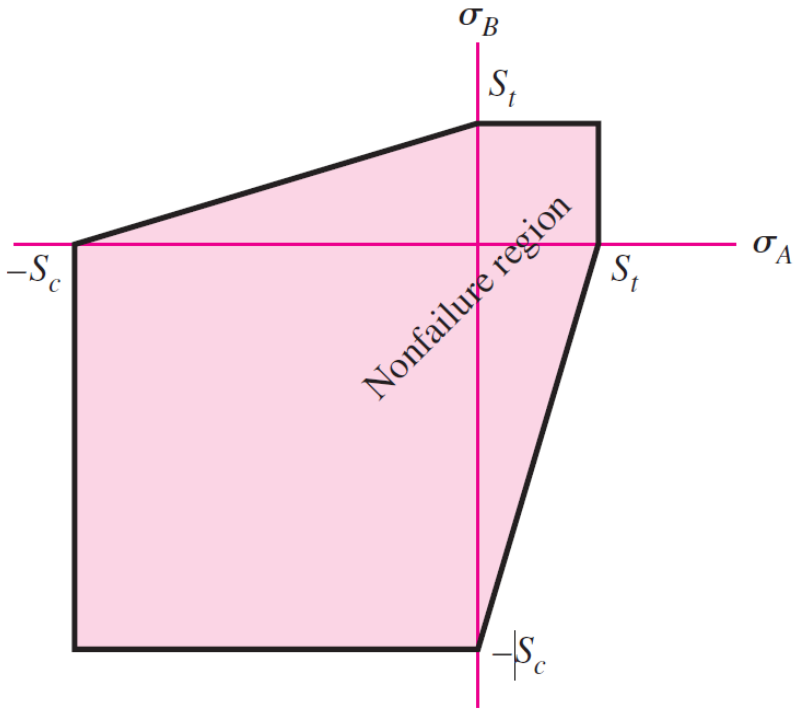

Figure 3.7: Depicts the Coulomb-Mohr yield criterion for ductile materials for the plane stress case (Budynas and Nisbett 2011).

The inelastic flow for three-dimensional stress states is determined with empirical relationships, even for uncomplicated isotropic materials. These empirical yield criteria are developed to match experimental observations with certain limitations.

Brittle Material Failure

According to the Maximum-Normal-Stress criterion, failure will occur when one of the principal stresses exceed the strength of the material, $\sigma_1 \geq S_{ut}$ or $\sigma_3 \leq -S_{uc}$. The Coulomb-Mohr theorem explained previously can also be applied to brittle materials by using the ultimate tensile and compressive stresses in Equation (3.7), this is shown by the dotted line in Figure 3.8 and highlights the inaccurate prediction by the Maximum-Normal-Stress theorem in the second and fourth quadrant. (Budynas and Nisbett 2011)

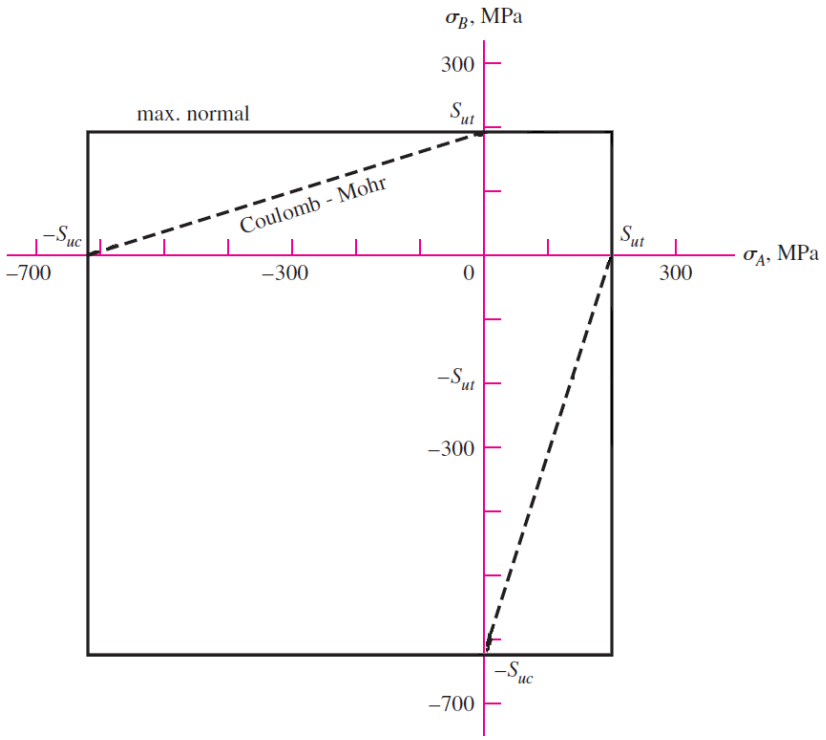

Figure 3.8: Brittle failure criterion (Budynas and Nisbett 2011).

3.3.2 Determining Failure of Refractory Materials

Refractories are often regarded as brittle materials, similar to concrete. Several investigations have used concrete material models to predict the behaviour of refractories (Liang et al. 2007). These models were used to evaluate the stress-strain relationship of refractory lined systems; however, refractories only behave in this manner at lower temperatures (close to room temperature), whereas at higher temperatures refractories behave in a more ductile manner.

In Schacht (1995) several concerns with the use of concrete material models to approximate failure in refractories are highlighted, the most noteworthy is the difference in loading conditions. As already discussed, refractories are subject to strain-controlled loads whereas concrete structures are subject to stress-controlled loads in most cases. The temperature range also creates different reactions in refractories than in concrete. (Schacht 1995)

For refractories the ultimate crushing and tensile strength is highly dependent on the dimensionality of the stress state, the rate at which the loading is applied, and the temperature at which the load is applied. Both the ultimate crushing and tensile strengths are typically provided by the refractory manufacturer. One of the challenges with assessing stress and failure in a lining is the multidimensionality of a stress state at any point of interest. Investigations have shown that for brittle materials, a multidimensional stress state has a large influence on the ultimate strength of the material. In other words, it is possible to have stresses that exceed the ultimate compressive stress which is obtained using a uni-axial strength test. (Schacht 1995)

That said, very little investigative work has been done on the influence of the dimensionality of the stress state on the ultimate strength of refractories. There are several investigations that have been done for typical brittle materials such as concrete. From these investigations it was observed that the ultimate tensile strength, which will give an indication if fracturing will occur, is not dependent on the dimensionality of the stress state. This means that the maximum tensile failure stress is not amplified due to the dimensionality of the stress state. (Schacht 1995)

For compressive stress the dimensionality plays an extremely important part. For a bi-axial stress state, depending on the ratio of the two principal compressive stresses, the crushing strength can

be 25 to 30% greater than the uni-axial compressive strength. Should all three principal stresses be kept equal, this can increase to 6 times for the three-dimensional state. (Schacht 1995) As discussed previously, refractories behave significantly different at higher temperatures than other brittle materials and so the material behaviour of refractories could deviate significantly from the observations discussed above. To illustrate this deviation, notice how the hot modulus of rupture increases with temperature especially for the higher temperature fired bricks in Figure 3.9.

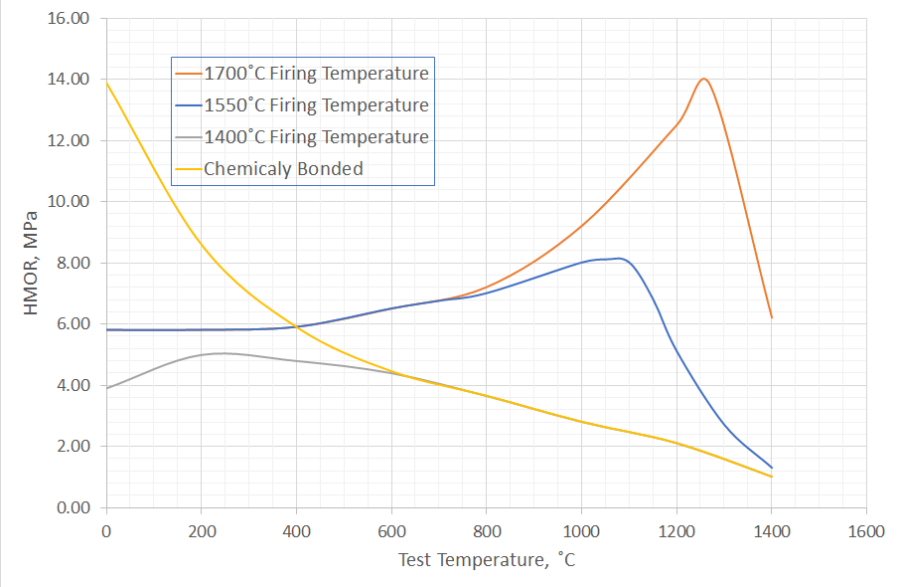

Figure 3.9: Variation of HMOR for magnesite-chrome brick with respect to firing temperature (Schacht 1995)

The crushing strength also changes at higher temperatures, it is then called the hot crushing strength. According to Schacht (1995), very limited information is available. For magnesia bricks with different ratios of CaO and SiO_2 Figure 3.10 shows a decrease in crushing strength as the temperature increases.

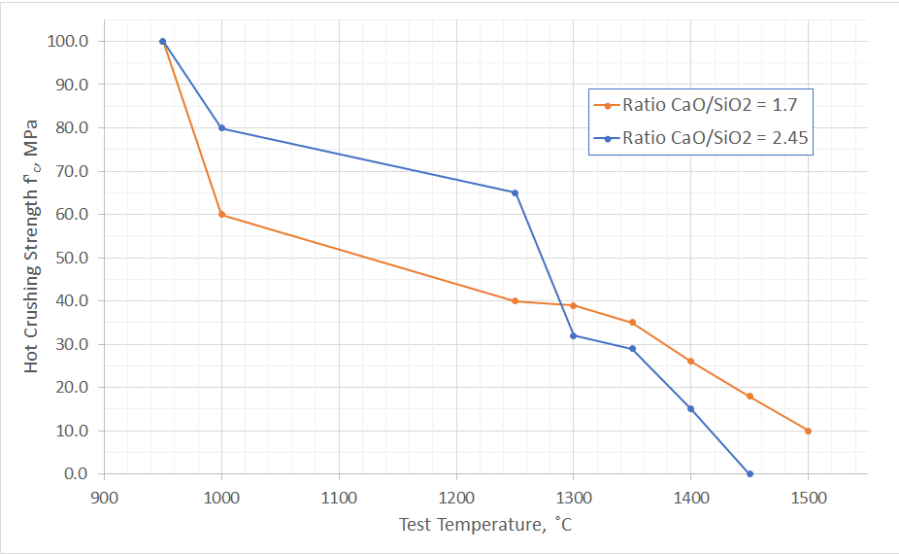

Figure 3.10: Variation of hot crushing strength for two types of magnesia bricks (Schacht 1995)

3.4 Application

Several considerations needs to be taken into account when using refractory materials for the lining of vessels. One of the most important factors to understand is the behaviour of joints. Joints allow some expansion which reduces stress in the lining. This expansion allowance becomes even more important for refractories with high coefficients of thermal expansion, such as magnesia and silica bricks. (Schacht and Maupin 2004) Expansion allowance will be discussed later in the document, first it is important to understand how joints function and the effect they have on the mechanical response of the lining.

3.4.1 Joints

There are two types of joints that are used; mortared and dry (also referred to as unmortared) joints. Both types of joints have significantly different stress-strain behaviour in compression to that of the surrounding refractory bricks. Joints cannot handle tension and would separate under tensile loading (Gasser, Terny-Rebeyrotte, and Boisse 2004).

For dry joints, material such as plastic inserts or cardboard are placed in the gaps between the bricks. These burn out at a relatively low temperature. (Schacht 1995)
For the scope of this study only dry joints will be considered.

Dry Joint Mechanical Behaviour

Figure 3.11 show the compressive stress-strain data for samples at two different temperatures with and without dry joints. Note how the inclusion of dry joints result in about half the stress for the same strain compared to the specimen without dry joints. An important factor to consider is that the two surfaces that make up the dry joint are not completely flat. This will result in greater compressive stresses at the contact points, causing greater deformations. (Schacht 1995)

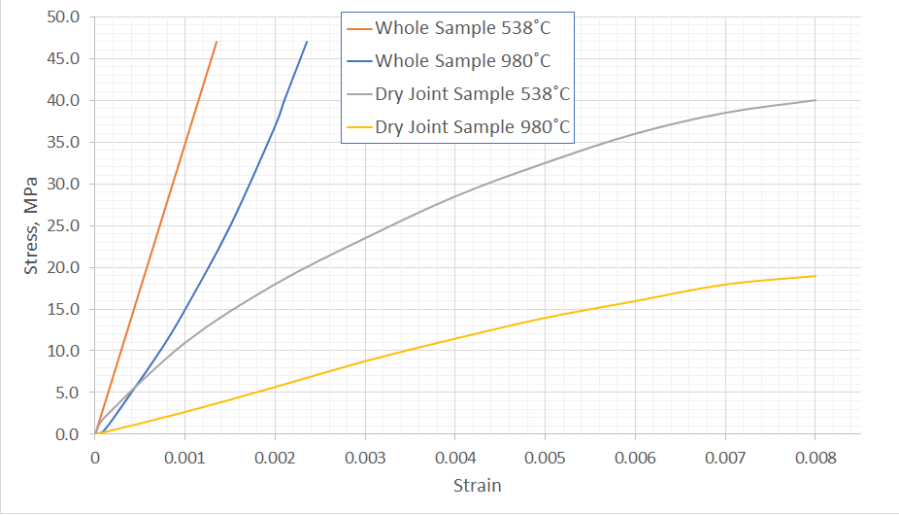

Figure 3.11: Effect on the compressive stress-strain data due to the inclusion of a dry joint in the sample (Schacht 1995).

Equation (3.8) can be used to determine the effective modulus of elasticity for a joint. From this the stiffness of the joint can be compared at the two different testing temperatures introduced in Figure 3.11. The results are shown in Figure 3.12 for an assumed joint thickness of 1 mm. (Schacht 1995)

Notice the effect of the small contact area at a lower temperature versus at a higher temperature. Due to thermal expansion larger areas of the neighbouring bricks will be in contact resulting in a decrease in the modulus of elasticity for the joint at higher temperatures.

$$E_j = \frac{E_{jb} E_b t_j}{t_b (E_b - E_{jb})} \tag{3.8}$$

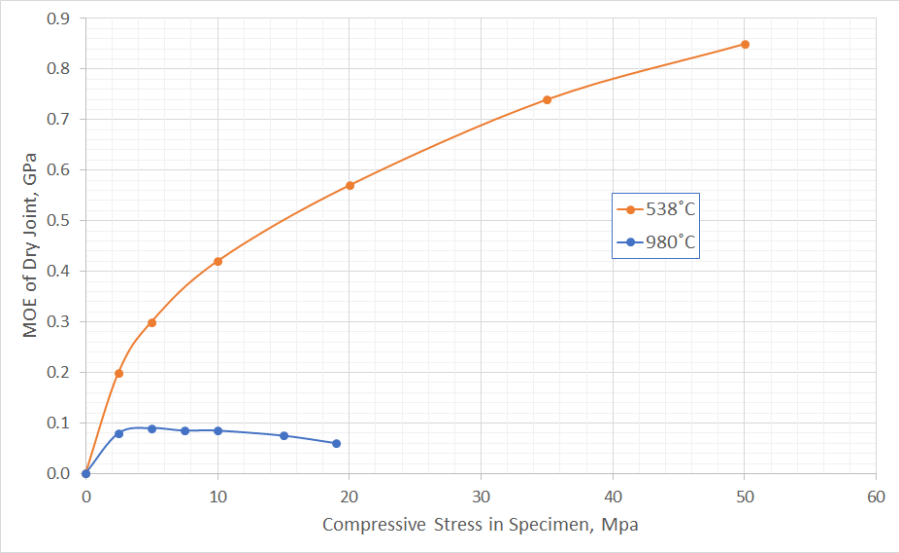

Figure 3.12: Compressive MOE data on a Dry Joint for Assumed thickness of 1 mm (Schacht 1995)

Hinges in Joints

At the joints in a refractory lining system hinges, or pivot points, can form during heat-up. A hinge is formed when there is a tensile loading on one end of the joint and a compressive loading on the other, resulting in a large portion of the joint to separate. The locations of these hinges in a refractory shell-type structure are not arbitrary, but will form at locations where a minimum strain energy is present.

Figure 3.13 shows that as these hinges develop, the load bearing structure of the lining also changes. Hinges do not form on a single joint but rather affects the entire area of the refractory shape. This is shown in Figure 3.13 where the darker section is the load bearing area in the arch. All joints surrounding the hinge also separates and is shown by the darker lines in Figure 3.13. (Schacht 1995)

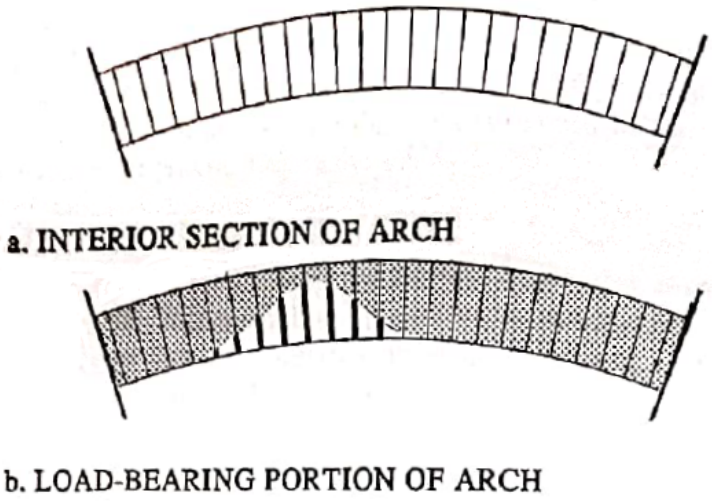

Figure 3.13: Effect of a hinge on the load bearing area of an arch (Schacht 1995)

When considering a structure such as an arch it is obvious where hinges might form and this can be accounted for in design. However, in more complicated loading conditions and geometries the location of hinges is not as obvious. Detailed structural analysis needs to be done in order to know where hinges may form. (Schacht 1995)

3.4.2 Brick-lined Cylindrical Linings

The purpose of any refractory-lined process vessel is to contain the process material. Due to the vessel being exposed to a combination of operating pressures and temperatures the installation and design is extremely important. According to Schacht (2004) the most common geometry used in industrial process vessels is the cylindrical vessel. Because it is so commonly used, the scope of this study is limited to these cylindrical brick-lined vessels.

The brick lined cylindrical vessel is contained by a steel shell which provides the tensile strength to constrain the lining in the heated condition. The steel has a higher thermal expansion than the lining and any increase in the shell temperature will affect the tensile constraint the shell will have on the lining. In addition, most structural steel cannot be exposed to temperatures in excess of 350 °C to 450 °C. Hence, the refractory lining needs to insulate the steel structure from excessive temperatures. (Schacht 1995)
Following from this, the purpose of the lining can be summarised as follows:

1. Insulate the process materials
2. Isolate the support structure from process temperatures
3. Control heat loss from the process:
    - Heat loss control can be aimed at a more economic operation
    - Heat loss control can be required in order to maintain a stable temperature inside the vessel for product quality

Most linings are made up of several layers of different quality refractories as there is an expected temperature gradient through the lining. Lining choices can be based on temperature distribution, mechanical properties, or chemical resistance to corrosion. The part of the lining that is exposed to the process is referred to as the working lining, or the hot face of the lining. (Schacht 1995)

Stresses and Displacements in Cylindrical Geometries

A method to calculate the stresses in the lining is described below along with the assumptions guiding the approach.
The assumptions are:

- Refractory material is linearly elastic.
- The temperature gradient is linear through the lining thickness, this implies steady state.
- The brick joints cannot support tensile loading.
- A lining thickness is used that ensures the expansion of the lining is greater than the expansion of the shell.
- No expansion allowance is taken into account.

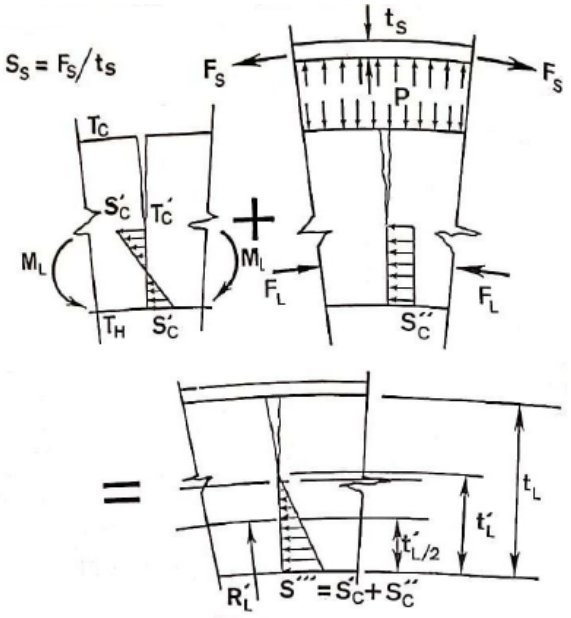

Figure 3.14: Components of the expansion stress in a cylindrical lining (Schacht 1995).

In this approach the effect of temperature and subsequent thermal expansion in the lining is divided into two components, the average temperature over the lining and the gradient portion of the temperature distribution in the lining (Figure 3.14). The average temperature is the driving force for the expansion forces which result in the uniform lining stress, S''_C. F_L is the lining expansion force and F_S is the shell expansion force. (Schacht 1995)

The temperature distribution in the lining results in a thermal moment (M_L) which only acts on the portion of lining that is under compression. The resultant stress from the thermal moment is S'_C. On the hot face S'_C adds to the compressive stress while on the cold face it subtracts from the compressive stress. The final stress state, which is the addition of S''_C and S'_C is S'''. Equations (3.9) to (3.20) demonstrate the basic behaviour of the cylindrical vessel lining system. (Schacht 1995)

The hoop or circumferential stress (S_C) is described using Equation (3.9) for the shell. Where R is the vessel radius, t is the vessel thickness and P is the radial pressure. This is assuming the vessel lining can be approximated as a thin walled pressure vessel with the ratio of the vessel radius to the vessel thickness greater than ten.

$$S_C = \frac{PR}{t} \tag{3.9}$$

From here the hoop strain (ε_C) can be calculated by dividing both sides by the modulus of elasticity (E):

$$\varepsilon_C = \frac{PR}{tE} \tag{3.10}$$

By making use of the incremental change in the circumferential length ΔC, Equation (3.10) can be expanded into Equation (3.12) using Equation (3.11). Because $\Delta C = 2\pi\Delta R$, it can be said that the change in radial displacement can be described with Equation (3.13).

$$\varepsilon_C = \frac{\Delta C}{2\pi R} \tag{3.11}$$

$$2\pi R\varepsilon_C = \Delta C = \frac{2\pi PR^2}{tE} \tag{3.12}$$

$$\Delta R = \frac{PR^2}{tE} \tag{3.13}$$

Since it is assumed that the radial displacement of the shell will be less than that of the lining there will be a radial pressure which exists between the two bodies. Equations (3.9) to (3.13) can be applied to both the refractory lining and the steel shell. P will be the same on the shell and the lining.

The inward pressure on the lining will result in a radial displacement of the lining defined as:

$$\Delta R_L = \frac{PR_L'^2}{t_l' E_L} \tag{3.14}$$

The only part of the lining that contributes to the outward pressure on the shell is the area that is under compression loading, therefore full lining thickness t_l will not be used. To obtain t_l' a thickness will be iterated over until a zero tensile pressure is obtained. Using a similar equation to Equation (3.14), but with the properties of the shell, the outward displacement of the steel shell due to the pressure P can be determined.

The sum of the shell and lining radial displacement can then be defined as:

$$\Delta\delta_P = P\left(\frac{R_L'^2}{t_l' E_L} + \frac{R_S^2}{t_S E_S}\right) \tag{3.15}$$

Thus far, only the mechanical effects on the lining and shell have been described. Equation (3.16) can be used to calculate the thermal expansion of the lining and Equation (3.17) for the shell. ΔT_L is calculated as the mid-thickness (at R_L') temperature change from room temperature.

$$\Delta R_{TL} = \alpha_L R_L' \Delta T_L \tag{3.16}$$

$$\Delta R_{TS} = \alpha_S R_S \Delta T_S \tag{3.17}$$

As previously assumed, the lining will expand more than the shell. The difference in the radial thermal growth is defined as the thermal interference and can be calculated with Equation (3.18).

$$\Delta\delta_T = \Delta R_{TL} - \Delta R_{TS} \tag{3.18}$$

Since the thermal and mechanical interference needs to be the same the thermal interference can be defined as:

$$\Delta\delta_T = P\left(\frac{R_L'^2}{t_l' E_L} + \frac{R_S^2}{t_S E_S}\right) \tag{3.19}$$

A shortfall of the approach is assuming a constant modulus of elasticity for the lining. To improve on the accuracy of this approach, the lining can be divided into thin cylindrical parts, Equation (3.19) can then be expressed as:

$$\Delta\delta_T = P\left(\sum_{i=1}^{n}\left(\frac{R_L'^2}{t_l' E_L}\right)_i + \frac{R_S^2}{t_S E_S}\right) \tag{3.20}$$

The approach described is very approximate and can be greatly improved by more sophisticated solving techniques, such as the finite element method; however, it does provide a basic understanding of lining behaviour. (Schacht 1995) Schacht (1995) used this approach to calculate a few example cases with the following conclusions:

1. The tensile stress calculated on the coldface indicates the opening of cracks or separating of joints.
2. Because the lining cannot develop any tensile stress, the steel shell develops the opposing tensile stress to the compressive stress in the lining.
3. The average temperature of the lining is used to calculate the expansion restraint of the vessel shell. The contribution of the thermal gradient is limited to the thermal stresses in the lining.
4. Because the lining joints pull apart toward the cold face of the lining, the centre of gravity of the compressive expansion stress shifts toward the hot face of the lining.
5. Depending on the lining, the loss of expansion interference, which can result in penetration of process materials, can be due to:
    - a lack of tightness in the lining installation
    - the inappropriate use of crushable material behind the working lining
    - expansion joint material that is either too thick or is too compressible
6. A lining must have sufficient crushing strength based on the stress on the hotface of the lining.

Since the average temperature is the only variable influencing the shell restraint, the gradient, which is influenced by transient conditions, need to be well understood to ensure that the stress and strain in the lining does not lead to failure. The importance of understanding the outward expansion and ensuring that the crushing strength is not exceeded even though enough tensile force on the lining is needed to prevent lining penetration shows the importance of accurately calculating the expansion allowance. All of these conclusions highlights the necessity for more accurate modelling of lining behaviour under both steady state and transient conditions.

Expansion Allowance

The percentage of expansion allowance needed is approximated as a percentage of the full expansion. In other words, the full expansion of the lining is not used as the allowed expansion as this will result in a non-compressive lining which could lead to process material penetration. (Schacht and Maupin 2004)

Reasons to install expansion allowance, according to Schacht (1995), is if the lining:

- has a high stiffness

- has a high coefficient of thermal expansion
- has a highly restraining support structure
- has high operating temperatures
- is exposed to high heatup rates

The cylindrical refractory lined vessel does not typically develop hinges, but rather shows a significant increase in stress-strain values as the temperature increase. However, hinges can still develop in areas such as the skewback area (where the hearth and the sidewall come together) as well as where the roof meets the sidewall. Several forms for expansion allowance can be used, the most common of these are (Schacht 1995):

- mortar joints
- dry joints with mortar sheeting material (such as cardboard or expansion sheets)
- compressive blanket material

A few equations are given by Schacht (1995) to give a better understanding of the relief offered by the use of expansion allowance. There is a critical balance with the use of expansion allowance, too much will result in a loose lining where too little will result in cracking and lining deterioration.

To gain initial insight, the ratio of lining stiffness to shell stiffness can be calculated using Equation (3.21) where E_l is the Young's modulus of the lining, t_L is the lining thickness, E_S is the Young's modulus of the shell, and t_S is the thickness of the shell. If $ST_{\frac{L}{S}}$ approaches 1 at any given temperature, expansion allowance needs to be considered. Under normal conditions the expected stiffness of the shell is much higher than that of the lining and hence the outcome of Equation (3.21) should be less than one. As it approaches one the stiffness of the shell is not enough to contain the lining and expansion should be considered. As already mentioned not the entire thickness of the lining contribute to the lining stiffness and the working thickness should be determined using the approach described in Section 3.4.2.

$$ST_{\frac{L}{S}} = \frac{E_L t_L}{E_S t_S} \tag{3.21}$$

The ratio of hoop to radial stress is dependent on the lining thickness and radius, as shown in Equation (3.22) where S''_C is the hoop stress, P is the radial stress, t'_L is the critical lining thickness, and R'_L is the effective mid-thickness radius of the lining. Based on this it is clear that the hoop stress will be significantly higher than the radial stress. The higher hoop stress means that the expansion joints along the circumference of the lining will be compressed more than those along the radial direction, it then follows that there will be more joints in the circumferential direction than the radial. The total expansion allowance can be accounted for using Equation (3.23), where N_C and N_R are the number of expansion joints in the circumferential and radial directions respectively. Although this only provides a very rough estimate of the effect, it does allow for a better understanding of the influences of the number of joints in each direction. (Schacht 1995)

$$S''_C = P(\frac{R'_L}{t'_L}) \tag{3.22}$$

$$R_{expansion} = \frac{N_C R'_L}{N_R t'_L} \tag{3.23}$$

When using compressible blankets Schacht (1995) suggests using Equation (3.24) as an indication of the percentage a blanket will compress, if Q_B is the density of the blanket. Note that a thermal

analysis of the lining is important so that the maximum temperature rating of the blankets is not overshot. Temperatures above this can result in blanket deteriorating and too much expansion of the lining which would lead to loss of compressive stress and process material penetration. Use of blankets will also result in insulating effects, this should be taken into account when doing the thermal analysis.

$$C = 100 - 0.1Q_B \tag{3.24}$$

3.5 Summary

From this chapter it is clear that a limited amount of data is available for a refractory material's stress and strain relationship. This information is needed to accurately predict the behaviour of the lining. The use of concrete material models is not sufficient as refractories tend to behave in a more ductile fashion as the temperature increase. The load types that refractories are subject to is also something to consider and needs to be taken into account when doing modelling and analysis work. To accurately study the material behaviour of refractories the stress-strain relationship along with the correct failure criterion need to be used. Using a simple linear elastic ductile material modelling approach can give some insight; however, this needs to be expanded to consider the inelastic behaviour at higher temperatures. These investigations are complex and need the aid of more sophisticated modelling methods such as the FEM (Zienkiewicz, Taylor, and Zhu 2013).

Chapter 4

Thermal Cycles

This section investigates the influence of thermal cycles on furnace linings. Thermal cycles can include any change in the temperature that the lining is exposed to. This can be due to shut-downs, permanent and temporary, start-ups or fluctuations in operating temperature. For the purpose of this study focus will be on the largest of these, namely the start-ups and shut-downs.

4.1 Effects of Rapid Thermal Cycles

Rapid heat-up causes higher expansion forces as shown in Figure 4.1, and causes local fracture and progressive deterioration in the lining. (Schacht 1995)

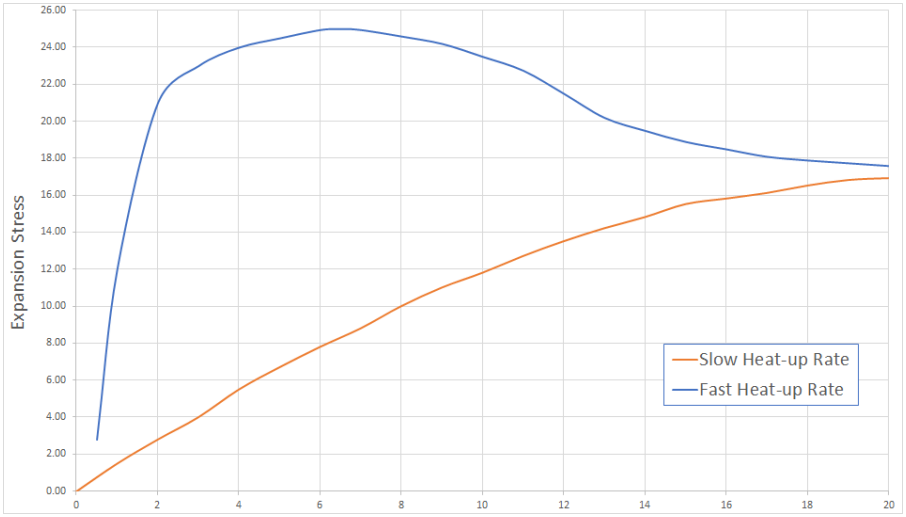

Figure 4.1: Graphic representation of the influence of heatup rate on lining and shell expansion stress (Schacht 1995).

This causes thermal shock fracturing, which is one of the most investigated modes of failure. Any rapid change in temperature during heating or cooling causes a tensile thermal stress that develops in the lining. Usually thermal shock fracturing is evaluated using the MOR (modulus of rupture, or ultimate tensile strength). However, since thermal tensile loading is strain controlled, data for the stress-strain relationship should be used as the MOR cannot accurately predict failure. (Schacht 1995)

In order to obtain this information the work-of-fracture (WOF) test can be used. The WOF test is a modification of the MOR test and measures the strain along with the applied loading, this allows for a complete load-displacement relationship to be measured. By using the WOF, classical fracture mechanics can be applied to refractories. (Schacht 1995)

To evaluate tensile fracture the material needs to resist the start and growth of cracks. There are two parameters that define the resistance of the material to crack growth; the fracture toughness, calculated with Equation (4.1) and Equation (4.2), and the resistance to crack growth, which can be calculated using either Equation (4.3) or Equation (4.4).

$$K_{IC} = \sigma_f Y C_{critical}^{0.5} \tag{4.1}$$

$$K_{IC} = \varepsilon_f Y C_{critical}^{0.5} E \tag{4.2}$$

$$R = \frac{\sigma_f (1-\nu)}{\alpha E} \tag{4.3}$$

$$R = \frac{\varepsilon_f (1-\nu)}{\alpha} \tag{4.4}$$

For the case of strain loading ε_f needs to be increased in order to increase the resistance to crack growth (Equation (4.4)) where as σ_f needs to be increased for the case of stress loading (Equation (4.3)). These increases result in vastly different WOF curves as shown in Figure 4.2.

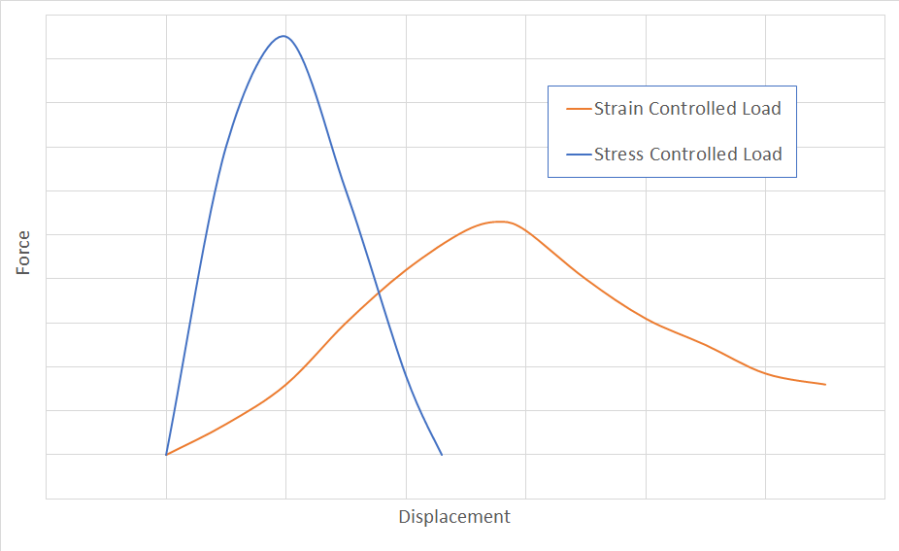

Figure 4.2: Optimisation of WOF curves for different load type imposed on refractory materials (Schacht 1995).

The three main causes for failure are summarised below (Schacht 1995):

1. *slabbing, spalling, flaking or peeling* - This is thermal fracture that originates inside the brick close to the hotface and have crack propagation parallel to the hotface of the brick.

2. A crack originates in the centre of the hotface and propagate perpendicular to the hotface, there are no names in literature for this type of failure

3. *pinch spalling* - This refers to the crushing of the corners of the radial brick joints, this is the result of concentrated compressive stresses and results in failure due to shear fracture of the brick. This can also be referred to as *cobbing* in its more advanced stages.

In Figure 4.3 the compressive load due to the restraining shell on a lining element is shown, as a result of this restraint the brick element will experience a maximum deformation just behind the part of the joint that caries the compressive load. The result of this can be seen in Figure 4.4 when the lining has a linear temperature distribution. Notice how a tensile crack can develop behind the compressive load at the hotface of the brick. The location where *pinch spalling* can occur is also

indicated. Both figures show the loading and stress for a linear thermal distribution, during heat-up the same effects will be present but will increase in severity. (Schacht 1995)

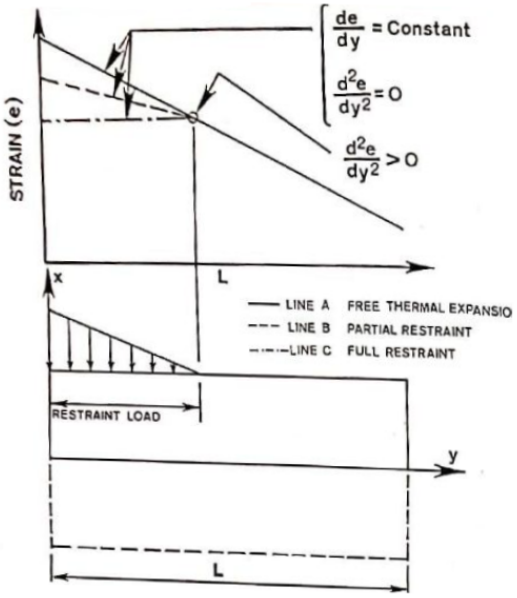

Figure 4.3: Effect of restrained lining compressive load on strain in a lining brick element (Schacht 1995).

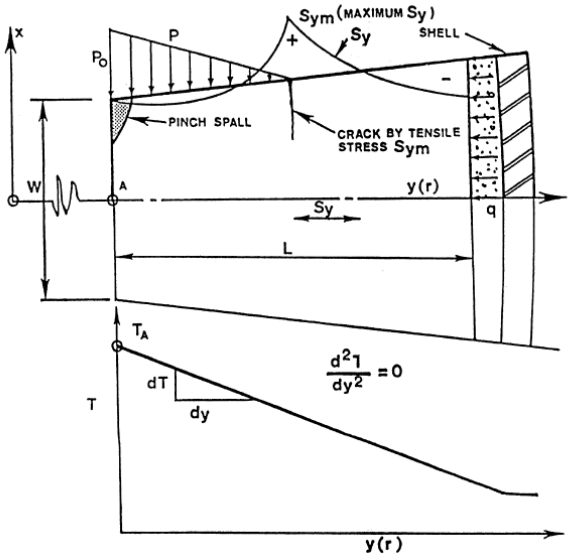

Figure 4.4: Restraint stress in lining component with a linear temperature gradient (Schacht 1995).

Figure 4.5 show the loading condition when the lining starts to cool down. The hotface joint will start separating as the lining cools down, rapid cooldown can result in more severe forms of this loading condition. A crack can then be initiated at the hotface side of the compressive load. (Schacht 1995)

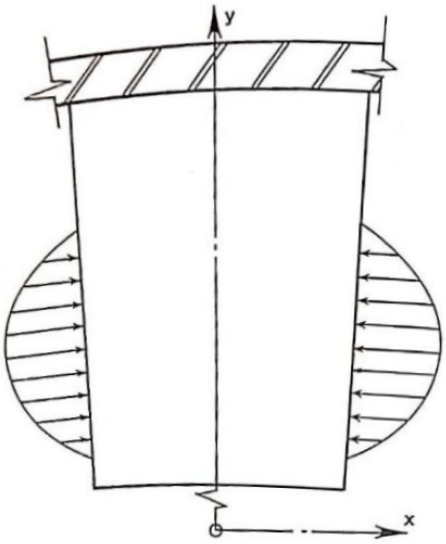

Figure 4.5: Restraint force in radial joint during transient cooldown (Schacht 1995).

4.2 Results from Analytical and Modelling Simulations

In Schacht (1995) several cases for temperature variations are analysed, both analytically and with FEM modelling. The conclusions of the effect of this on linings were:

- When the hotface of a constrained refractory lining has been heated past the plastic strain threshold temperature, which results in compressive plastic strain, amplification of the tensile thermal stress during cooldown will occur.
- Due to the restraint on the lining by the shell, the tensile loading in the radial direction is reduced, a single circumferential stress fracture occurs behind the the circumferential restraint load along the radial joint.
- Once the lining has been heated above the plastic strain threshold temperature, realistic critical cooling rates cannot be predicted using an analytical approach.
- For the prediction of heating rates for a restrained lining, an elastic analytical approach can be sufficient.
- During rapid cooldown the maximum radial tensile stress develop at both ends of the restraint load along the radial joint, the maximum circumferential tensile stress is located in the centre of the width of the hotface due to the elongation of the refractory lining.
- Due to the strain discontinuity between the unrestrained and restrained surfaces in the radial joint, a maximum radial tensile stress develops.
- The maximum radial tensile stress at the tail of the restraint load along the radial joint away from the hotface is independent of the rate of heating on the hotface and therefore thermal spalling can occur even due to slow heating.
- The maximum tensile stress at the tail of the restraint load along the radial joint closest to the hotface is dependant on the rate of heating or cooling as well as the compressive plastic strain of the hotface.

- The maximum circumferential tensile stress, which occurs at the middle width of the hotface of a lining component, is dependant on the plastic strain of the hotface as well as the heating and cooling rate.
- Cooldown resulted in more tensile failures than heat-up.
- The maximum tensile stress in a restrained refractory lining component is a function of the following:
  - time
  - heating or cooling rate
  - refractory thermal diffusivity
  - refractory thermal expansion
  - refractory elastic modulus
  - refractory plastic modulus
  - Poisson ratio of refractory
  - refractory component size
  - stiffness of the vessel shell
  - temperature of the refractory lining component prior to heating or cooling
  - plastic strain threshold temperature
  - expansion allowance
  - slope of the temperature gradient through the refractory brick at the point of the maximum radial tensile stress

4.3 Summary

Schacht (1995) concludes by stating that thermal tensile failure is an extremely complex phenomena and that it needs to be evaluated for each case independently. It is clear from the information captured in this chapter that the transient conditions greatly affect the life span of a refractory lining. This combined with the loading type and material model uncertainty explained in the previous chapter highlights the necessity for studies as conducted by Schacht (1995). It was also interesting to note that the cooling down period could result in more tensile fractures in the lining than the heat-up phase; however, ideally a furnace with a refractory lining will only undergo cooldown once the lining needs to be replaced. Using an elastic approach to consider the effects of heatup is an important conclusion as this will allow for easier modelling of typical heatup rates. It is also clear that even though considering the lining as a continuous solid can give some insights, individual brick modelling will be needed to investigate the various different way failure can occur due to the loading conditions in the lining.

Part III

Model Development

Chapter 5

System Analysis

5.1 System Description

The system that is modelled is shown in Figure 5.1 with each section indicated by a number. The system originates from numerous drawings of different systems used in the industry and represents a generic ilmenite smelting furnace. No specific dimensions will be described as geometrical effects are outside the scope of the study. The system shown is made up of a DC smelting furnace which includes a metal and slag bath as well as a transitional area between the two. An electrode is also included along with a freeboard. The system, as shown, also includes a roof, this is included for accurate heat transfer in the freeboard of the furnace and will not be evaluated for stress, strain and displacement.

The ambient conditions are taken as the average for Richards Bay in Kwazulu-Natal, South Africa. (*November Climate History for Richards Bay Country Club* 2019)

Table 5.1: Climate in Richards Bay South Africa

	Value	Unit
temperature	22	°C
humidity	79	%

The material properties applied for each section of the system is described in Section 6.4 while the key phenomena for each section are listed in Table 5.2. How each of these will be accounted for in the models will be described in Chapter 6. In addition, the allowed expansion in the joints will also be considered as explained below:

Allowed expansion in joints Joints are present between bricks in both the hearth and the sidewall refractories. The joints allow for expansion to take place that will not result in total thermal expansion of the lining. How much of this, where and the exact effects of it need to be considered.

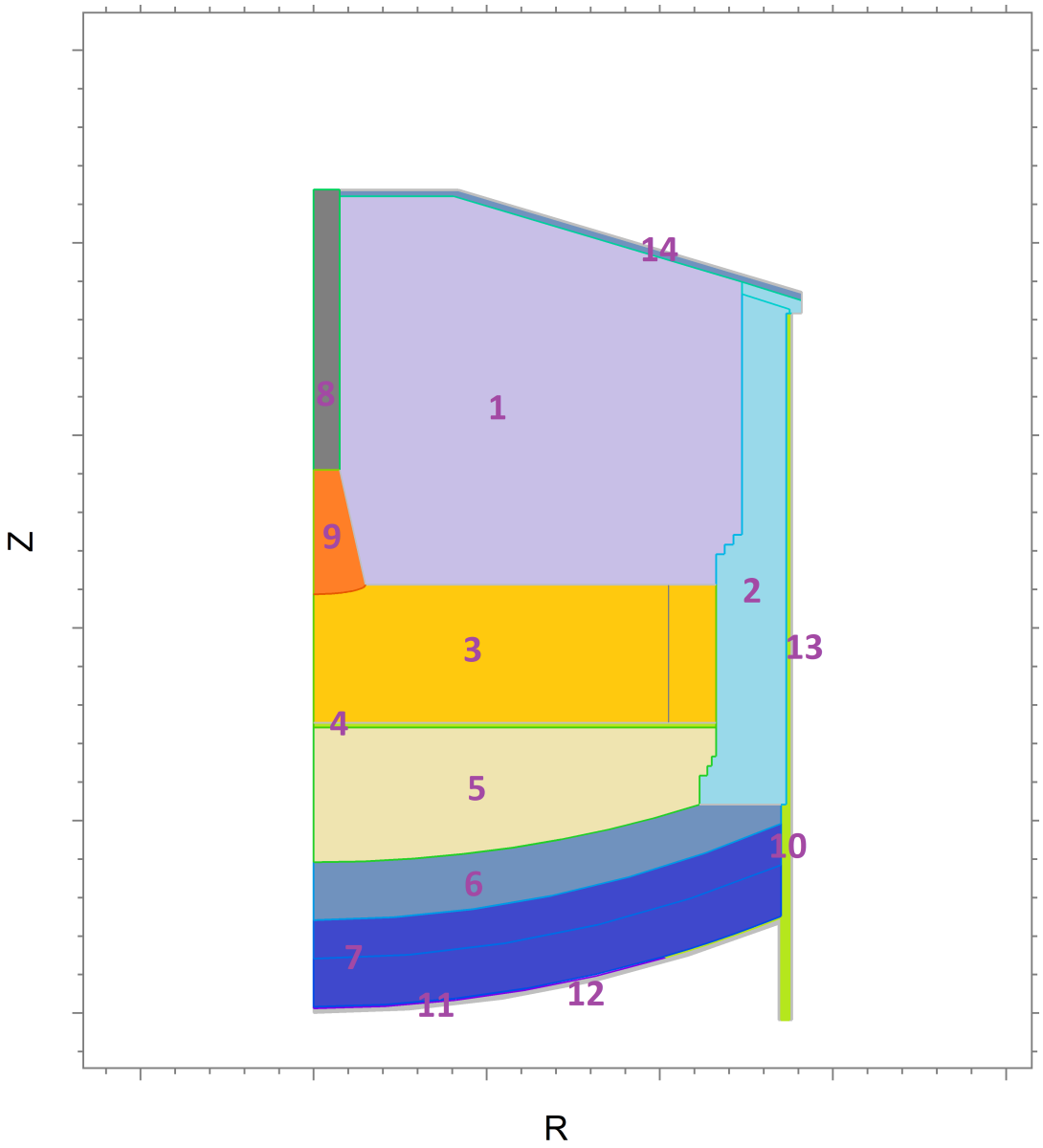

Figure 5.1: The system used to model the effects of expansion allowance and material properties on the stress, strain and displacement in the lining. Each numbered section is defined in Table 5.2

Table 5.2: Description of sections as numbered in Figure 5.1

Number	Section	Description	Key Phenomena
1	Freeboard	The Freeboard consists of air dust and fumes from the process.	Radiative Heat Transfer Conductive Heat Transfer Convective Heat Transfer
2	Sidewall	Uniform refractory throughout the entire sidewall.	Conductive Heat Transfer Displacement Stress and Strain
3	Slag Bath	Consists of a separate area where a freeze lining can form against the sidewall.	Conductive Heat Transfer Convective Heat Transfer
4	Transition Zone	Consists of the same material as the slag bath	Conductive Heat Transfer Convective Heat Transfer
5	Metal Bath	Consists of a highly conductive material and has no freeze lining area	Conductive Heat Transfer Convective Heat Transfer
6	Hearth Top Layer	Consists of the refractory material in contact with the metal	Conductive Heat Transfer Displacement Stress and Strain
7	Hearth Bottom Layer	This can be a different refractory material than the hearth top layer	Conductive Heat Transfer Displacement Stress and Strain
8	Electrode	Made from a graphite material	Conductive Heat Transfer
9	Arc	This is the area in which the arc will most likely be.	Conductive Heat Transfer Radiative Heat Transfer
10	Ramming Material	This is a softer material between the refractory materials and the shell which allows for compression due to thermal expansion of the lining	Conductive Heat Transfer Displacement Stress and Strain
11	Copper Plate	The copper plate acts as the anode for the DC current	Conductive Heat Transfer Displacement Stress and Strain
12	Hearth Shell	The hearth shell is cooled and supports the mechanical load of the hearth refractory	Conductive Heat Transfer Displacement Stress and Strain
13	Sidewall Shell	The sidewall shell is also cooled and mechanically constrains the sidewall refractory during thermal expansion	Conductive Heat Transfer Displacement Stress and Strain
14	Roof Refractory and Shell	The roof is only included for the accuracy of the temperature distribution in the freeboard	Conductive Heat Transfer

Chapter 6

Model Formulation

6.1 Overview

To solve the heat transfer and deformation equations the FEM is used on triangular meshes. The software used is a general partial differential equation (PDE) solver which uses the FEM and is called FlexPDE. The mesh can be refined in areas with large errors, this is done automatically by a procedure in FlexPDE. The version of FlexPDE used is 6.50

Since FlexPDE is a general PDE solver the formulation of the model and all phenomena for which it solves are described in the formulation files as well as in the following sections. The following phenomena is mathematically described in the FlexPDE models:

- Conductive heat transfer
- Stress, strain and displacement
- Radiative heat transfer

In order to account for the expansion allowance, a method is formulated to adjust the strain of the refractory lining due to thermal expansion. This method is described in detail along with an extension which allows for the calculation of the degree to which the lining has been sealed mechanically; all joints are in a compressive state, this is referred to as keying. This method is inline in approach to the work of Gasser, Terny-Rebeyrotte, and Boisse (2004).

6.1.1 Variables and Initial Values

The variables used in the models are shown in Table 6.1. Each simulation will address a specific phenomena and will not necessarily solve for each of the variables.

Table 6.1: Variables used in the model

Variable	Description	Initial value	Units
Tn	temperature	22	°C
u	displacement in r direction	0	m
v	displacement in z direction	0	m
$i0$	zero-order moment of radiation intensity	0	$\mathrm{W\,sr\,m^{-2}}$

6.2 Assumptions

An assumption refers to a value or condition which is unknown and assumed for the purposes of the model. This should not be confused with simplifications in which case the value or condition is known but is purposefully changed in order to reduce solving times or non-linearities in the solution.

Assumptions can have a large impact on the usability of the model, and it is important to understand the assumptions and how it affects the results obtained in simulations. The assumptions made in this model are described in the sections below:

6.2.1 Geometry

The geometry used in all models are a combination of various geometries used in industry and is therefore not representative of a specific furnace. Since the geometry is assumed actual results cannot be directly interpreted as realistic values, but rather the change in expansion, stresses, strains and displacements in the lining can be evaluated for different simulations.

The metal and slag baths are included in the model, in order to consider the impact these will have on the lining. In addition, a freezelining thickness needs to be assumed. For all simulations a freeezelining thickness of 16% of the total slag bath thickness is used.

6.2.2 Materials

Since the models were not built for a specific furnace the material properties that were used are based on properties available in literature and is listed in Table 6.2. In some cases the value was assumed, as indicated.

Table 6.2: Assumed properties of materials

Furnace Area	Property	Value	Units	Reference
Freeboard	k	50	$\mathrm{W\,m^{-1}\,K^{-1}}$	Assumed [a]
Metal Bath	k	200	$\mathrm{W\,m^{-1}\,K^{-1}}$	(Holman 1989) [b]
Slag Bath	k	30	$\mathrm{W\,m^{-1}\,K^{-1}}$	(Kotze and Pistorius 2009) [b]
Freezelining	k	1	$\mathrm{W\,m^{-1}\,K^{-1}}$	(Kotze and Pistorius 2009) [c]
Carbon Ramming	k	25	$\mathrm{W\,m^{-1}\,K^{-1}}$	(Brulin et al. 2011)
Carbon Ramming	c_P	700	$\mathrm{J\,K^{-1}}$	(Brulin et al. 2011)
Carbon Ramming	ρ	1330	$\mathrm{kg\,m^{-3}}$	(Brulin et al. 2011)
Carbon Ramming	E	900	kPa	Assumed [d]
Carbon Ramming	μ	0.25		(Brulin et al. 2011)
Carbon Ramming	α	3.3×10^{-6}	$^{\circ}\mathrm{C}^{-1}$	(Brulin et al. 2011)
Electrode	ϵ	0.3	N/A	(Reynolds 2002)
Dust Particle	ϵ	0.3	N/A	Assumed

[a] The thermal conductivity in the freeboard is assumed higher than that of air to account for the contribution of the dust and fumes to conduction, as well as the movement of air in the freeboard resulting in mixing and convective heat transfer.

[b] The thermal conductivity of the liquid slag and metal was chosen to be higher to account for the movement in the baths, resulting in mixing and convective heat transfer.

[c] At 450 °C to 500 °C

[d] The Young's Modulus was iterated and slowly increased until the ramming was not compressed to the point of penetration of refractory sidewall into the steel shell.

6.2.3 Radiative Heat Transfer

Larger particles in the freeboard cause reflection and the smaller particles causes refraction (change in direction etc). Large particles were defined as dust with a mean radius of 1×10^{-5} and small particles was defined as fume with a mean radius of 1×10^{-7}. The gas and fume production rate was assumed to be $450\,\mathrm{kg\,h^{-1}}$ and the ratio was assumed to be $\frac{9}{10}$ fume to dust production. Finally, the refractive index for the fume was assumed to be 1.5. Note that these are assumed values and could impact the thermal distribution in the freeboard; however, the freeboard temperature should closely relate to the temperature of the slag bath, if the simulation results show a close correlation, the assumed values will not be iterated further.

The total projected area of the dust particles in the gas allows for the calculation of absorption. The attenuation coefficients for absorption and scattering are determined as described by Reynolds (2002) For all bodies in the furnace an emissivity of 0.7 was assumed unless otherwise indicated in Table 6.2 (Reynolds 2002).

6.2.4 Conductive Heat Transfer

By approximating the body as a solid it is also assumed that the contact thermal resistances between components are negligible. The second assumption made for conductive heat transfer is that the thermal fluxes are not influenced in the angular direction, allowing an axisymmetric idealization.

6.2.5 Boundary Conditions

It was assumed that:

- boundary conditions are constant over the surface for which it is applied
- bulk fluid temperatures are used in all boundary conditions
- the bulk cooling temperature of the cooling air on the hearth was taken as 25 °C
- the bulk cooling temperature of the cooling water on the sidewall steel shell was assumed to be 22 °C
- the alloy and slag baths have a constant temperature of 1550 °C and 1700 °C respectively

6.3 Simplifications

Simplifications are made when the value used or the physics applied are known to be incorrect. Simplifications allow for models to be accurate within a certain degree, it is therefore important to ensure that the simplifications and the impact they will have are well understood.

6.3.1 Convective Heat Transfer

Convective heat transfer is not modelled explicitly for the freeboard and the slag and metal baths. To account for this the conductive heat transfer coefficient for these sections is increased. This could result in a better temperature distribution in these sections than would be achieved in practise.

6.3.2 Geometry

To decrease computational intensity the arc is not specifically modelled. This could result in a lower temperature experienced by the sidewall and roof exposed to the freeboard. However, as proven by Reynolds (2002) the greater influence to radiative heat transfer in the freeboard is the slag bath and not the arc.

The furnace is also modelled using a cylindrical coordinate system. This means that any geometrical inconsistencies in the angular direction, such as tapholes or cooling blocks, was not considered in this study.

6.3.3 Stress, Strain and Displacement

For the stress, strain and displacement calculations the following simplifications were made:

- The contents of the furnace (metal and slag baths) are not taken into account when considering the displacement, stresses and strains of the furnace lining. This could result in slightly lower stress levels in the lining and slightly more displacement. However, the effect of the weight of the contents on the hearth stresses is estimated to be three orders smaller than any observed stresses in the lining. This simplification should therefore not have a significant impact.
- A linear elastic material model was used, this is not a true reflection of the behaviour of refractory materials as discussed in Part II. This will result in significantly higher stresses in the lining. The results obtained by the model is therefore not an accurate reflection of the actual displacements, stresses and strains that will be present in a furnace lining.
- The model approaches the entire furnace as a single solid, this means no relative movement between different layers, sections, and bricks in the furnace can be considered by the model. Higher stresses and less displacement can therefore occur in certain areas. It is also possible that some influences of different furnace sections on each other can give a false perception of the actual influence the furnace sections might have on each other.
- Not considering the roof displacement and the effect that it might have on the sidewall could yield inaccurate results, especially around the sidewall-roof interface.

6.3.4 Thermal Radiation Heat Transfer

In order to calculate the thermal radiation heat transfer in the freeboard the P_1 differential approximation was used. The P_N formulation approximates the integral equations of radiative heat transfer with a set of differential equations. For an infinite number of terms the series will yield the exact result; however, according to (Siegel and Howell 2002) the P_1 approximation yields satisfactory results for most cases. The P_3 approximation will increase the computational cost and will only have a significant impact on the results if the effects of an arc on freeboard gas temperatures are studied. For the purposes of this study the P_1 formulation will yield satisfactory results.

6.4 Materials

Even though the model was built for a fictional furnace the material properties applied in certain sections are based on materials that would typically be used in a DC arc furnace for Ilmenite smelting. These material properties are listed below. It should also be noted that some of these material properties will be varied for the different scenarios that are investigated using the model, in such cases all the properties that will be used are shown.

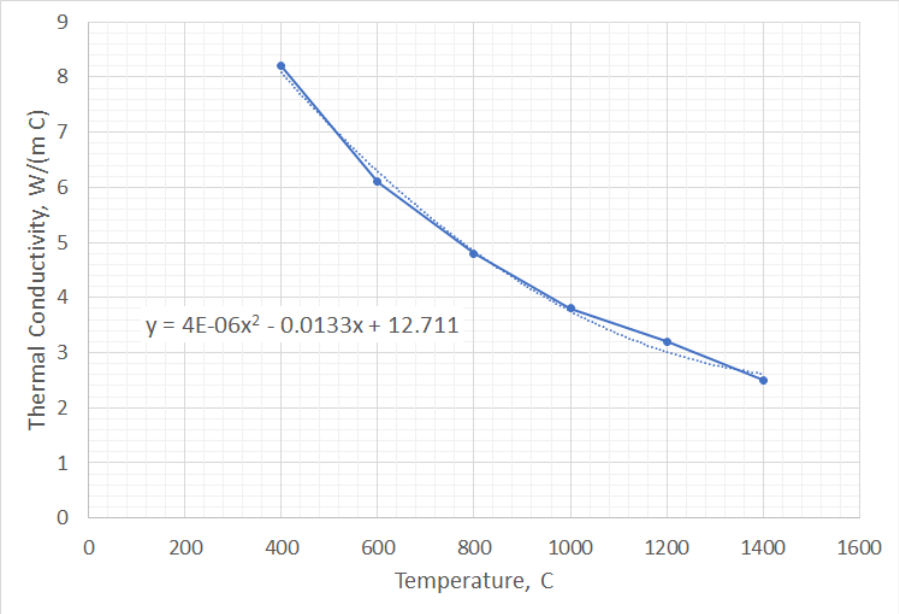

Figure 6.1: Thermal conductivity of Magnesia refractory bricks (China Firebrick 2017)

Hearth, Sidewall and Roof Refractories

The refractory data used are based on theoretical data sourced from various sources. All properties are kept constant over all sections except for the Young's Modulus, which is varied for different scenarios. The thermal conductivity is calculated using the equation as shown in Figure 6.1.

The density was taken as 3000 kg m^{-3} (Made-in-China.com 2019) and the Poisson ratio as 0.15 (Benavidez et al. 2015). From Part II the thermal expansion coefficient was taken as 14.1 $\times$ 10^{-6} K^{-1}. Finally, the different Young's modulus were extracted from Figure 6.2 and are listed in Table 6.3. For the cases at higher temperatures where non-linearity exists the Young's modulus is simplified by using the last known data point.

Table 6.3: Young's modulus of Magnesia refractory bricks at different temperatures as extracted from Figure 6.2

	1093 °C	1316 °C	1482 °C
Direct Bond Brick 1	22.7 GPa	none	2.55 GPa
Direct Bond Brick 2	44.5 GPa	8 GPa	none
Direct Bond Brick 3	62.5 GPa	14.687 GPa	1.583 GPa

Hearth, Sidewall and Roof Shell

For the shell, general steel properties were used and are summarised in Table 6.4.

Copper Plate

For the copper plate that acts as the anode, the material properties used are shown in Table 6.5

6.5 Radiative Heat Transfer

The partial differential equation solving for the radiative heat transfer in the freeboard is described in Equations (6.1) to (6.3). A detailed view of the derivation can be found in ?? (Siegel and Howell

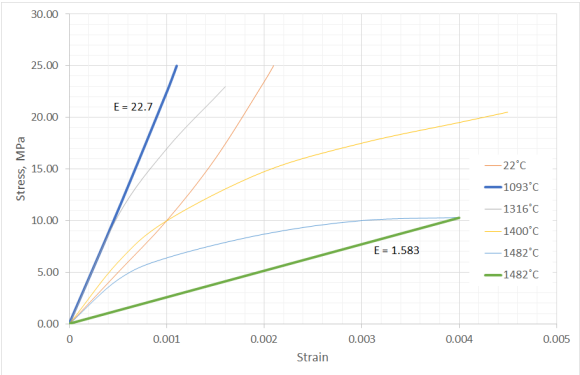

(a) Direct Bond Brick 1

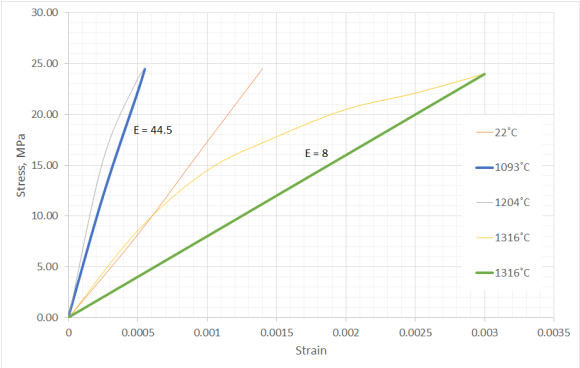

(b) Direct Bond Brick 2

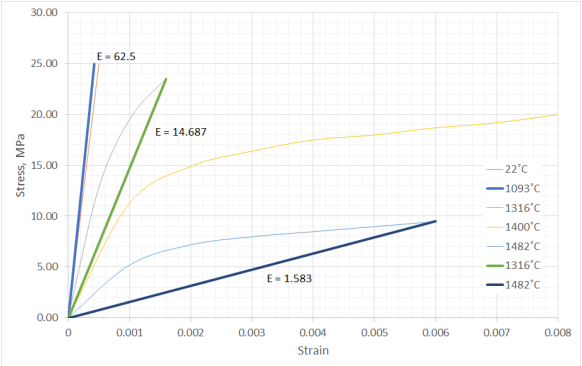

(c) Direct Bond Brick 3

Figure 6.2: Young's Modulus at different temperatures extracted from Figure 3.5, note the linear approximations made at the higher temperatures

Table 6.4: Properties of steel

Property	Value	Units	Reference
k	$2.1 \times 10^{-8}Tn^3 - 1.68 \times 10^{-5}Tn^2 - 3.03 \times 10^{-2}Tn + 55$	$W\,m^{-1}\,K^{-1}$	(Holman 1989)
ρ	7.86×10^3	$kg\,m^{-3}$	(Ameswebinfo 2019)
C_P	434	$J\,K^{-1}$	(Ameswebinfo 2019)
E	200	GPa	(Ameswebinfo 2019)
μ	0.32	N/A	(Ameswebinfo 2019)
α	11.7×10^{-6}	N/A	(Ameswebinfo 2019)

Table 6.5: Properties of copper

Property	Value	Units	Reference
k	$9.52 \times 10^{-6}Tn^2 - 6.0 \times 10^{-2}Tn + 3..86e2$	$W\,m^{-1}\,K^{-1}$	(Holman 1989)
ρ	8.3×10^3	$kg\,m^{-3}$	(Ameswebinfo 2019)
C_P	420	$J\,K^{-1}$	(Ameswebinfo 2019)
E	115	GPa	(Ameswebinfo 2019)
μ	0.34	N/A	(Ameswebinfo 2019)
μ	0.34	N/A	(Ameswebinfo 2019)
α	18.4×10^{-6}	N/A	(Ameswebinfo 2019)

2002; Liu, Swithenbank, and Garbett 1992). Equation (6.4) is used to describe the radiative flux at the boundaries of the freeboard.

$$\nabla \cdot \nabla(i^{(0)}(S)) = 3(1-\Omega)(i^{(0)}(s) - 4\pi i_b(S)) \tag{6.1}$$

$$\Omega = \frac{\sigma_S}{\kappa + \sigma_S} \tag{6.2}$$

$$i_b(S) = \frac{\sigma_S T^4}{\pi} \tag{6.3}$$

$$\frac{\partial i^{(0)}(S)}{\partial x_1} = \frac{3\beta_m \varepsilon_w}{2(2-\varepsilon_w)} \left(4\pi i_b(S) - i^{(0)}(S)\right) \tag{6.4}$$

$$\beta_m = \sigma_m + \kappa_m$$

6.6 Conductive Heat Transfer

In order to model for the heat fluxes through all materials included in the model, conductive heat transfer was included. Heat fluxes are due to the temperature gradient. All thermal gradients are introduced through boundary conditions simulating actual phenomena. In order to calculate the thermal conductivity the partial differential equation as shown in Equation (6.5) is used. For boundary conditions the heat flux (Equation (6.6)) on the boundary can be specified or a fixed temperature can be prescribed. (*FlexPDE 6 Help* 2017)

$$\nabla \bullet (k\nabla(Tn)) = \rho c_P \frac{\partial Tn}{\partial t} \tag{6.5}$$

$$q = h(Tn - T_b) \tag{6.6}$$

6.7 Stress, Strain and Displacement

In order to calculate the displacement, stresses, and strains in the lining the following equations are used. The strain is defined as shown in Equations (6.7) to (6.10) (Backstrom 2005).

$$\varepsilon_r = \frac{\partial u}{\partial r} \tag{6.7}$$

$$\varepsilon_\theta = \frac{u}{r} \tag{6.8}$$

$$\varepsilon_z = \frac{\partial w}{\partial z} \tag{6.9}$$

$$\gamma_{rz} = \frac{\partial u}{\partial z} + \frac{\partial w}{\partial r} \tag{6.10}$$

In order to relate the strain to the stress, Hooke's law can be used and is shown in Equations (6.11) to (6.15). These equations can then be rewritten as shown in Equations (6.16) to (6.21), note that the thermal expansion is now included by subtracting it from the strain due to displacement (Equation (6.21)).

$$\varepsilon_r = \frac{1}{E}(\sigma_r - \mu\sigma_\theta - \mu\sigma_z) \tag{6.11}$$
$$\varepsilon_\theta = \frac{1}{E}(-\mu\sigma_r + \sigma_\theta - \mu\sigma_z) \tag{6.12}$$
$$\varepsilon_z = \frac{1}{E}(-\mu\sigma_r - \mu\sigma_\theta + \sigma_z) \tag{6.13}$$
$$\gamma_{rz} = \frac{\tau_{rz}}{G} \tag{6.14}$$
$$G = \frac{E}{2(1+\mu)} \tag{6.15}$$

$$\sigma_r = C\left((1-\mu)\eta_r + \mu\eta_\theta + \mu\eta_z\right) \tag{6.16}$$
$$\sigma_\theta = C\left(\mu\eta_r + (1-\mu)\eta_\theta + \mu\eta_z\right) \tag{6.17}$$
$$\sigma_z = C\left(\mu\eta_r + \mu\eta_\theta + (1-\mu)\eta_z\right) \tag{6.18}$$
$$C = \frac{E}{(1-2\mu)(1+\mu)} \tag{6.19}$$
$$\tau_{rz} = G\gamma_{rz} \tag{6.20}$$
$$\eta_i = \varepsilon_i - \alpha_i(T) \tag{6.21}$$

Equation (6.22) and Equation (6.23) are the PDE's that is solved for in FlexPDE for the displacement in a cylindrical coordinate system. (Backstrom 2005)

$$\frac{\partial r\sigma_r}{\partial r} + \frac{\partial r\tau_{rz}}{\partial z} - \sigma_\theta = 0 \tag{6.22}$$
$$\frac{\partial r\tau_{rz}}{\partial r} + \frac{\partial r\sigma_z}{\partial z} + rF_z = 0 \tag{6.23}$$

Finally, the model needs to be able to cater for the allowed expansion in the lining. This is done by introducing a key factor. The key factor indicates how much of the allowed expansion has been used, i.e. how much keying has taken place in a certain area; 1 indicating complete keying and 0 no keying. It is calculated using

$$key_{factor} = \max(0.0, \min(1.0, \frac{lte}{\varepsilon_{expansionSheets}})) \tag{6.24}$$

.

In order to include this phenomena into the displacement calculations, the strain as a result of the thermal expansion are kept at zero until keying has taken place i.e. $\alpha_i(T) = 0$ and at 1 should the linear thermal expansion (lte) be more than the allowed expansion. Since the hearth that is modelled is conical and the coordinate system is cylindrical the linear thermal expansion will have to be calculated as the z and r components. The following equations can be used to calculate the radial and axial lte respectively:

$$lte_r = max(0.0, \alpha\Delta T - \varepsilon_{expansionSheets})\cos(\beta) + \alpha\Delta T\sin(\beta) \tag{6.25}$$
$$lte_z = max(0.0, \alpha\Delta T - \varepsilon_{expansionSheets})\sin(\beta) + \alpha\Delta T\cos(\beta) \tag{6.26}$$

.

The expansion allowance can be calculated using

$$\varepsilon_{expansionSheets} = \frac{number\ of\ sheets \times sheet\ thickness}{number\ of\ bricks \times brick\ thickness} \tag{6.27}$$

for a specific section in a furnace. The simulations studied with the model will use different allowed expansions and compare the results.

6.8 Boundary Conditions

Since the models and simulations used in this study is not based on an actual furnace and furnace data, the boundary conditions that were applied had to be based on assumptions. The following boundaries and boundary conditions had to be supplied:

- Cooling on the furnace sidewall
- Cooling of the hearth
- Cooling on the roof of the furnace

In order to determine the heat transfer coefficient on the boundaries the following approach was taken. The thermal resistance was calculated for each segment along the cooling path using:

$$R_{cond} = \frac{1}{k}\int_{r_1}^{r_2}\frac{dr}{A} \tag{6.28}$$

$$R_{conv} = \frac{1}{hA} \tag{6.29}$$

$$T_{total} = R_{cond} + R_{conv} \tag{6.30}$$

In order to determine the effect that any changes to the boundary condition would have on the overall result, the % contribution the boundary condition has to the overall heat transfer had to be determined. If the boundary condition has a low contribution to the heat transfer it can be deduced that variations of the boundary condition would have a small impact on the heat transfer and the thermal distribution in the lining.

6.8.1 Sidewall

In order to predict the mechanical behaviour of the furnace lining, the bottom part of the steel shell is restricted in all direction up to where the bottom of the hearth meets the sidewall. This is in accordance with several industrial furnace designs that restrict the movement of the hearth shell.

Considering the thermal resistance through the sidewall in the freeboard area, the results are shown in Table 6.6. The largest contributor to the thermal resistance is the refractory material, the impact of the convection is thus quite low in comparison. A heat transfer coefficient of $1000\,\mathrm{W\,m^{-2}\,K^{-1}}$ was used. Using the same approach, the heat transfer through the freezelining region was calculated and again the results show a very low sensitivity to the choice of heat transfer coefficient (Table 6.7).

6.8.2 Hearth

The bottom of the hearth steel shell is completely restricted from movement in all directions.

Cooling air is blown over the steel plate at the bottom of the hearth. The sensitivity analysis shows a thermal resistance contribution of 15.6% for the convection with a chosen heat transfer coefficient

Table 6.6: Upper sidewall thermal resistance analysis for a heat transfer coefficient of 1000 W m^{-2} K^{-1}

Component	Refractory	Ramming	Steel	Convection	Total
k	4.46	25.000	53.96		
T_{inside}	1600.00	50.87	36.18	31.10	
$T_{outside}$	50.87	36.18	31.10	22.00	
$T_{average}$	825.44	43.52	33.64	26.55	
ΔT	1549.13	14.70	5.07	9.10	1578.00
$R_{thermal}$	4.08×10^{-3}	3.87×10^{-5}	1.34×10^{-5}	2.40×10^{-5}	4.16×10^{-3}
Contribution	98.17%	0.93%	0.32%	0.58%	100.00%

Table 6.7: Sidewall thermal resistance analysis inline with the freezelining for a heat transfer coefficient of 1000 W m^{-2} K^{-1}

Component	Freezelining	Refractory	Ramming	Steel	Convection	Total
k	1.0	11.08	25.000	54.23		
T_{inside}	1700.00	225.50	29.36	25.61	24.32	
$T_{outside}$	225.50	29.36	25.61	24.32	22.00	
$T_{average}$	962.75	127.43	27.49	24.97	23.16	
ΔT	1474.50	196.14	3.75	1.29	2.32	1678.00
$R_{thermal}$	3.73×10^{-2}	4.96×10^{-3}	9.48×10^{-5}	3.26×10^{-5}	5.87×10^{-5}	4.24×10^{-2}
Contribution	87.87%	11.69%	0.22%	0.08%	0.14%	100.00%

of 30 W m^{-2} K^{-1}. This shows a significantly larger contribution than that of the convection on the sidewall; however, the contribution is significantly less than that of the refractory material and since the cooling fluid is air and not water the chosen heat transfer coefficient is within acceptable bounds. The reader should note that choosing a different heat transfer coefficient for the hearth will have a much larger impact on the results than altering the coefficient of the sidewall heat transfer.

Table 6.8: Hearth sensitivity analysis for a heat transfer coefficient of 30 W m^{-2} K^{-1}

Component	Refractory	Copper	Steel	Convection	Total
k	8.641	366.65	43.55		
T_{inside}	1550	271.55	271.24	263.01	
$T_{outside}$	271.55	271.24	263.01	25.00	
$T_{average}$	910.78	271.39	267.13	144.01	
ΔT	1278.45	0.31	8.22	238.01	1525.00
$R_{thermal}$	3.25×10^{-3}	7.97×10^{-7}	2.09×10^{-5}	6.04×10^{-4}	3.87×10^{-3}
Contribution	83.83%	0.02%	0.54%	15.61%	100.00%

6.8.3 Roof

Since the roof is not included in the scope of this study no particular cooling is applied here. However, in order to have a more realistic temperature on the roof natural convection is applied to the roof boundary using Equations (6.31) to (6.33). (Hibbeler 2011)

$$Ra = \frac{g\beta L_c^3(T_{surface} - T_{ambient})}{\alpha\nu} \tag{6.31}$$

$$Nu = 0.15Ra_L^0.33 \tag{6.32}$$

$$L_c = \frac{A}{p} = \frac{r}{2} \tag{6.33}$$

6.9 Verification

Since the modelled furnace is not based on an actual production furnace no industry data could be used to validate the results obtained during modelling; however, the results could be verified to ensure the correct implementation of the model and the physics described above. In order to verify the implementation of the model into FlexPDE the following steps were taken:

- Application of Boundary Conditions: Checking that boundary conditions are applied to the correct boundary:
- Thermal calculations: Comparison of 1D thermal resistance calculations to simulation results.
- Displacement calculations: To verify this the implementation of the PDE's were used to solve the same problem as presented in Backstrom (2005) and the results were compared.

6.9.1 Application of Boundary Conditions

To verify that the boundary conditions are applied correctly in FlexPDE boundary condition values are set at different, excessive values and the results for the first iteration is considered, the boundary on which the boundary condition is applied then clearly shows as different from the initial conditions and gives a view of where the boundary is applied (Figure 6.3). This is necessary as FlexPDE problem definition is completely text based and no visual confirmation of the boundary conditions when and where they are applied form part of the model definition.

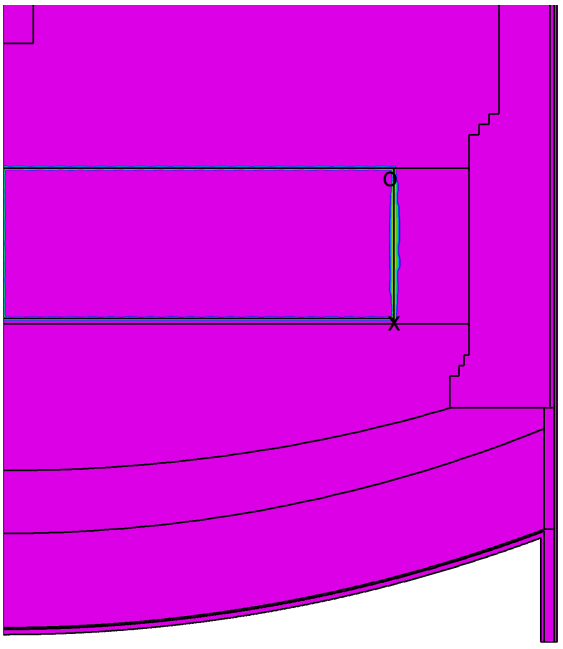

Figure 6.3: Illustrating the verification of the temperature boundary condition to the slag bath

6.9.2 Thermal Verification

From Table 6.8 the temperature on the outside of the refractory lining should be 271.55 °C, the actual result obtained is 160 °C. This deviance can be ascribed to the choice of thermal conductivity coefficient for the resistance calculations of $k = 8.641$, when the average of the temperatures on the lining inside and outside are taken from Table 6.8 and used to calculate the thermal conductivity coefficient it becomes $k = 3.9$. This then results in a temperature on the outside of the refractory lining of 147 °C (Table 6.9). The close correlation between the actual result and the result obtained from the thermal resistance calculation serves as verification that the heat transfer and boundary conditions in the model are applied correctly.

Table 6.9: Hearth second iteration of resistance calculations

Component	Refractory	Copper	Steel	Convection	Total
k	3.9	366.65	43.55		
T_{inside}	1550	147.11	146.96	142.88	
$T_{outside}$	147.11	146.96	142.88	25.00	
$T_{average}$	848.56	147.03	144.92	83.94	
ΔT	1402.89	0.16	4.07	238.01	1525.00
$R_{thermal}$	2.72×10^{-3}	7.97×10^{-7}	2.09×10^{-5}	6.04×10^{-4}	3.87×10^{-3}
Contribution	91.99%	0.01%	0.27%	7.73%	100.00%

6.9.3 Displacement Calculations

In order to verify that the displacement stresses and strains were implemented correctly several problems from Backstrom (2005) were replicated to achieve the same results. Since the implementation for the cylindrical coordinate system stresses and strains were sourced from Backstrom (2005) this served as verification that the implementation was done correctly.

Part IV

Simulation Results and Discussion

Chapter 7

Steady State

Using a steady state linear elastic modelling approach, investigations can be done to provide insight into the influences of refractory material properties and expansion allowance on the displacement, stresses, and strains of the refractory lining. Firstly, the influence of expansion allowance on keying is investigated. Using these results as input, the impact of different Young's modulus on the furnace is simulated.

FlexPDE has mesh refinement algorithms already built into the software which allows for refinement of the mesh in areas where the error is large. It can be seen that the mesh has been refined in all areas where rapid heat transfer is expected to take place. Additionally, the mesh was refined in areas where specific values were plotted through key areas, the final mesh that was used can be seen in Figure 7.1.

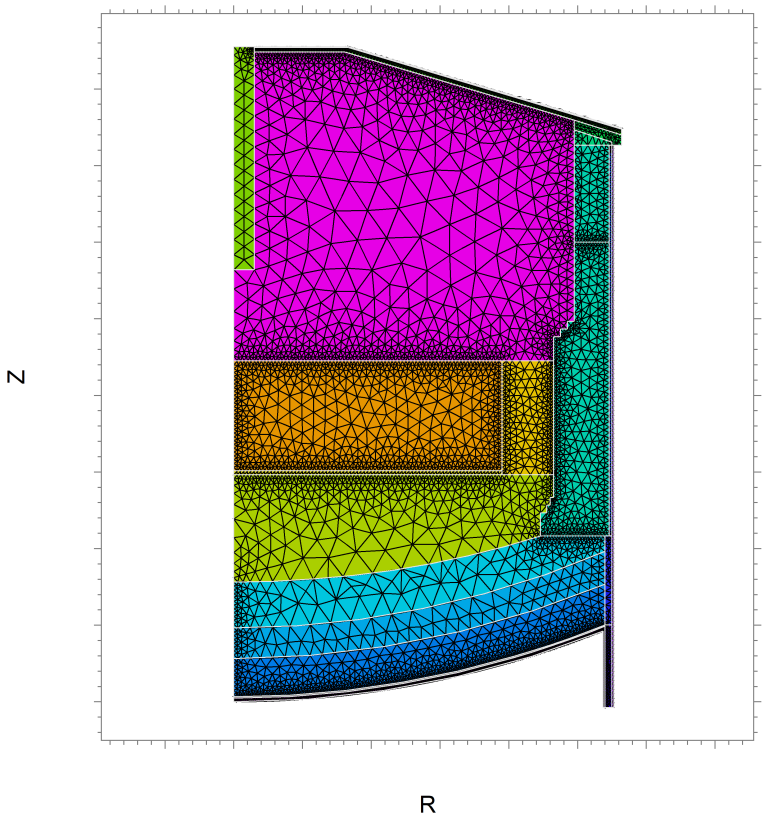

Figure 7.1: The final mesh used for all simulations

7.1 Thermal Distribution and Keying

7.1.1 Thermal Distribution

The temperature in the furnace is controlled by the pre-set metal and slag bath temperatures. In the freeboard the temperature is mainly due to the radiative heat transfer from the slag bath but also includes conductive heat transfer. It can be seen from Figure 7.2 that the freezelining has a significant impact on the heat transferred to the sidewall. This is shown in more detail in Figure 7.3c. The freeboard is observed to be close to the temperature of the slag bath which is set at 1700 °C.

Due to the high thermal conductivity of the graphite electrode, the entire electrode is at the same temperature as the freeboard. The slight temperature gradient through the roof can be attributed to the natural convection boundary condition on the outside of the roof. Since the roof is not included in the scope of this study, no further analysis of the roof temperature gradient will be done.

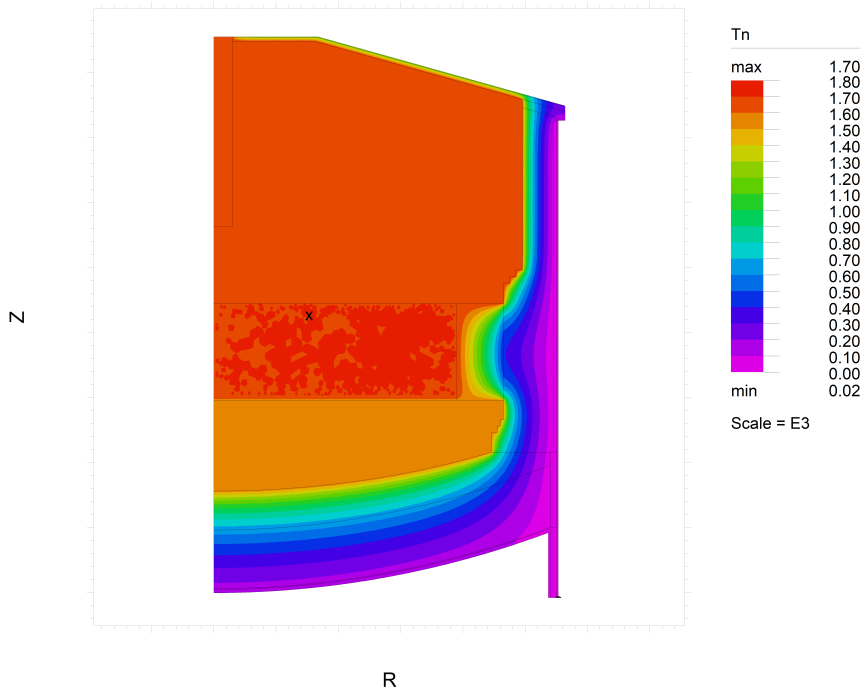

Figure 7.2: Temperature distribution through the furnace

The temperature drops significantly through the first part of the hearth as shown in Figure 7.3a. This same behaviour is observed in the skewback region (Figure 7.3b) and can be explained by the low thermal conductivity of the refractory bricks along with the cooling on the sidewall and hearth shells. The influence of the freezelining on the hotface temperature of the sidewall is significant with the sidewall temperature dropping to 400 °C directly behind the freezelining. The hotface temperature is close to the freeboard temperature above the freezelining.

7.1.2 Keying

Table 7.1 shows the different allowed expansion that was modelled for the three areas of the furnace. In each case the chosen allowed expansion is gradually increased. For the hearth, the allowed expansion is included for the directions parallel and tangential to the curvature of the hearth. For the walls, the expansion allowance is only considered in the tangential direction.

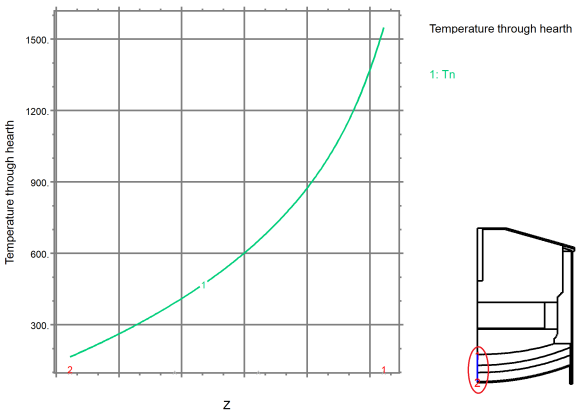

(a) Temperature through the centre of the hearth refractory

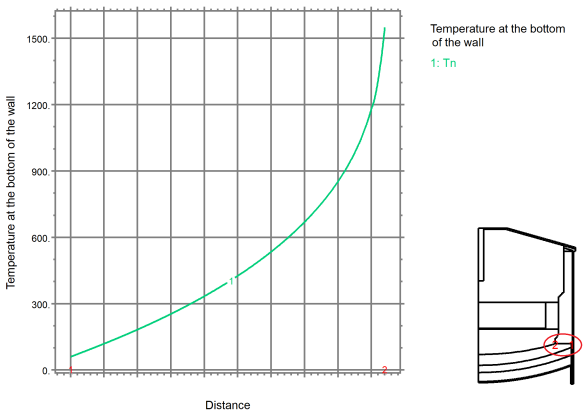

(b) Temperature through the skewback

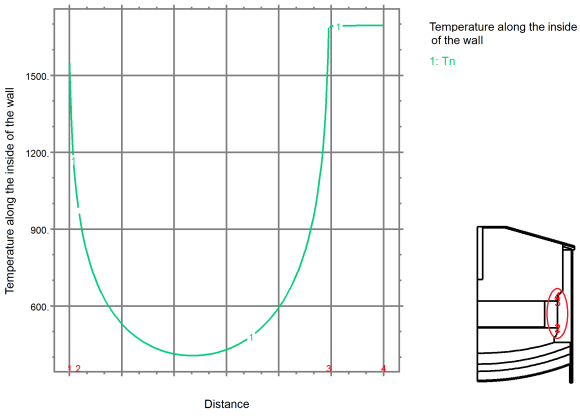

(c) Temperature along the hotface of the wall behind the freezelining

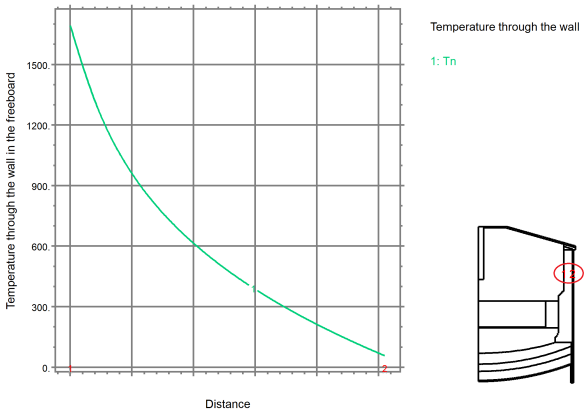

(d) Temperature through the upper wall exposed to the freeboard

Figure 7.3: Temperature distribution through key areas of the furnace

Table 7.1: Expansion allowance in each of the three sections of the furnace for six different cases

	expansion allowance		
	Hearth top	Hearth bottom	Walls
Case 1	1.00%	0.30%	0.50%
Case 2	1..25%	0.50%	0.75%
Case 3	1.35%	0.60%	1.00%
Case 4	1.50%	0.75%	1.10%
Case 5	1.75%	0.80%	1.20%
Case 6	2.00%	1.00%	1.50%

Hearth

As expected, for a lower allowed expansion, the keying factor increases in the hearth. A high keying factor is good; however, in anticipation of determining the stresses and strains, the higher keying factor could result in higher stresses in the lining. This is due to the fact that a greater area of the hearth can be under compressive load as all the allowed expansion has already been used. More detailed information on the keying through the centre of the hearth can be seen in Figure 7.5. For Case 1 the hearth top is 85% and the hearth bottom is 80% keyed through the thickness at the hearth centre. For both the hearth top and the hearth bottom the lowest percentage of keying is

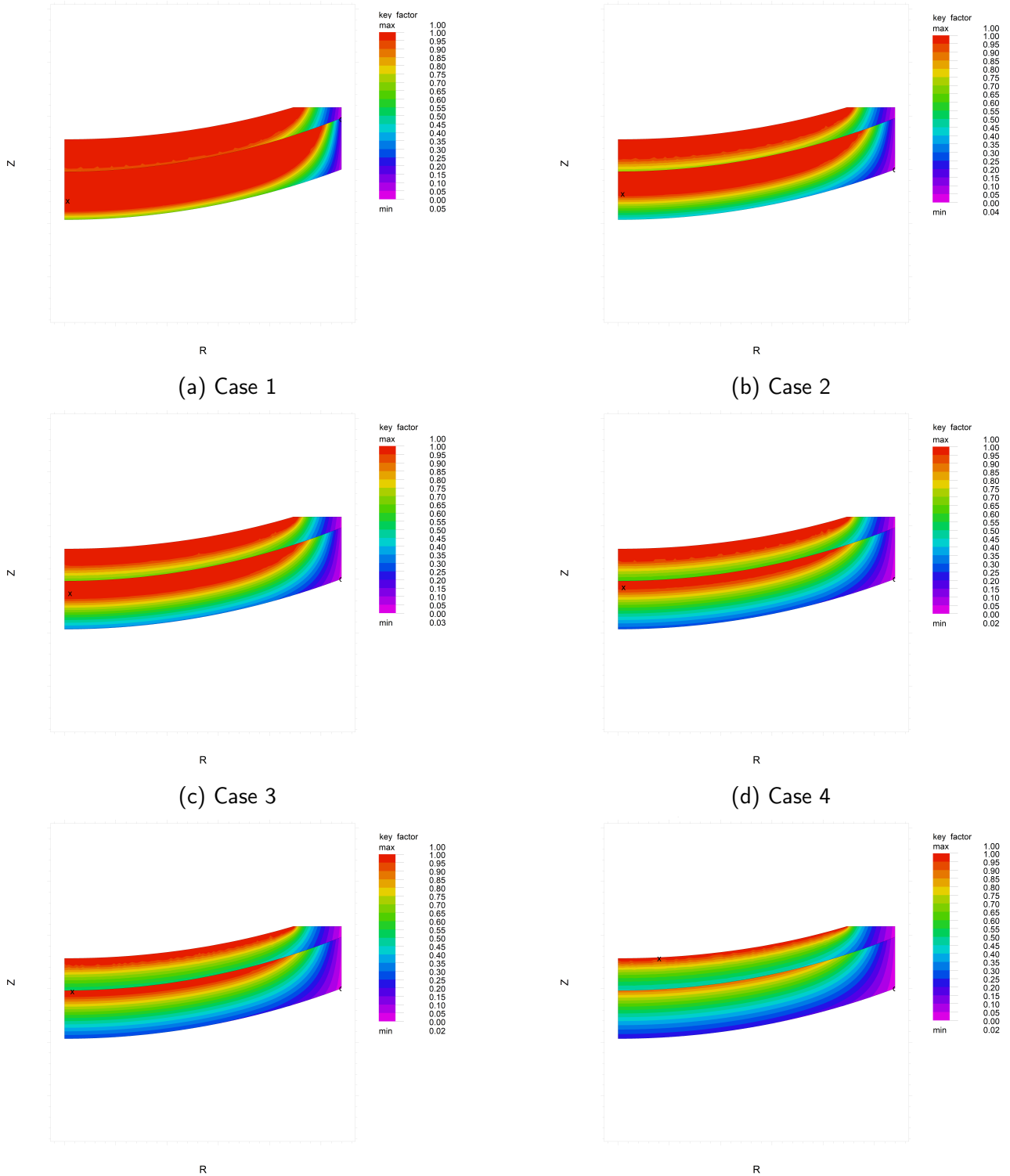

(a) Case 1

(b) Case 2

(c) Case 3

(d) Case 4

(e) Case 5

(f) Case 6

Figure 7.4: Keying in the hearth

well above 60%.

For Case 3 (Figure 7.4c and Figure 7.5c) the top of the hearth is keyed through 50% of its thickness and 30% through the thickness of the hearth bottom. There is no keying in the hearth bottom for Case 6, however the top 13% of the hearth top is still keyed (Figure 7.5f). Of greater concern for Case 6 is the keying in the skewback region; only the very tip of the skewback region is keyed, as seen in Figure 7.4f.

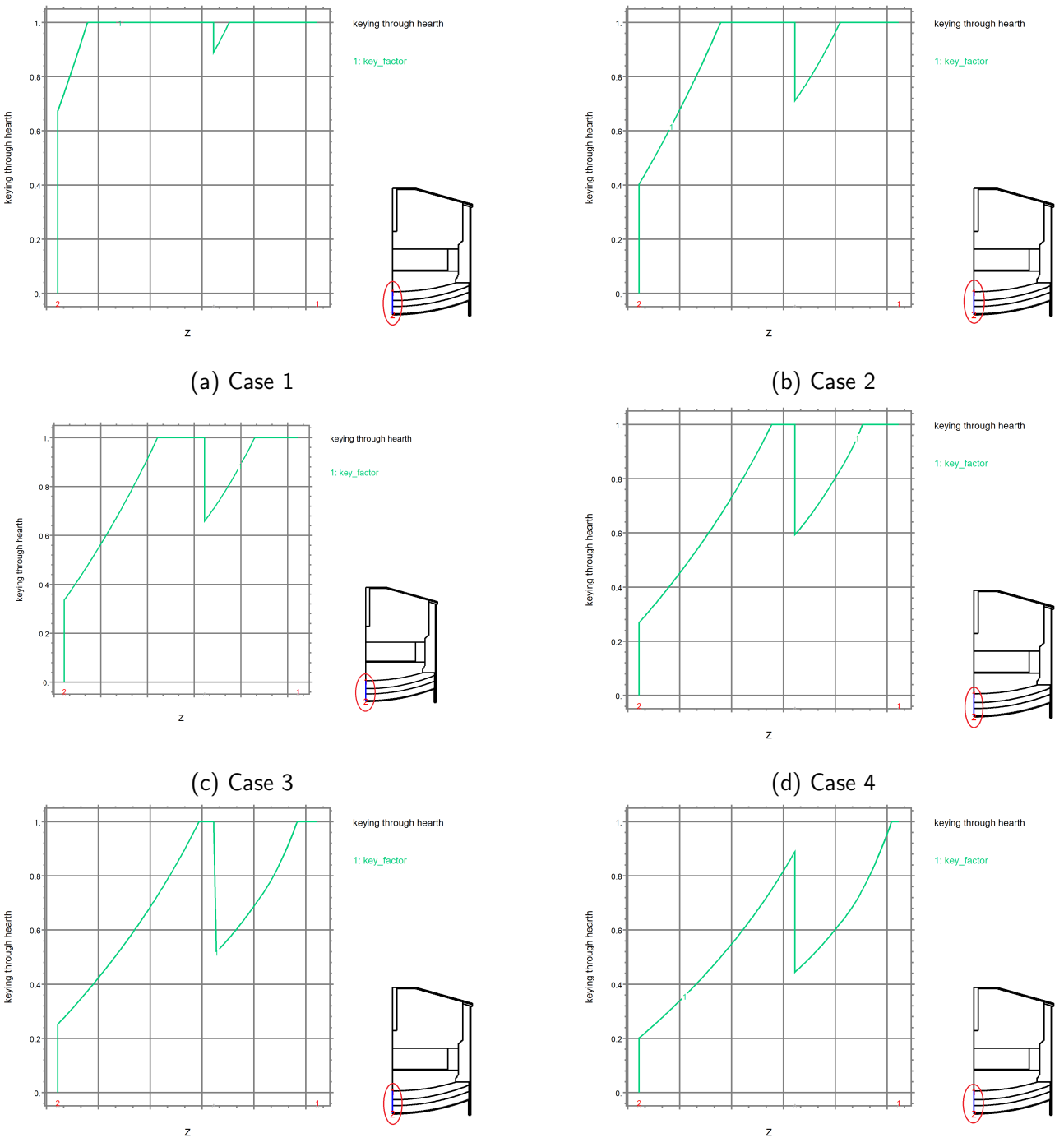

(a) Case 1

(b) Case 2

(c) Case 3

(d) Case 4

(e) Case 5

(f) Case 6

Figure 7.5: Keying through the hearth centre

Refractory Walls

The keying percentage through the wall thickness is slightly different between the wall top and bottom. This is driven by two factors; a thicker wall at the bottom and a lower metal bath temperature. The freezelining has a significant impact on keying in the sidewall, with all the cases except Case 1 showing no keying directly behind the freezelining. This effect gets progressively worse the higher the allowed expansion. Behind the freezelining only 50% of the allowed expansion has been closed for Case 4, Figure 7.6d. Also, note Case 4 where keying has taken place for only 5% of the wall thickness, this decreases to 1% for Case 6.

The allowed expansion is inserted to reduce the stress due to the thermal expansion in the

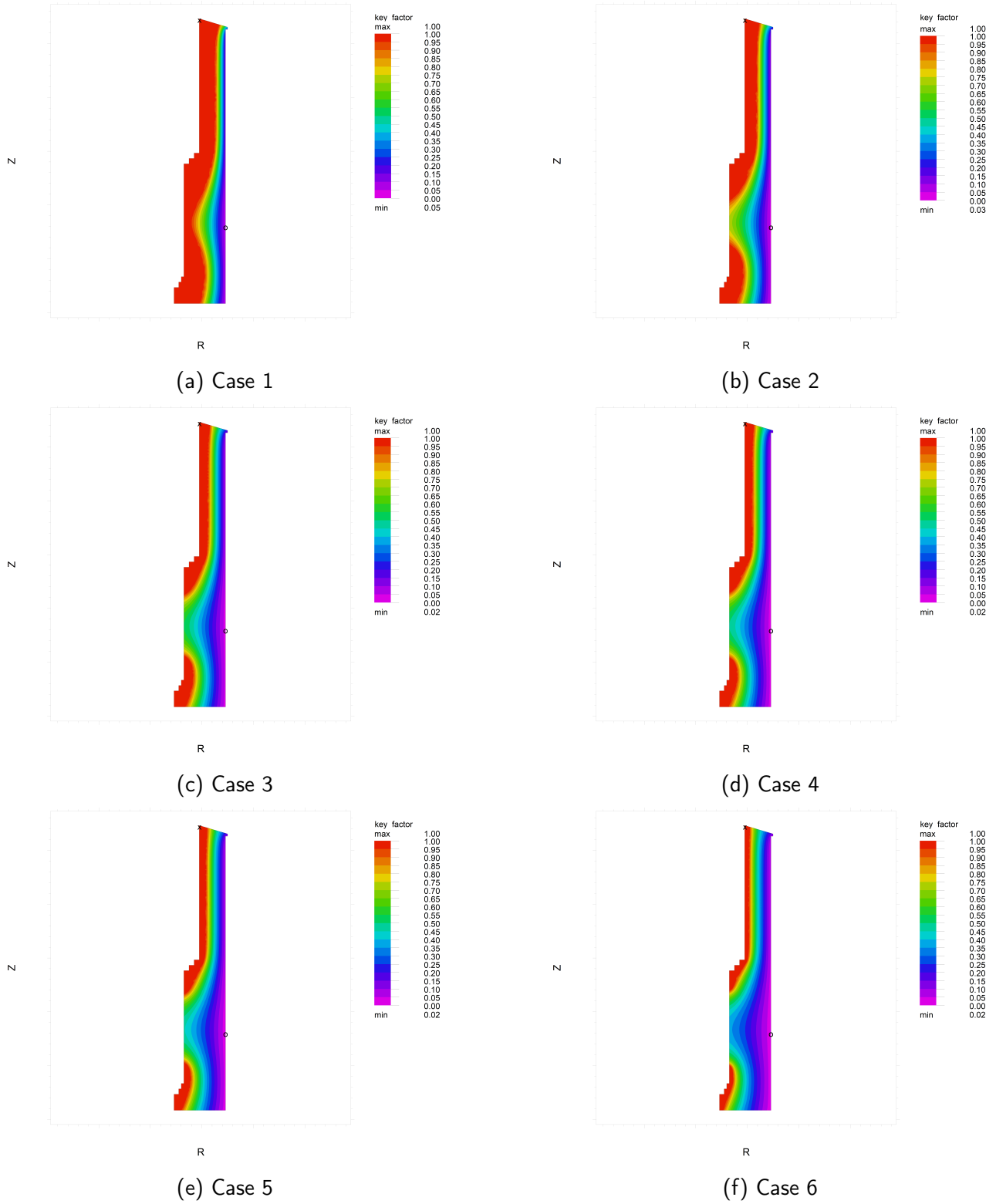

(a) Case 1

(b) Case 2

(c) Case 3

(d) Case 4

(e) Case 5

(f) Case 6

Figure 7.6: Keying in the refractory sidewall

lining. It is important that all gaps are closed to prevent metal penetration. For the case where the freezelining blocks heat transfer to the wall from the slag bath, the risk of lining penetration is significantly reduced as the freezelining is solidified slag. There is still a risk that should the freezelining thickness greatly reduce at a rapid rate that thermal shock can cause cracks in the lining. It could even result in lining penetration if the entire freezelining comes of at once. This is highly unlikely and to make use of lower allowed expansion, as for Case 1, carries the risk of

extremely high stresses in the lining, which could result in lining failure.

7.2 Displacement, Stresses and Strains

Based on the evaluation of keying for different allowed expansions, the stresses and strains were evaluated using the allowed expansions of Case 4. The factors considered were:

- Has the hearth top and sidewall hotface keyed?
- Is there keying in the skewback region?
- Has the hearth bottom keyed on the hotface?

From Table 6.3 four different cases were evaluated using different combinations of Young's Moduli across the three sections in the furnace. These are shown in Table 7.2. After evaluating the displacements, stresses and strains it might be useful to increase the allowed expansion; however, the keying of the skewback region should be monitored closely.

Table 7.2: Young's modulus for different simulation cases to evaluate the displacements, stresses and strains

	Young's Modulus		
	Hearth top	Hearth bottom	Walls
Case E 1	44.5 GPa	22.7 GPa	44.5 GPa
Case E 2	44.5 GPa	62.5 GPa	22.5 GPa
Case E 3	22.7 GPa	44.5 GPa	62.5 GPa
Case E 4	62.5 GPa	44.5 GPa	44.5 GPa

7.2.1 Displacement

The radial and axial displacements were evaluated independently. Considering the radial displacement as shown in Figure 7.8 Figure 7.9 and , the first thing to take note of is the displacement of the ramming between the steel shell and the sidewall bricks. Figure 7.7 shows this in more detail for Case E1. The ramming should compress to decrease the stress in the lining due to thermal expansion. It should, however, be stiff enough to prevent the wall from expanding more than the shell. The Young's Modulus of the ramming was chosen as 900 kPa based on several iterations where the value was increased gradually with each simulation until the desired outcome was achieved.

Radial Displacement

One of the most important factors to note is how the choice of material properties for one section of the furnace will affect the rest of the furnace. Compare Figure 7.8a with Figure 7.8d and notice how the sidewall has slightly different radial displacement values even though the Young's Modulus in both cases are the same for the sidewall. It is therefore important to evaluate the furnace displacements and subsequent stresses and strains for each individual case, as any changes to material properties in one area will have a knock-on effect elsewhere.

For all cases the largest displacement is at the top of the sidewall, the displacement then decreases the gradually toward the bottom of the wall. A similar behaviour is observed for the inward displacement of the sidewall at the step just above the slag bath level. The displacement of the upper sidewall is expected as the sidewall shell was only clamped in at the bottom and the moment

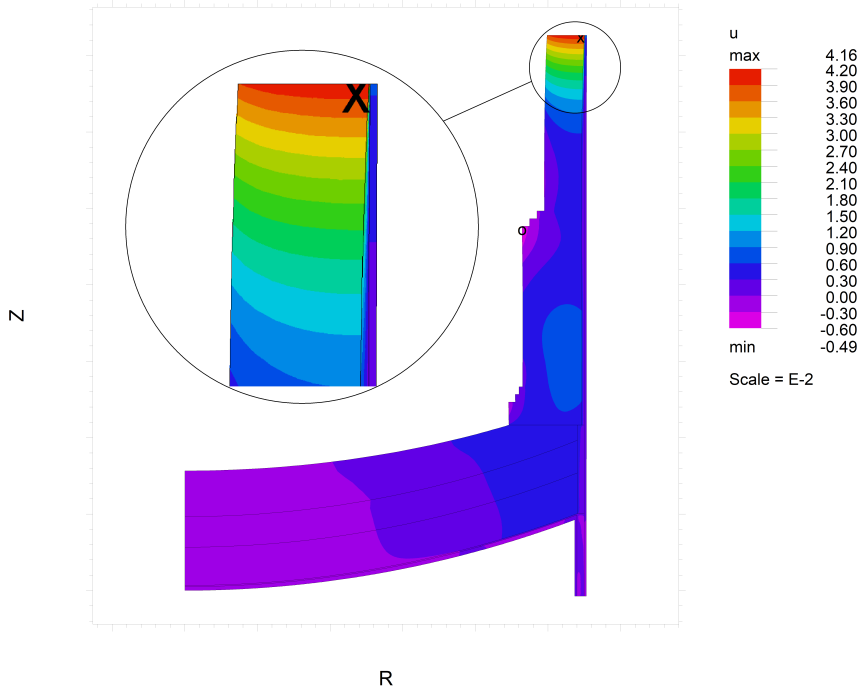

Figure 7.7: Radial displacement for Case E1 showing the compression of the ramming material between the refractory wall and the steel shell

caused by the distributed load on the sidewall shell will result in the greatest displacement outward the furthest from the support.

The expansion of the lining is also expected to increase in the freebard region due to the higher hotface temperatures. Comparing only the sidewall, it can be seen that the stiffer sidewall case exhibits lower overall expansion (Figure 7.8c). When evaluating the general distribution of displacement in the hearth, a similar pattern emerges for cases E1 and E4. This is supported by both having a stiffer brick in the hearth top than the hearth bottom.

From the displacement in the hearth, it can be seen that Case E3 has the lowest radial displacement, from Table 7.2 the hearth top, exposed to the highest temperatures is the least stiff of all the cases. The less stiff material thus shows a lower movement toward the ramming material. Contributing to this is the significantly stiffer wall which is connected to the hearth and can influence the results. The influence of the wall on the hearth top displacement can be seen when comparing Figure 7.8a and Figure 7.8b. Both have the same stiffness for the hearth top, however the displacement of the hearth at the skewback is significantly higher for Case E2 due to the increased movement of the wall in this area.

Another interesting observation is that the top of the wall radial displacement is the highest for Case E3 where the wall is the stiffest and the lowest for Case E2 where the wall has the lowest stiffness. However, the middle to lower wall of Case E2 has higher displacement than any of the other cases.

Axial Displacement

General observations regarding the axial displacement shows positive displacement upward of the hearth. Since the weight of the contents of the furnace is not included, this might be slightly more than what can be expected. In all cases the point with the highest positive movement is the hotface of the wall top. Since no expansion allowance is made in a vertical direction for the sidewall, this is not unexpected. Coupled with no resistance to outward movement, the hotface of the top of the wall will displace the most. Case E3 has the highest expansion in this region with 55.38 mm.

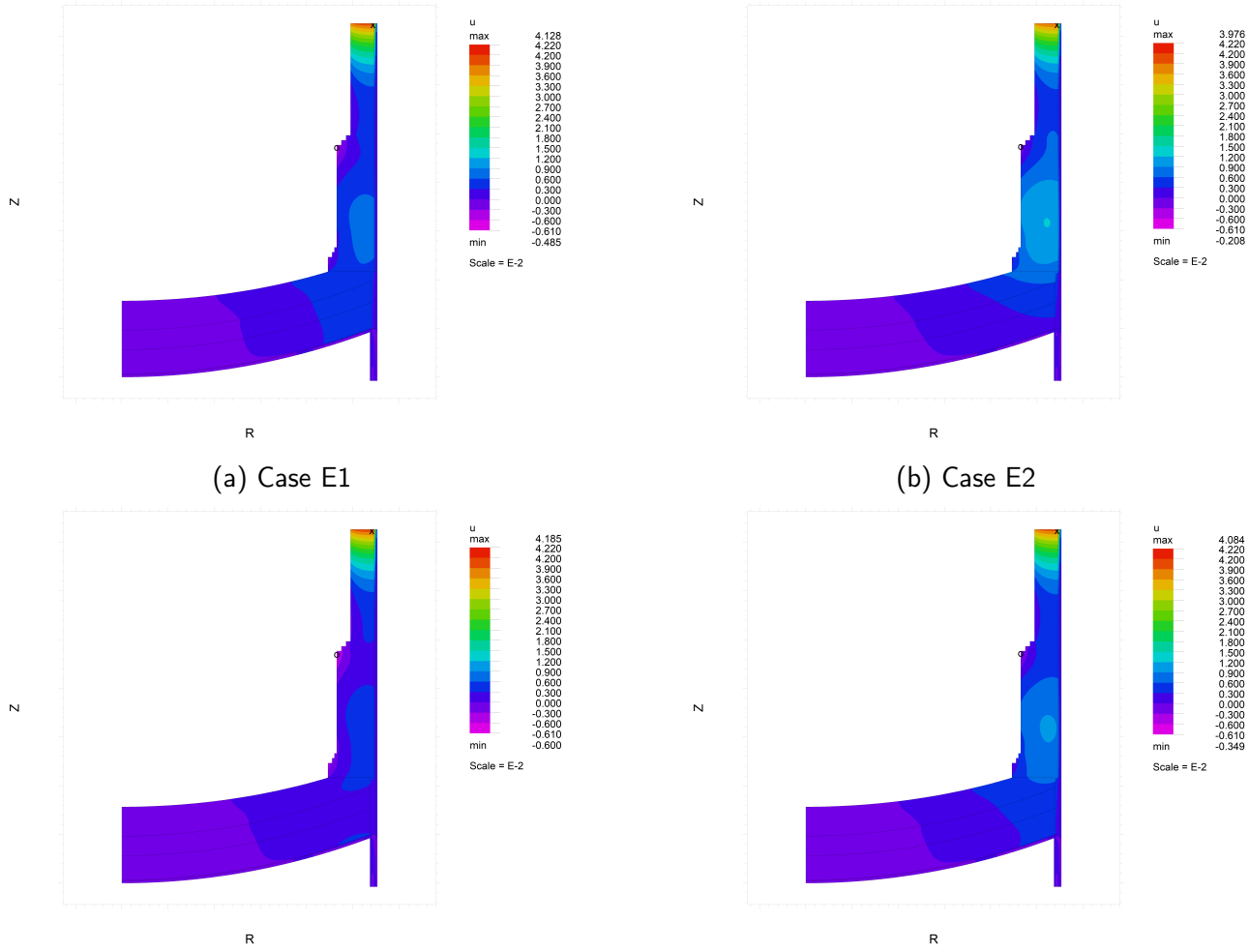

(a) Case E1 (b) Case E2

(c) Case E3 (d) Case E4

Figure 7.8: Radial displacement for the evaluated cases plotted on the same scale

The movement in the skewback region cold face is the least for Case E2 with expansion of between 0 mm to 3 mm as opposed to 6 mm of the other cases. This can be explained by the low stiffness of the sidewall and the medium stiffness of the hearth top, collectively having a low stiffness in the skewback region which results in low expansion.

Interesting to compare is the vertical displacement of Cases E1 and E4. Both cases have a wall stiffness of 44.5 GPa; however, there is a slight difference between the vertical expansion at the top of the walls. Upon closer observation it can be seen that this change already shows itself at the skewback region. The stiffer hearth top of Case E4 shows less movement at the skewback coldface.

Displacement of Key Areas

From Figure 7.10 it can be seen the vertical displacement is higher at the hotface than the cold face for the cases where the top of the hearth is stiffer than the wall (Case E2 ad E4), a plausible explanation is the wall pulling the hearth upward on the coldface, rather than the hearth pushing the wall upward. For both the other cases the vertical displacement decreases from the coldface to the hotface. This can be attributed to the hearth not compressing under the load from the wall but rather forcing the wall upward at the hotface.

For cases E1 and E3 the coldface displacement is significantly higher than that of E2 and E4. even though E1 and E3 exhibit the same behaviour the displacement at the hotface of E1 is higher than that of E3, which can be due to the stiffer hearth top. Since the hearth at the skewback is

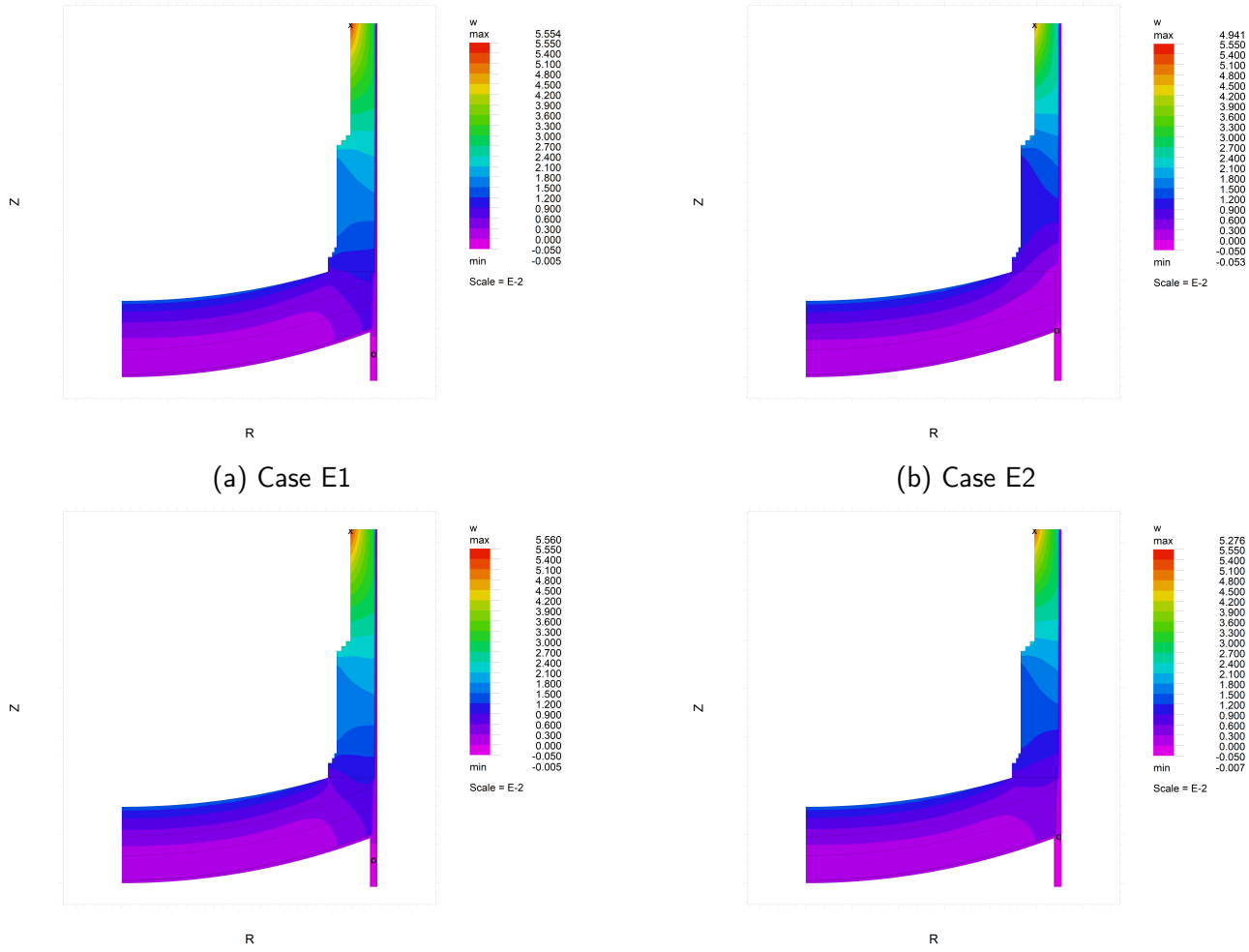

(a) Case E1 (b) Case E2

(c) Case E3 (d) Case E4

Figure 7.9: Axial displacement for the evaluated cases plotted on the same scale

cooler due to the proximity of two cooling surfaces, the lower expansion of the cold face of the skewback can be attributed to the stiffer material being the hearth top and limiting expansion of the less stiff material in this region.

From Figure 7.11 it can be observed that the stiffness of the wall has got little to no effect on the radial displacement. Although the stiffness influences the amount of displacement, the behaviour is similar through the wall for the vertical displacement of all cases. Again the influence the hearth has on the sidewall displacement is seen by comparing the stiffer wall of Case E1 which shows very similar vertical displacement values to that of Case E3.

Case E2 has the biggest difference between the highest and lowest displacement in the radial direction, differing with 11.5 mm, Figure 7.12. Cases E1 and E4 have 9 mm and 10 mm respectively. Case E3, with the highest stiffness, has a difference of 8 mm. The less stiff wall (Case E2) also has the highest radial displacement below the freezelining and expands inward the least. The stiffest wall expands the most inward above the freezelining.

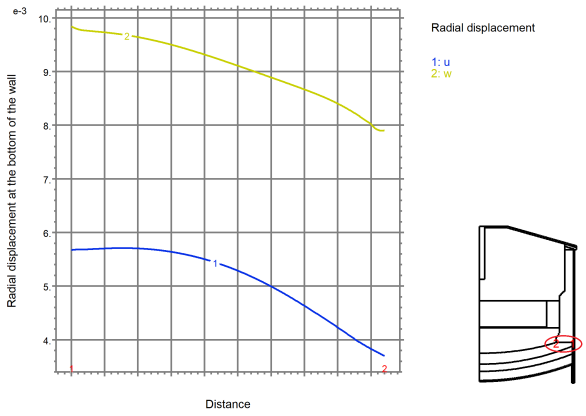

(a) Case E1

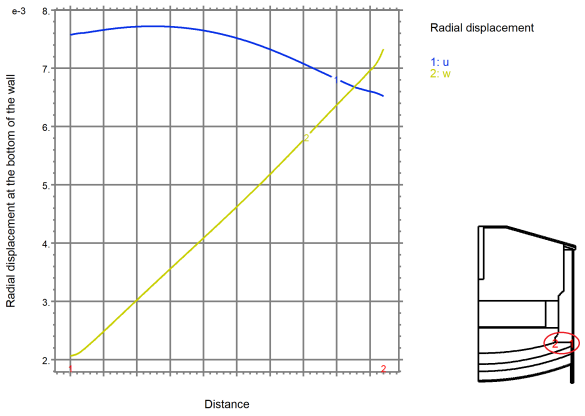

(b) Case E2

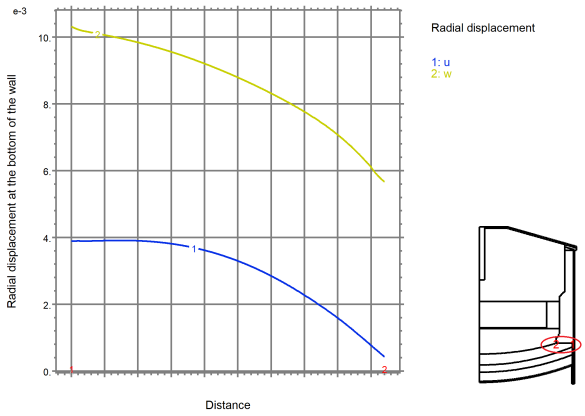

(c) Case E3

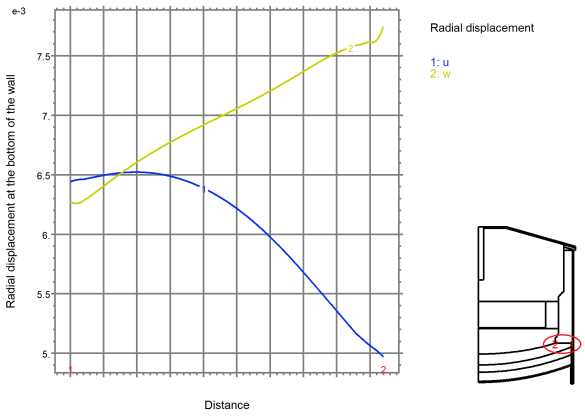

(d) Case E4

Figure 7.10: Displacement in the skewback region

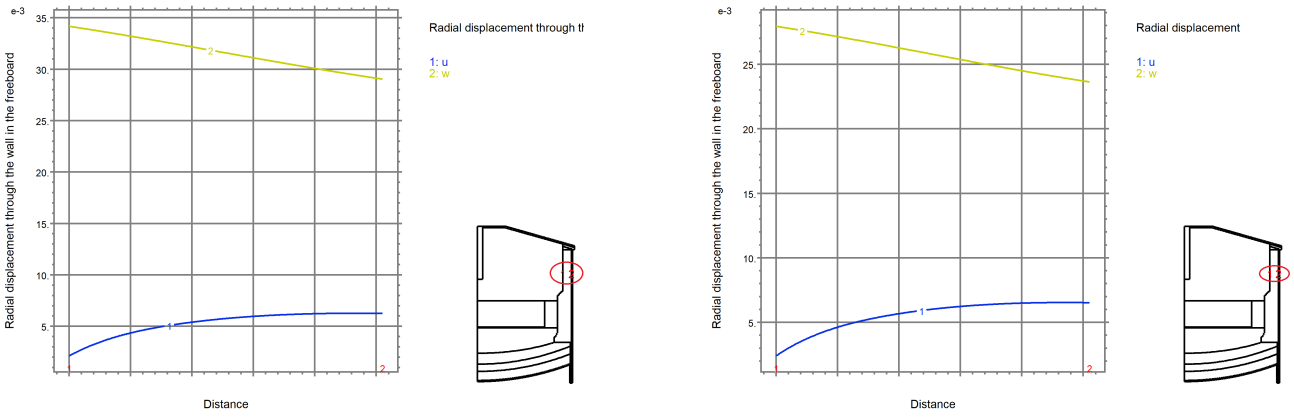

(a) Case E1

(b) Case E2

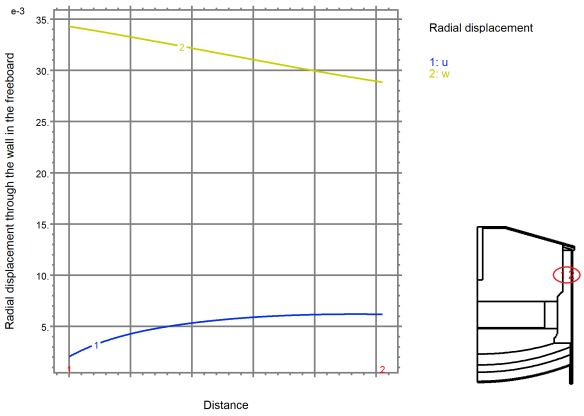

(c) Case E3

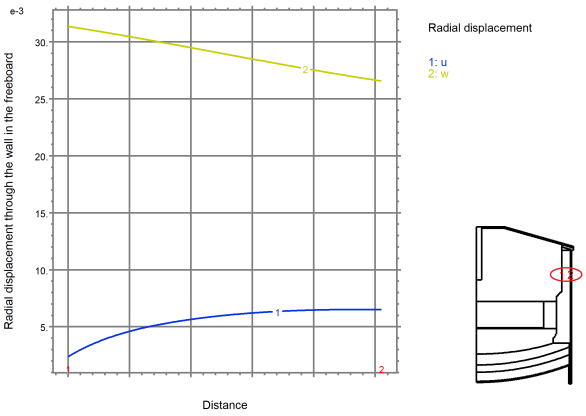

(d) Case E4

Figure 7.11: Displacement in the upper wall

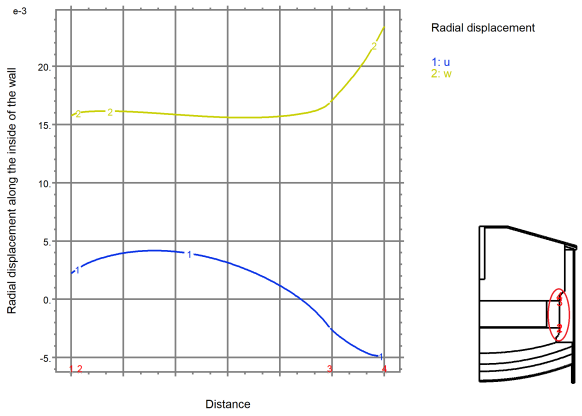

(a) Case E1

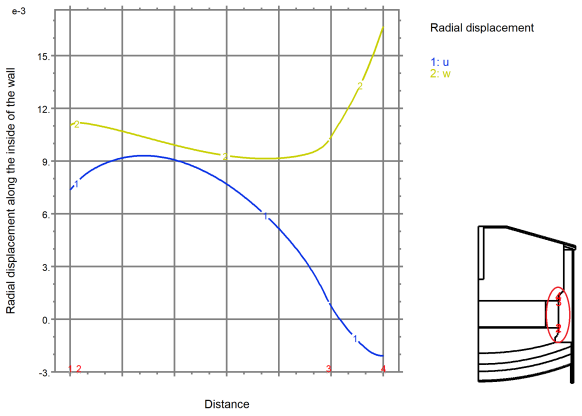

(b) Case E2

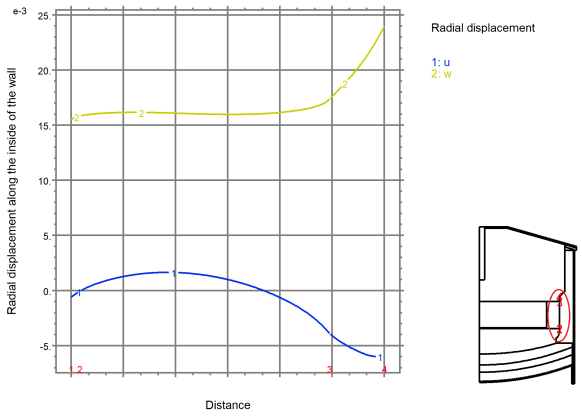

(c) Case E3

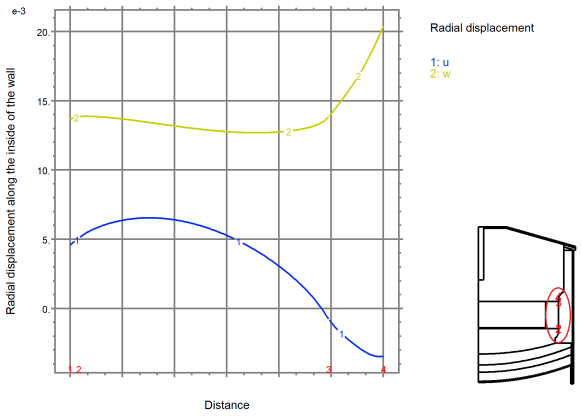

(d) Case E4

Figure 7.12: Displacement along the inside of the sidewall inline with the freezelining

7.2.2 Stress and Strain

Radial Stress and Strain

From Figure 7.13, the maximum compressive stress (negative stress) is in the skewback area for all cases. Even though a compressive stress is desired here to ensure no metal penetration, too high pressure could result in fracturing of the refractory material. In all cases the high stress is observed in the hearth as it approaches the skewback area. The stress in Figure 7.13b is observed to be the lowest in this area. This can be attributed to the softer wall which is compressed under the pressure from the hearth top as it expands radially.

In all cases the hearth top shows a compressive stress and an increased stress at the hotface of the bottom layer of the hearth. This is expected as these are the areas in keying (Figure 7.4). A tensile stress is seen at the intersection of the copper plate and the ramming. This can be attributed to the influence of the change in thermal expansion between the materials.

The furnace is modelled as a single solid; the different furnace sections might exhibit a higher influence on each other than what would be observed in an actual furnace. In all cases a stress concentration is observed at the steps in the sidewall, especially in the freeboard area where the temperature is higher. Should the bricks be modelled independently the compression in the radial direction could be less; as bricks would have some relative movement to each other. Despite this, it is important to consider the steps in the furnace wall an area where compressive failure might occur.

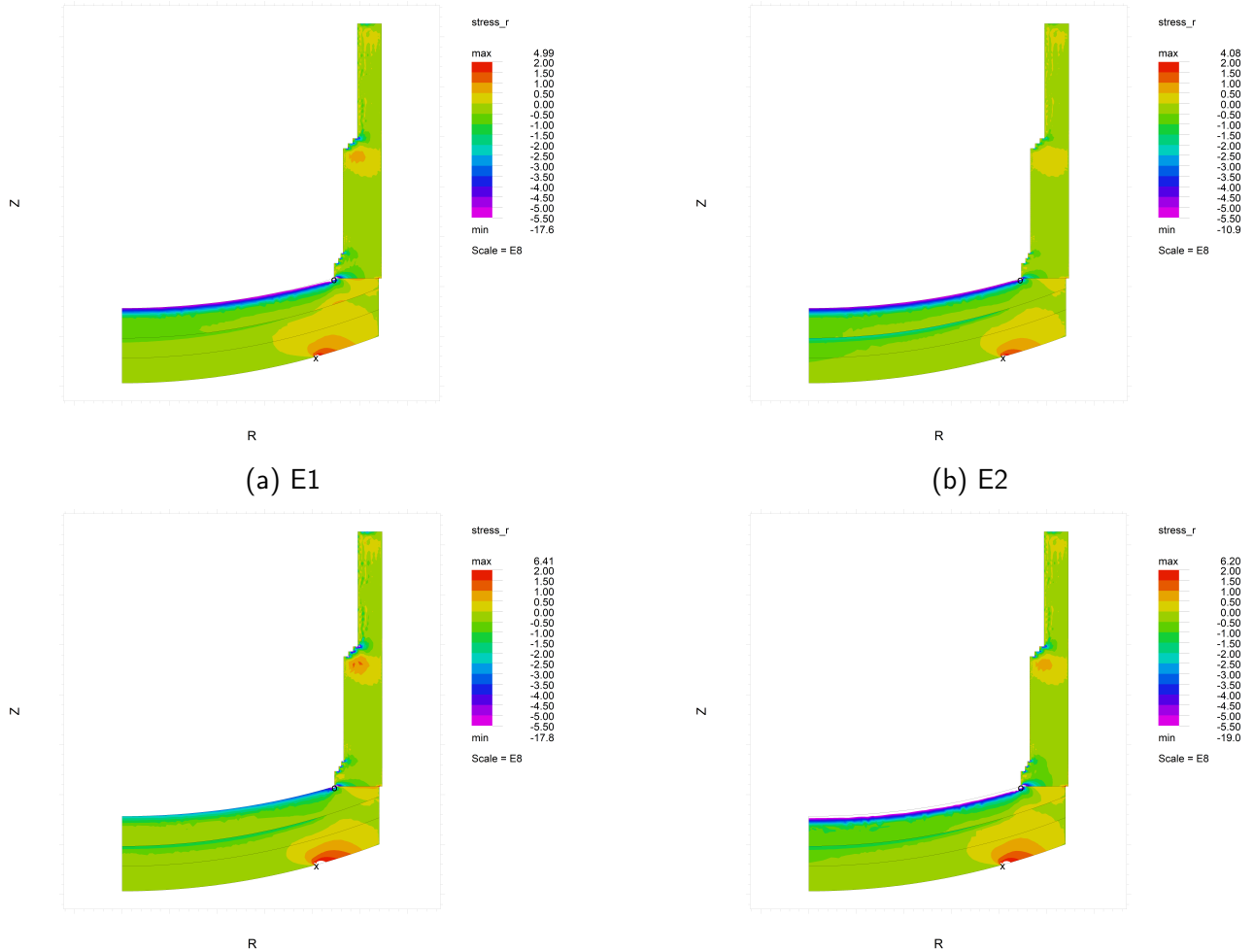

(a) E1 (b) E2

(c) E3 (d) E4

Figure 7.13: Radial stress for the evaluated cases plotted on the same scale

Despite a low stress state on the hotface of the sidewall exposed to the freeboard, there is a

significant positive strain in this area. The entire sidewall hotface has a positive strain, although a bit less. The negative strain on the hearth hotface is an indication of the compressive state in this region. The thermal displacement is limited due to all the allowed expansion gaps being filled. These general trends are observed for all cases in Figure 7.14.

Except for the values in the areas with the highest and lowest strain the results are closer related than that of the stress with the overall dispersion of strain in the refractory lining being very similar for all four cases. This can be explained by considering the nature of what the strain results are presenting. When a piece of the lining moves, the strain can still reflect as zero, even though the displacement is not. Hence, due to the magnitude of strain in certain key areas, the displacement of the furnace as a whole can look vastly different for the four cases considered. In the areas under significant load the difference in strain is resultant from the material's capacity to deform based on the resultant stress due to that deformation. Notice how the magnitude of strain might differ even though the distribution is closely related.

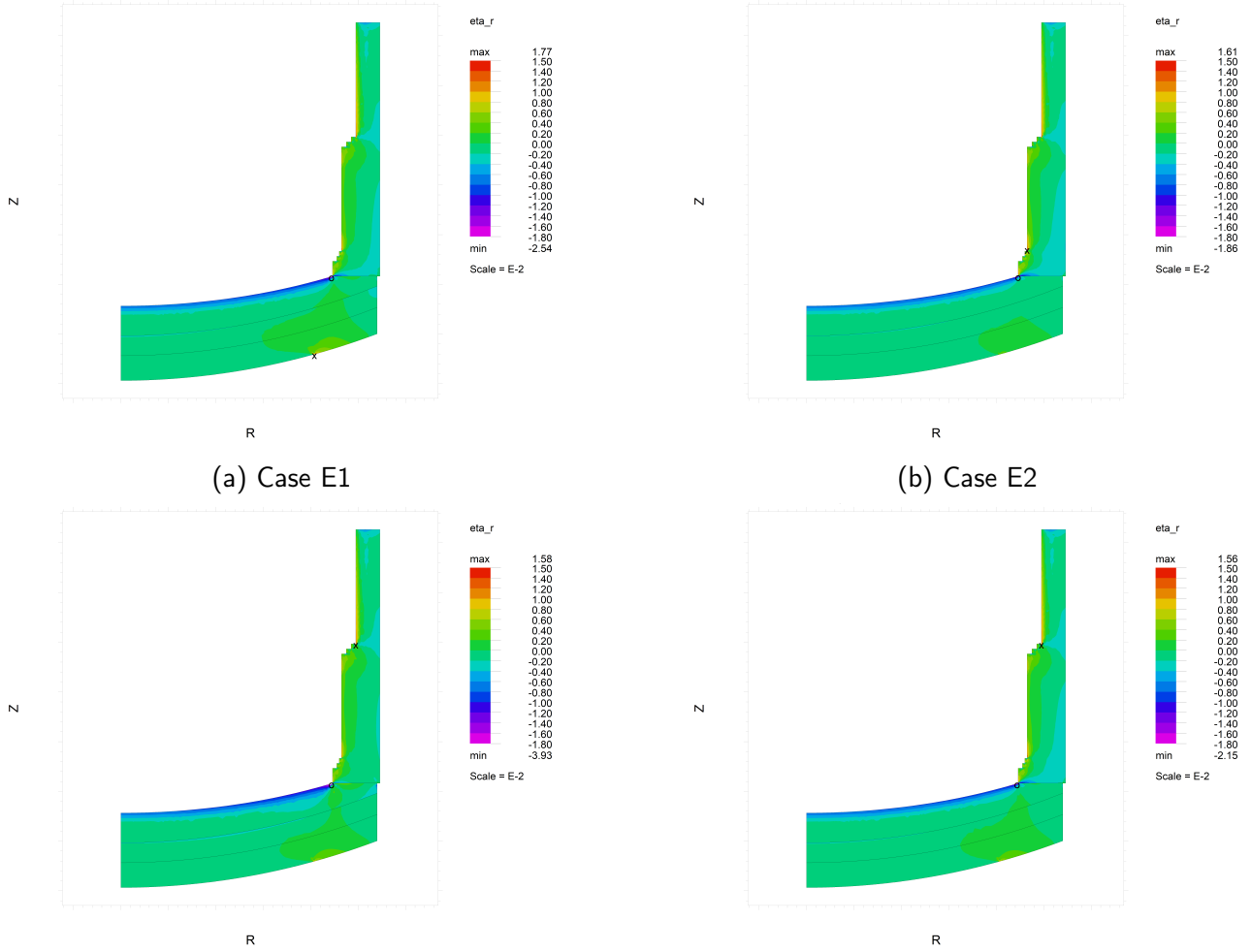

(a) Case E1 (b) Case E2

(c) Case E3 (d) Case E4

Figure 7.14: Radial strain for the evaluated cases plotted on the same scale

Tangential Stress and Strain

The highest compression stress observed is in the skewback area on the hearth and the bottom of the sidewall for all cases. The wall shows tensile stress on the coldface increasing in magnitude toward the wall top. Due to the lower stiffness, the stress in the wall for Case E2 is less than that of the other cases. The correlation between the high stress and the stiffer material is also evident

by the higher compression loading on the hearth top hotface in Case E4 in comparison to Case E3. From Figure 7.15c it is clear that the stiffer wall not only results in higher compressive stresses on the hotface but also an increased tensile stress in the wall coldface which could lead to separation. As noted in Chapter 4, this could result in a very small area of the brick carrying the compressive load and circumferential cracks forming in the individual bricks.

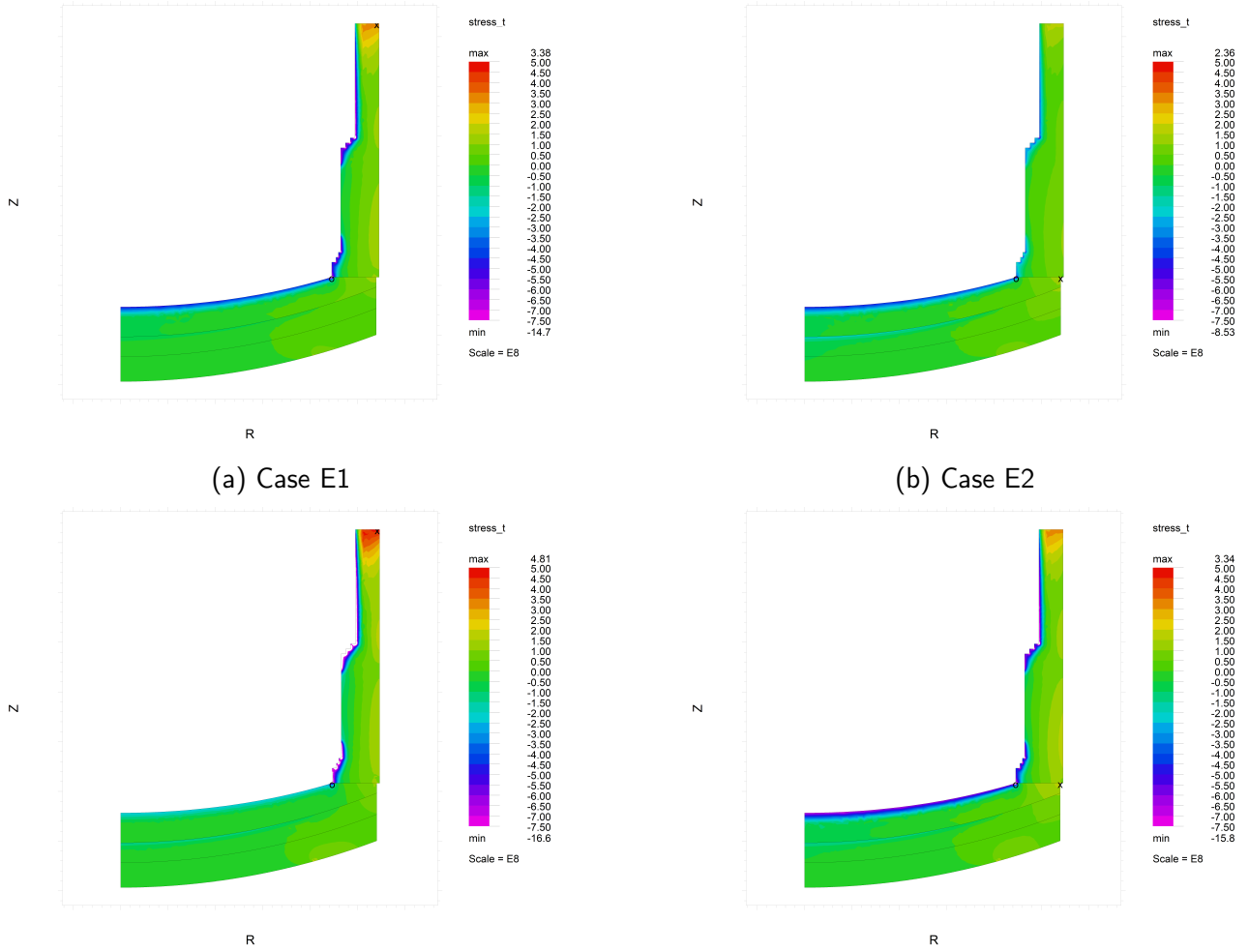

(a) Case E1 (b) Case E2

(c) Case E3 (d) Case E4

Figure 7.15: Tangential stress for the evaluated cases plotted on the same scale

Again the distribution of the strain is closely related for all cases in Figure 7.16. However, a difference is observed in the lower sidewall for the different cases. Since there is no keying in this area, the strain will be purely mechanical and will not be as a result of the thermal expansion. The difference in strain can be attributed to the effect of the hoop loading on the hotface, which is in a compressive state. The result is that the combination of this and the outward movement along the radial direction (Figure 7.8b) will force the coldface of the refractory lining to pull apart in the tangential direction. The softer lining in Figure 7.16c shows this effect the most. This is the same phenomena that drives the high positive strain in the upper sidewall on the coldface, which is seen for all cases.

Axial Stress and Strain

The most significant observation from Figure 7.17 is the tensile stress on the coldface of the sidewall. This will result in an opening between the layers on the coldface of the wall. In all cases a significant tensile stress is also present on the coldface for the skewback, this could pose a danger for metal

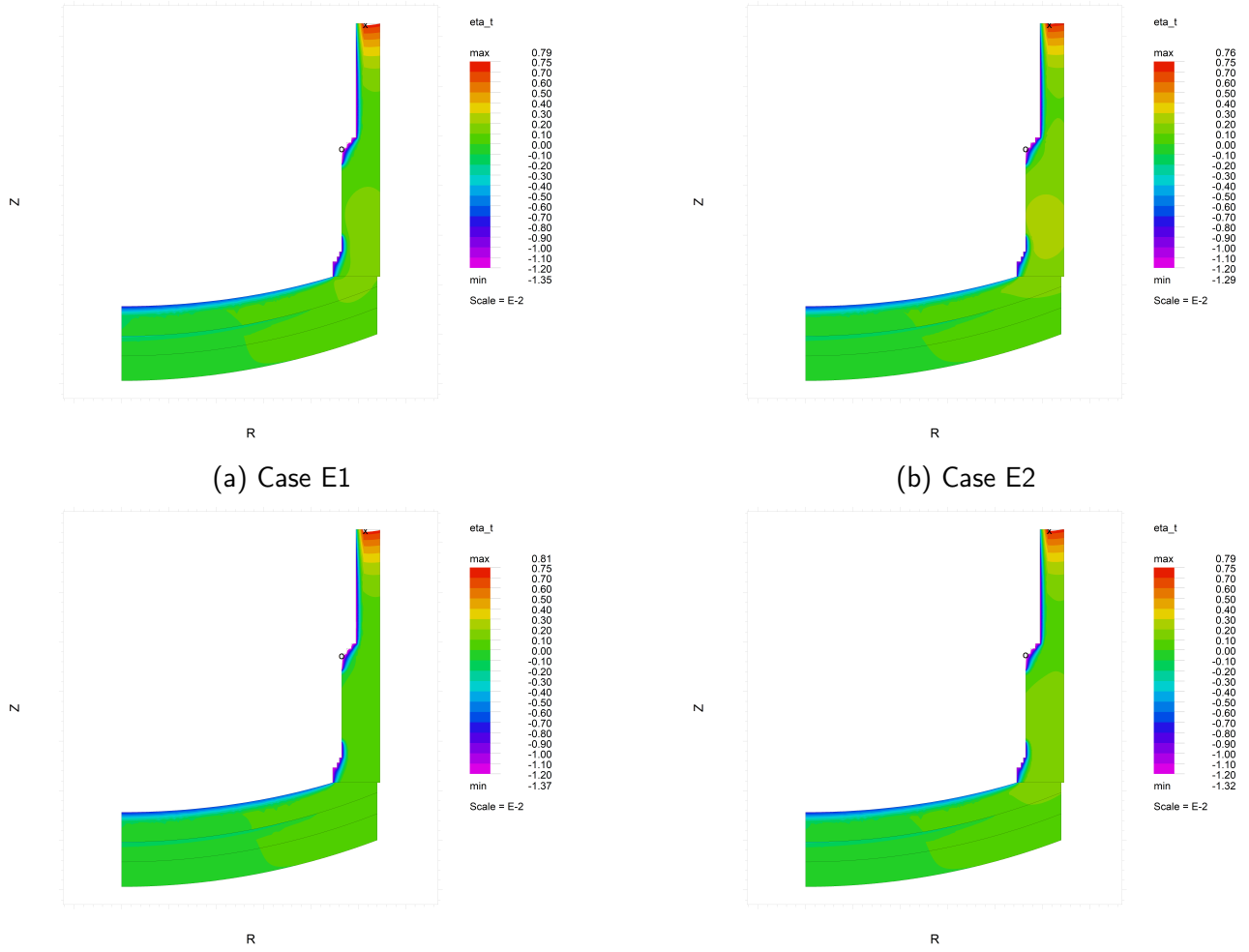

(a) Case E1 (b) Case E2

(c) Case E3 (d) Case E4

Figure 7.16: Tangential strain for the evaluated cases plotted on the same scale

penetration should the hotface of the lining fail. The hearth is in a general state of compressive loading. A high compressive load is present at the steps in the freeboard area, due to the higher thermal expansion. This could be due to the stress concentration caused by modelling the wall as a continuum solid. However, it could be an area of concern as the lower step might expand more in the area where no pressure from above contains it and which might result in cracks forming in these areas.

As with the strain for the radial and tangential directions, the strain distribution in the lining is largely similar for all four cases. Figure 7.18c show a different strain distribution around the outside of the hearth top where it meets the sidewall bottom. A tensile strain here indicates the wall and the hearth pulling apart significantly more than any of the other cases. As shown in Figures 7.18c to 7.18d the influence of the stiffer wall and softer hearth results in the large strains in the hearth whereas the stiffer hearth and softer wall shows the negative strain in the wall rather than the hearth. In these areas the wall restrict the expansion of the hearth in the axial direction which results in large strains in this area. This gives a good indication of one of the reasons that the skewback region needs to be carefully considered when designing a furnace and selecting the mechanical material properties.

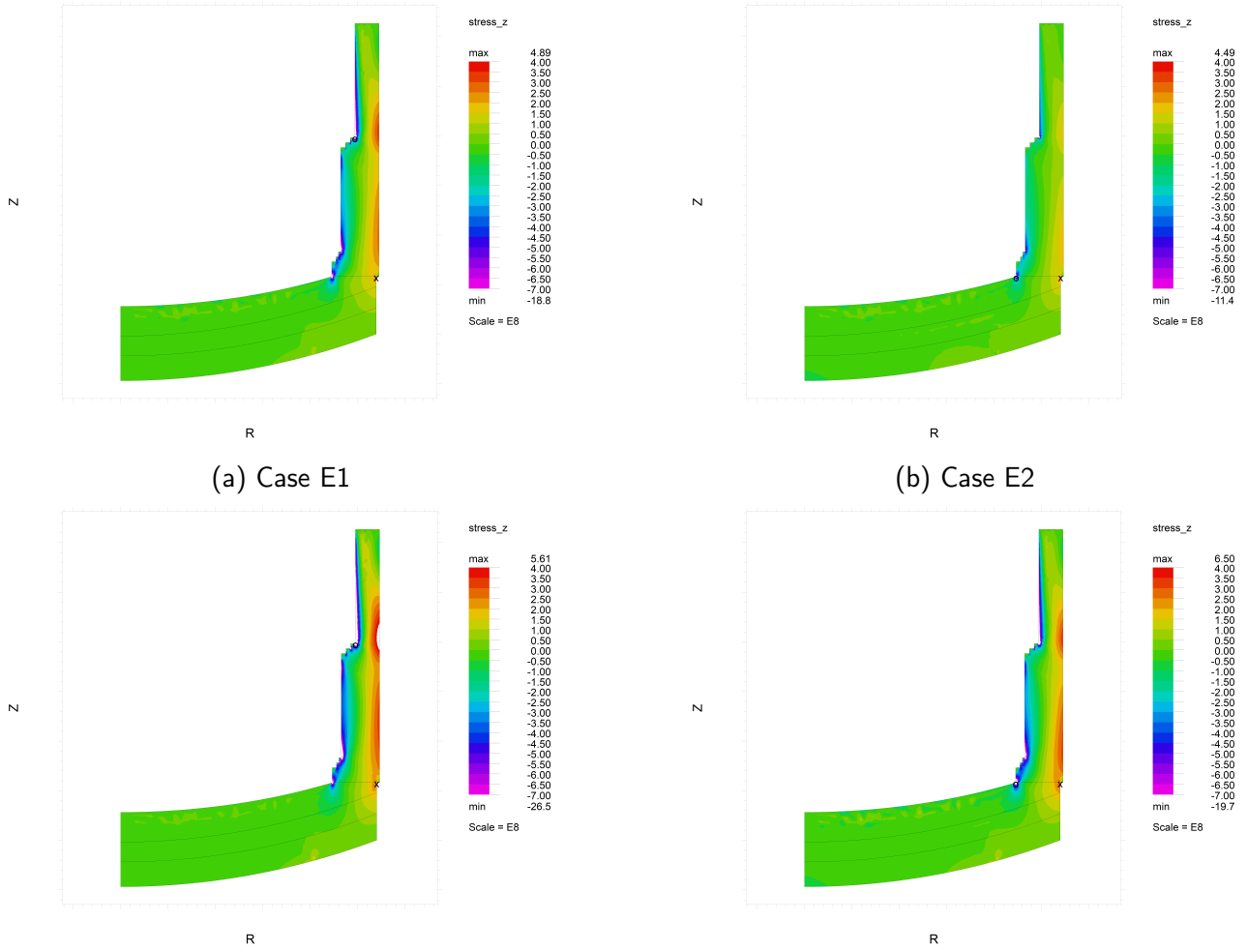

(a) Case E1

(b) Case E2

(c) Case E3

(d) Case E4

Figure 7.17: Axial stress for the evaluated cases plotted on the same scale

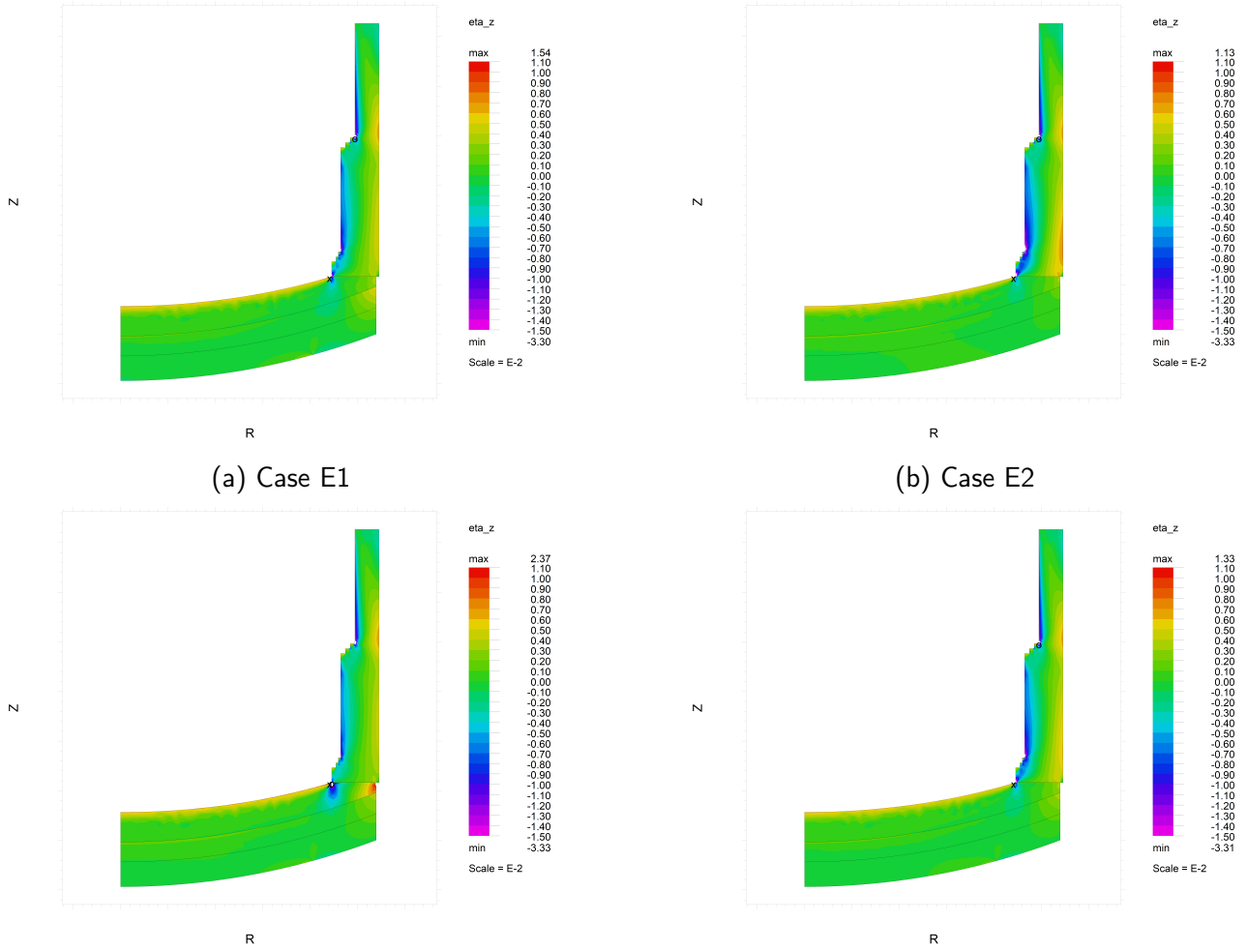

(a) Case E1

(b) Case E2

(c) Case E3

(d) Case E4

Figure 7.18: Axial strain for the evaluated cases plotted on the same scale

7.2.3 Influence of Allowed Expansion on Stresses

To further illustrate the impact of the allowed expansion on the stress state in the lining the material properties for Case E1 as described in Table 7.2 were used for Case 1 and Case 6 of allowed expansion as listed in Table 7.1. The stress states are shown in Figures 7.19 to 7.21.

Considering the radial stress, the largest area impacted by the allowed expansion is the hearth hotface, notice how the highest compressive stress is almost double in Figure 7.19a compared to Figure 7.19b. Also noteworthy is the low impact on the sidewall of the extra allowed expansion for stresses in the radial direction with only a slight impact in the hearth bottom.

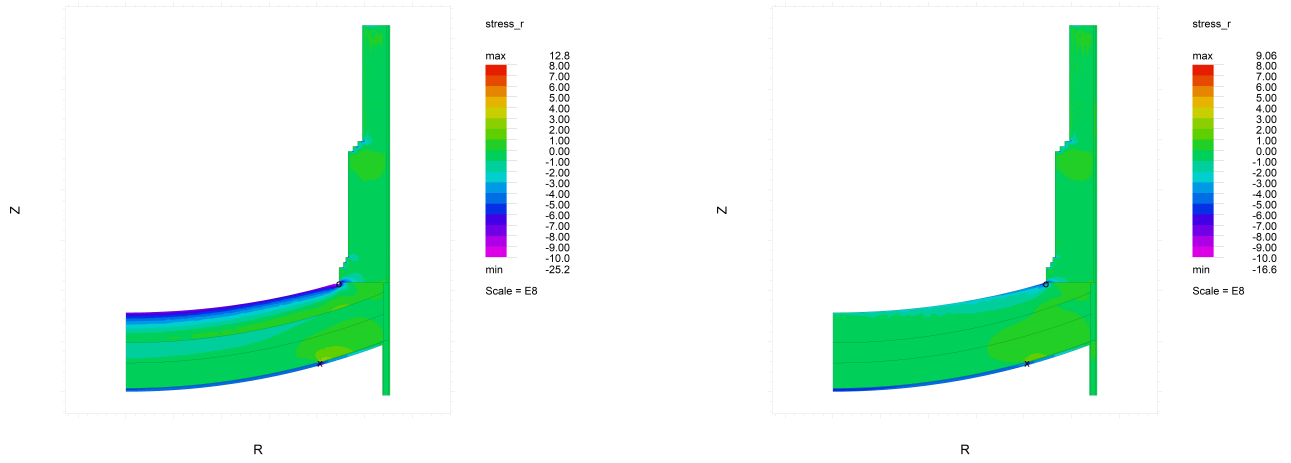

(a) Case K5 (b) Case K6

Figure 7.19: Radial stress for the comparison of low and high allowed expansion

The tangential stress is impacted the most by the allowed expansion. A significantly higher stress state in all areas are observed for Figure 7.20a when compared to Figure 7.20b. Note the effect of the increased compressive tangential stress on the sidewall hotface leading to the higher tensile stress toward the sidewall coldface. This indicates a separation of the bricks which could increase the lining failure risk due to cracks forming on the smaller sections of the bricks that are now load bearing.

Tensile loading is also observed on the hearth top coldface indicating separation due to the high compressive load on the hotface. It is thus worth noting that less allowed expansion could actually result in more separation of lining coldface and increase the stress even more on the hotface driving lining failure.

The impact of the allowed expansion on the axial stress is low with very few and slight differences observed in Figure 7.21.

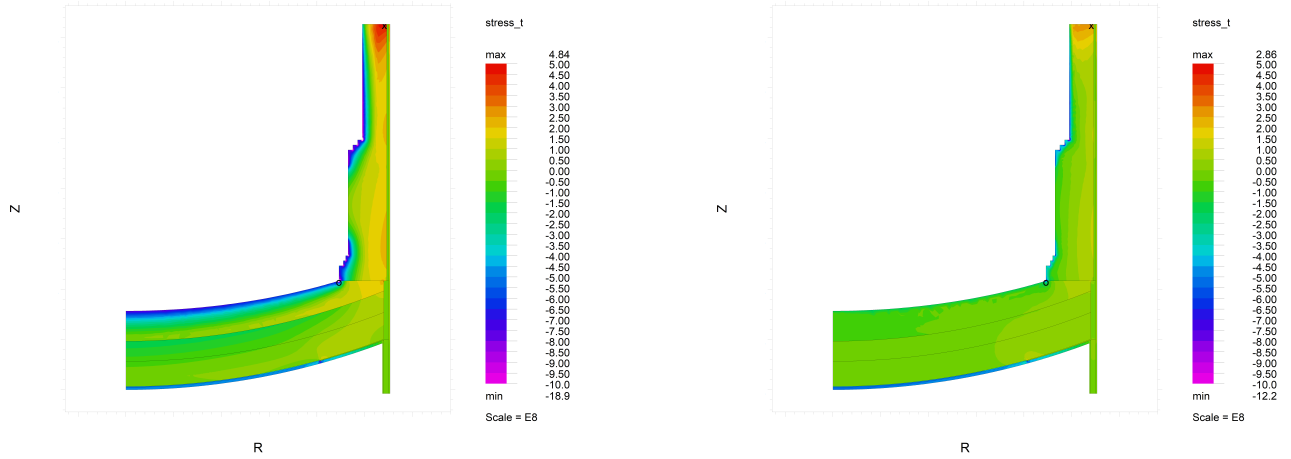

(a) Case K5 (b) Case K6

Figure 7.20: Tangential stress for the comparison of low and high allowed expansion

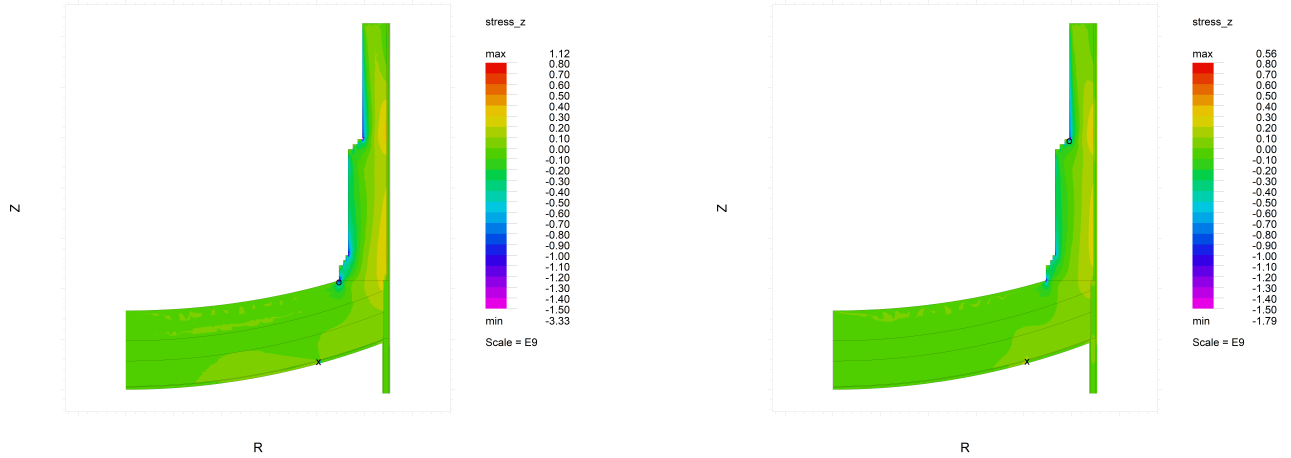

(a) Case K5 (b) Case K6

Figure 7.21: Axial stress for the comparison of low and high allowed expansion

7.2.4 Von Mises Stresses and Failure

Using the results shown in Figure 7.22, the impact of the material properties can be evaluated for the three main sections where the input was varied; the hearth top, hearth bottom, and sidewall. Comparing Figure 7.22a and Figure 7.22b for the hearth bottom: the results do not vary much when looking at the stress distribution, there is a magnitude difference and a higher stress state on the hearth top and bottom interaction for Figure 7.22b. From these results the impact of the hearth bottom material properties is not as significant and some variation is tolerable.

Comparing Figure 7.22c and Figure 7.22d can give an indication of the influence of the mechanical material properties for the hearth top. In this case it shows a much higher stress state on the hearth hotface for Figure 7.22d. In addition, the stress state in the skewback region is vastly different.

The sidewalls show the largest impact of different material properties. The stiffer material used for the sidewall in Case E3 shows a significantly higher stress state than the softer material choice for Case E2. The stress concentrations on the steps in the sidewall is also significantly more prominent for the stiffer material choice. This is predominantly driven by the tangential or *hoop* stress in the lining (Figure 7.15). This needs to be considered when choosing the allowed expansion and mechanical material property combination.

From Part II the cold crushing strength is expected to be between 20 MPa to 69 MPa; however, it

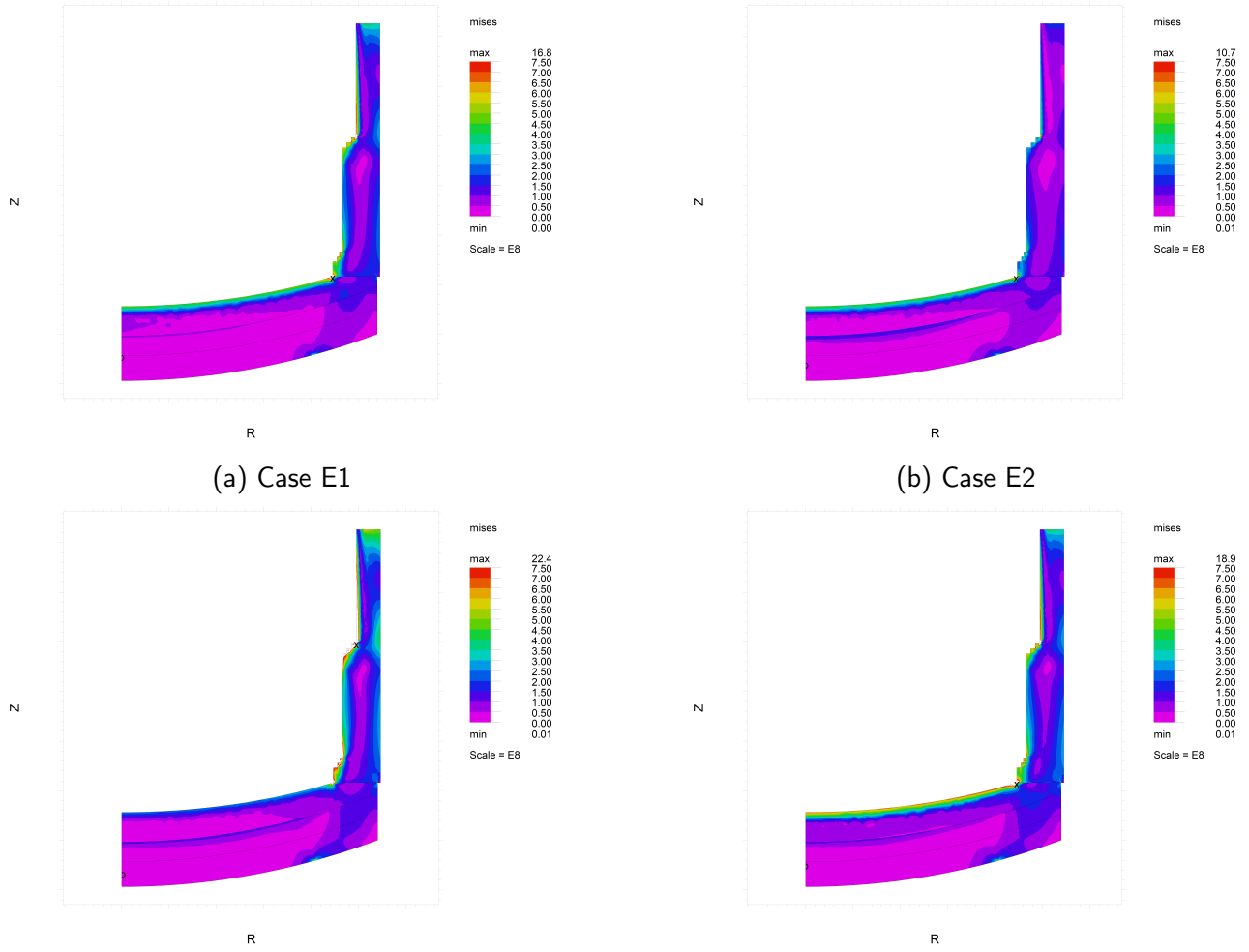

(a) Case E1

(b) Case E2

(c) Case E3

(d) Case E4

Figure 7.22: Von Mises Stress

was also demonstrated that the cold crushing strength does not always act as an accurate indication of the hot crushing strength and can therefore only provide a limited insight. In addition, the linear elastic material model used, does not take into account the ductile like behaviour of refractories as the temperature increases. To use the Von Mises stress to evaluate the failure of the lining, based on the limitations of the model as well as the limitation of the failure criterion, is not adequate. It can, however, still be used to give an indication of critical areas where failure could occur and where additional investigation might be needed should similar models be used for designing purposes. In such investigations more accurate material models can be used for refractories at a higher temperature along with the Coloumb-Mohr failure criterion. The impact of the linear elastic material model can clearly be seen in the magnitude of the stresses in Figure 7.22.

In order to better understand the effect of the linear material model used some additional simulations were run, for these the Young's modulus was kept constant over all sections of the furnace but significantly lower values were used (Table 7.3). These values were extracted from Figure 6.2 and Table 6.3. Note the vastly lower stress values in the refractory lining as shown in Figure 7.23. This serves to illustrate the importance of using the correct stress-strain relationship. In order to accurately predict the behaviour of the lining, non-linear and temperature dependant stress-strain curves need to be used to describe the material behaviour. The simulations were done for the keying Case 4.

Table 7.3: Young's modulus for additional stress evaluations

	Young's Modulus
Case E5	1.583 GPa
Case E6	2.55 GPa
Case E7	8.0 GPa
Case E8	14.687 GPa

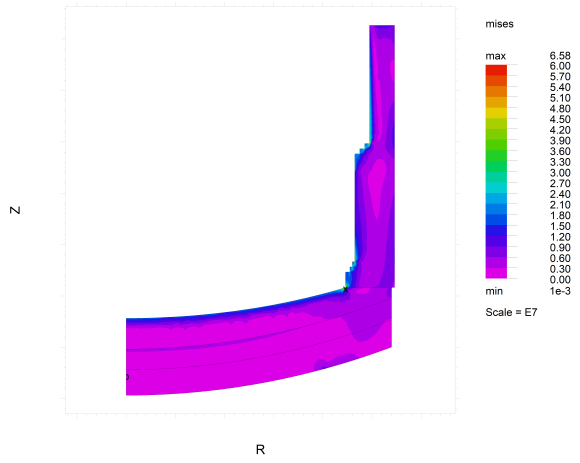

(a) Case E5, note the maximum stress of 65.8 MPa

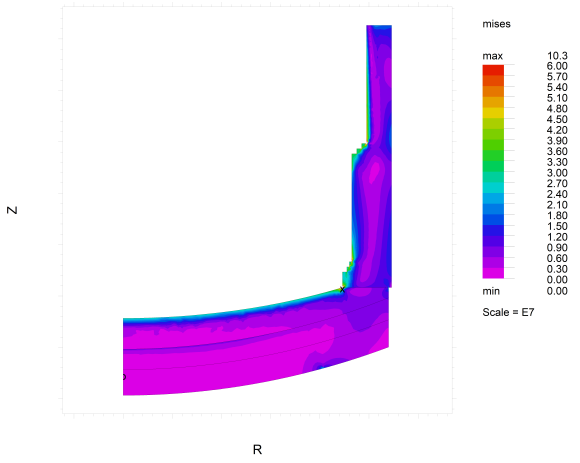

(b) Case E6, note the maximum stress of 100.3 MPa

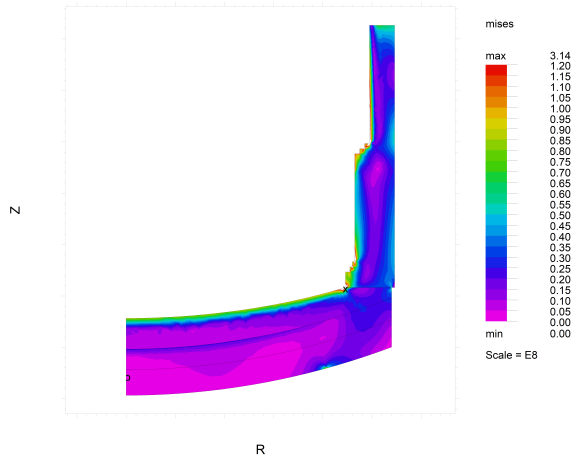

(c) Case E7, note the maximum stress of 314 MPa

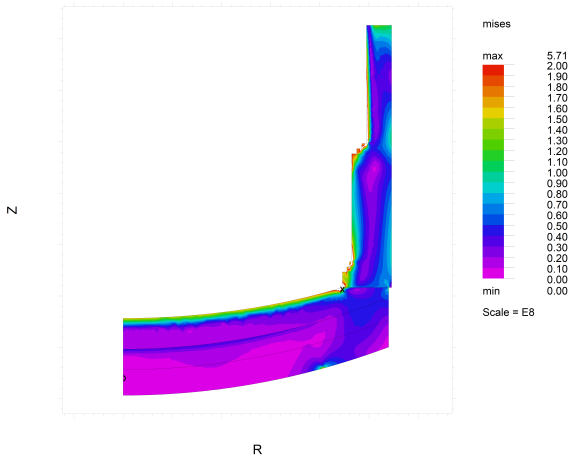

(d) Case E8, note the maximum stress of 571 MPa

Figure 7.23: Von Mises Stress for different Young's modulus as listed in Table 7.3

Part V

Closure

Chapter 8

Conclusions

From this study several conclusions can be drawn with regards to the impact of using a linear stress-strain approximation to the behaviour of refractories. From the work of Schacht (1995) the temperature dependence of this relationship was clearly stated. When using a linear approximation, the stresses can be severely over estimated especially for areas with high deformation due to the high temperature distribution. The simulation results showed these excessive stresses, but also showed the significantly reduced stresses when using a Young's Modulus that approximates the behaviour of the refractory material at higher temperatures. This study again highlights the need for the stress-strain relationship, especially at higher temperatures. According to Schacht (1995), this data is not freely available and is often not supplied by refractory manufacturers. In order to achieve the ultimate goal of full-scale furnace modelling and including all phenomena this data will have to be obtained for the specific refractories that will be used in the model. Over and above the need for this data, the linear elastic material model has been shown to be ineffective and not suitable to model the furnace.

Several literatures sources already highlight the importance of expansion allowance, a method has been presented which allows for an easy view of the effect of the expansion allowance and allows for calculation of the keying factor. This can be used to investigate changes in operational temperatures, the inclusion of additional refractories or a change in refractory material properties. It has also been shown that the degree of keying has a significant effect on the stress in the lining. As shown from Chirasha and Shoko (2007) the improper consideration of expansion allowance can lead to lining failure. In the case of the tangential stress in the sidewall a 70% increase is shown for three times less expansion allowance. Given that this is toward the cold face of the lining, in which case the linear elastic material model is more applicable than toward the hot face, this relationship gives an indication of the impact of expansion allowance has on the crushing forces in the lining. In addition, from the simulation results it is evident that more investigation needs to be done to determine the best distribution of allowed expansion, this is especially true for the sidewall where the separation of the cold face leads to crack initiation and growth on the hotface.

No simulation studies of thermal cycles were included in this study, from the Literature Review the importance of studying these have been highlighted. Before this can be attempted, however, the challenges identified with the steady state models to the use of linear elastic material models needs to be addressed. From Schacht (1995), the factors that need to be investigated would be the rate of heating of the furnace, along with in depth analysis of crack initiation and growth due to these thermal fluctuations in the lining. This would require individual brick modelling to achieve. It has been shown from Schacht (1995) that this is a significant contributor to lining failure, in combination with the fluctuating electrical supply in South Africa a more in depth look at this is critical.

The results obtained in the simulation studies does yield some insights to furnace behaviour and can be used to make observations about critical areas and material tenancies. The material properties

used were based on general Magnesium Oxide refractory properties and is thus not completely arbitrary. From the simulation results it is evident that a softer material (lower Young's Modulus) results in lower stresses and displacements in critical areas such as the skewback. The simulations also show an increase in the stresses at the sidewall steps, this can be attributed to the increased area exposed to higher temperatures and the stress concentrations in the area. The simulations also indicate the tendency of the lining to separate in specific areas; however, to estimate this behaviour more accurately modelling will have to be done considering the sections of the furnace not as a solid, but as individual pieces with contact forces between them. Using simulations as presented here will thus contribute to identifying critical areas where more detailed investigations can focus.

Given the challenges industry faces this study summarizes historical work on this topic and presents a starting point to the use of multi-physics modelling to analyse and estimate furnace behaviour.

Chapter 9

Recommendations

Building of the work presented here, the following are recommended next steps:

- Incorporate a non-linear elastic material model with refractory material properties that are temperature dependant.
- It might be necessary to conduct an experimental procedure to obtain this information for a specific set of refractory materials.
- Once accurate material models are incorporated transient studies can be undertaken to investigate the effect of transient conditions.
- After identifying critical areas in the furnace, more detailed models should be developed which includes contact between sections and, if needed, between individual bricks.

References

Ameswebinfo (2019). *Material Properties*. URL: https://www.amesweb.info/Materials/Material_Properties.aspx.

Backstrom, G. (2005). "Axially Symmetric heating of a Cylinder". In: *Deformation and Vibration by Finite Element Analysis Using FlexPDE Version 5*. GB Publishing, 133–136.

Belt, C.K. (2011). "Business Analysis of Total Refractory Costs". In: *Light Metals*.

Benavidez, E.R. et al. (2015). "Thermal and mechanical properties of commercial MgO-C bricks". In:

Boisse, P et al. (2001). "Simulations of thermomechanical behavior of composite refractory linings". In: *Composites: Part B* 32, pp. 461–474.

Brulin, J. et al. (2011). "Characterization and modelling of a carbon ramming mix used in high-temperature industry". In: *International Journal of Solids and Structures* 48, pp. 854–864.

Budynas, R.G. and J.K. Nisbett (2011). *Shigley's Mechanical Engineering Design*. 9th ed. ISBN: 9780073529288.

China Firebrick (Oct. 2017). *Thermal conductivity of refractory bricks*. URL: http://www.chinafirebrick.com/Company_News_128.html.

Chirasha, J. and N.R. Shoko (2007). "REFRACTORY DESIGN EFFECT ON SUBMERGED ARC FURNACE LIFE AND PRODUCTION PERFORMANCE – THE ZIMBABWE ALLOYS EXPERIENCE". In: *Infacon XI*.

Enterfea (2019). *Difference between linear and nonlinear elastic material*. URL: https://enterfea.com/difference-between-linear-and-nonlinear-elastic-material/.

Ferber, M.K, A.A. Weresczak, and J.G. Hermrick (2006). *Compressive Creep and Thermophysical Performance of Refractory Materials*. Report. Oak Ridge National Laboratory. URL: https://www.osti.gov/servlets/purl/885151.

FlexPDE 6 Help (2017). PDE Solutions Inc. URL: https://www.pdesolutions.com/bookstore.html.

Gasser, A, K. Terny-Rebeyrotte, and P. Boisse (2004). "Modelling of joint effects on refractory lining behaviour". In: *Journal of Materials: Design and Applications*.

Gous, M. (2006). "An overview of the Namakwa Sands Ilmenite Smelting Operations". In: *Southern African Pyrometallurgy 2006*.

Hibbeler, R.C. (2011). *Mechanics of Materials*. Pearson Higher Education and Professional Group, 2018. ISBN: 9781292178202.

Holman, J.P. (1989). *Heat Transfer*. ISBN: 0071004874.

Jones, R.T. et al. (2011). "Some myths about DC arc furnaces". In: *Southern African Pyrometallurgy 2011*. Ed. by R.T. Jones and P. den Hoed.

Kearney, L (Aug. 2012). *Mining and minerals in South Africa*. URL: https://www.brandsouthafrica.com/investments-immigration/business/economy/mining-and-minerals-in-south-africa.

Kotze, H., D. Bessinger, and J. Beukes (2006). "Ilmenite Smelting at Ticor SA". In: *Southern African Pyrometallurgy 2006*.

Kotze, H. and P.C. Pistorius (2009). "A heat transfer model for high titania slag blocks". In: *The 7th International Heavy Minerals Conference*.

Larosche, C.J. (2009). "Types and causes of cracking in concrete structures". In: *Failure, Distress and Repair of Concrete Structures*.

Liang, X. et al. (2007). "Modeling of failure in a high temperature black liquor gasifier refractory lining". In: *Engineering Failure Analysis* 14.

Liu, F., J. Swithenbank, and E.S Garbett (1992). "The boundary condition of the P_N-approximation used to solve the radiative transfer equation". In: *Int. J. Heat Mass Transfer*.

Made-in-China.com (2019). *High Density Low Porosity Magnesia Refractory Brick*. URL: https://jucos1.en.made-in-china.com/product/zKXnTNUCYDRE/China-High-Density-Low-Porosity-Magnesia-Refractory-Brick.html.

Motsie, R. (2008). "AN OVERVIEW OF SOUTH AFRICA'S TITANIUM MINERAL CONCENTRATE INDUSTRY". In: *DIRECTORATE: MINERAL ECONOMICS*.

Naidoo, S. (2012). "Eskom pays smelters to shut down". In: *Mail and Guardian*.

National Productivity Council, India (2006). "Furnace and Refractories". In:

November Climate History for Richards Bay Country Club (2019). URL: http://www.myweather2.com/Golf-Courses/South-Africa/Richards-Bay-Country-Club/climate-profile.aspx.

Pan, Y., S. Sun, and S. Jahanshahi (2011). "Mathematical modelling of heat transfer in six-in-line electric furnaces for sulphide smelting". In: *J. S. Afr. Inst. Min. Metall.* 111.

Papathanasiou, T.K., F DalCorso, and A Piccolroaz (2016). "Thermomechanical response FEM simulation of ceramic refractories undergoing severe temperature variations". In: *Journal of the European Ceramic Society*.

Pistorius, P.C. (Jan. 2008). "Ilmenite smelting: the basics". In: *The journal of The Southern African Institute of Mining and Metallurgy* 108.

Reynolds, Q.G. (2002). "Thermal Radiation Modelling of DC Smelting Furnace Freeboards". In: *Minerals Engineering* 11.

— (2012). "The dual-electrode DC arc furnace-modelling brush arc conditions". In: *J. S. Afr. Inst. Min. Metall.* 112.

Reynolds, Q.G. and R.T. Jones (2004). "Semi-empirical modelling of the electrical behaviour of DC-arc smelting furnaces". In: *Journal of the Southern African Instiute of Mining and Metallurgy* 6, pp. 345–351.

Schacht, CA (1995). *Refractory Linings. Thermomechanical Design and Applications*. Ed. by Charles A. Schacht. Routledge. ISBN: 9781351419321.

Schacht, C.A. (2004). "Thermomechanical Considerations for Refractory Linings". In: *Refractories Handbook*. Ed. by Charles A. Schacht. CRC Press, 475–489. ISBN: 0824756541.

Schacht, C.A. and M. Maupin (2004). "Refractory Lining Design and Installation". In: *Refractories Handbook*. Ed. by Charles A. Schacht. CRC Press, 475–489. ISBN: 0824756541.

Siegel, R. and J. Howell (2002). "Energy and radiative transfer relations for an absorbing, emitting, and scattering medium with conduction and convection". In: *Thermal Radiation Heat Transfer 4th Edition*. Taylor and Francis, pp. 557–576.

Steyn, L. (2019). "Smelters will not survive 15 percent Eskom tariff hike, industry warns". In: *BusinessDay*.

Yilmaz, S. (2003). "Thermomechanical Modelling for Refractory Lining of a Steel Ladle Lifted by Crane". In:

Zienkiewicz, O.C., R.L. Taylor, and J.Z. Zhu (2013). *The Finite Element Method. Its Basics and Fundamentals*. 7th ed.

Zietsman, J.H. and C. Kok (2016). "auxi – Lending a helping hand to improve metallurgical processes". In: *New technology and innovation in the Minerals Industry Colloquium*.

Zietsman, J.H. and P.C. Pistorius (2004). "Process mechanisms in ilmenite smelting". In: *The Journal of The South African Institute of Mining and Metallurgy* 11, pp. 653–660.